

Final Project

Master in Energy Engineering (MUEE)

Wind turbine type IV simulation with grid-following and grid-forming control

UPC

January 23, 2023

Author: Mohammadhossein Tavanaeeshahroodi

Director: Vinícius Albernaz Lacerda

Director: Eduardo Prieto Araujo



Escola Tècnica Superior
d'Enginyeria Industrial de Barcelona



Abstract

The demand for renewable energy is rapidly increasing for several reasons, including global warming, environmental effects, and energy independence for nations that now import the majority of their energy needs. Europe, as a whole, imports more fossil fuels than any other region in the globe, but the continent made the bold choice to become carbon neutral by 2050. Utilizing as much renewable energy as possible, including wind and solar, will be crucial to meet that goal. In many European nations, wind energy is one of the major sources of electricity, and its proportion will rise. Since wind power over the oceans and seas is more plentiful and powerful than wind power on land, off-shore wind farms are one of the keys to advancing the higher penetration of renewables. Repairs and maintenance in offshore wind farms can be complex, in addition to the difficulties brought on by activities on the sea and the problems caused by humidity. The wind turbine Type IV is typically utilized in off-shore applications to reduce maintenance concerns since it may be gearless and may use a permanent magnet generator and full-scale converter. As the penetration of renewables with power converters grows, new control approaches must be considered, and the benefits and drawbacks of each control structure must be weighed. A wind turbine Type IV model with grid-following and grid-forming control was built in Simulink and PSCAD during this project, and their behavior in an IEEE 9-bus system was evaluated at the completion.

Contents

1	Introduction	9
1.1	Background	9
1.2	Current state of wind energy production	10
1.3	Power system challenges with high penetration of renewable energy	11
1.4	Objectives	12
1.5	Scope of the project	12
2	Wind energy technology	13
2.1	Wind origin	13
2.2	Wind energy potential	13
2.3	Wind turbine fundamentals	14
2.4	Power coefficient	15
2.4.1	Betz's law	16
2.4.2	Aerodynamic lift force	17
2.4.3	Restrictions on power	18
2.5	Types of wind turbine	19
2.5.1	Wind turbine Type I	19
2.5.2	Wind turbine Type II	19
2.5.3	Wind turbine Type III	20
2.5.4	Wind turbine Type IV	20
2.6	Grid stability	22
2.7	The swing equation and inertia	22
2.8	Permanent magnet synchronous machine (PMSG)	24
2.9	Power converters	27
2.9.1	Diode rectifier based converter	27
2.9.2	Back to Back converter	28
2.10	Control systems of wind turbines	29
2.10.1	Grid-following versus Grid-forming	29
2.10.2	Droop based with cascade control	30
2.10.3	Virtual synchronous machine	32
3	Converter's controller components	36
3.1	Park and inverse park transformation	36
3.2	Phase locked loop (PLL)	36
3.3	Current reference computation	38
3.4	DC voltage regulator	38
3.5	Current regulator (Grid-side)	40
3.6	Current regulator (Machine-side)	41
4	Methodology	43
4.1	Simulation in MATLAB/Simulink	43
4.2	Wind Turbine Model	44
4.2.1	Wind Turbine Power Model	45
4.2.2	Pitch Angle Controller Model	45
4.2.3	Shaft Model	46
4.2.4	MPPT	46
4.2.5	Permanent Magnet Synchronous Generator	47



4.3	Voltage source converter (VSC)	47
4.4	AC Voltage source	47
4.5	Converter's grid coupling filter	48
4.6	DC bus	48
4.7	Grid side VSC controller	48
4.7.1	Phase Locked Loop	49
4.7.2	Park Transformation	50
4.7.3	DC Voltage regulator	50
4.7.4	Q Loop	50
4.7.5	Current regulator	51
4.8	Machine side VSC controller	52
4.8.1	Angular and rotational speed measurement	52
4.8.2	Current reference calculation	52
4.8.3	Current regulator (Machine-side)	53
4.9	Simulation in PSCAD	54
4.10	Wind turbine model in PSCAD	54
4.11	Power circuit in PSCAD	55
4.12	DC-Chopper	56
4.13	DC voltage support	57
4.14	Grid-side controller in PSCAD (GFOL)	58
4.14.1	PLL model in PSCAD	58
4.14.2	DC voltage regulator in PSCAD	58
4.14.3	Grid-side current regulator in PSCAD	59
4.15	Grid-side controller in PSCAD (GFOR)	60
4.15.1	LCL filter	60
4.15.2	Voltage controller	60
4.15.3	Current controller	60
4.15.4	Active power droop	61
4.15.5	Reactive power droop	62
4.16	Machine-side controller in PSCAD	63
4.16.1	Rotational speed measurement in PSCAD	63
4.16.2	Current reference calculation in PSCAD	63
4.16.3	Machine-side current regulator in PSCAD	64
4.17	Automatic initialization in PSCAD	65
4.17.1	Providing wind turbine model's data	65
4.17.2	Reading the data from power flow results	65
4.17.3	Sending the data to PSCAD model	66
4.18	IEEE 9-bus system	67
5	Results and discussion	71
5.1	Simplified models results	71
5.1.1	Results of wind turbine model in Simulink (GFOL)	71
5.1.2	Results of wind turbine model in PSCAD (GFOL)	73
5.1.3	Results of wind turbine model in PSCAD (GFOR)	78
5.1.4	Results of simplified GFOL converter model with different grid strength	79
5.1.5	Results of simplified GFOR converter model with different grid strength	83
5.2	IEEE 9-bus system with GFOL converter	87
5.2.1	Normal operation	87
5.2.2	Symmetric fault	88



5.2.3	Load increase	90
5.2.4	Generator disconnection	91
5.3	IEEE 9-bus system with GFOL and GFOR converters	92
5.3.1	Normal operation	92
5.3.2	Symmetric fault	93
5.3.3	Load increase	95
5.3.4	Generator disconnection	96
Conclusions		98
Acknowledgements		100
Bibliography		101
Appendix		106



List of Figures

1	Evolution of installed renewables and renewable waste capacity (MW) in EU-27 [22]	9
2	Global wind energy share in electricity mix 2021 [35]	10
3	Global winds [24]	13
4	Onshore wind full load hours[kwh kw ⁻¹][6]	14
5	The energy extracting stream-tube of a wind turbine [12]	15
6	Betz limit [37]	16
7	Lift and drag force of wind turbine [56]	17
8	Power control regions of wind turbine [17]	18
9	Wind turbine Type I [31]	19
10	Wind turbine Type II [31]	20
11	Wind turbine Type III [31]	20
12	Wind turbine Type IV [31]	21
13	Details of PMSG connection for a Y configuration without neutral conductor [38]	24
14	Diode rectifier based converter topology [33]	27
15	Back to Back converter topology [33]	28
16	Grid-following (left) vs Grid-forming (right)	29
17	Droop characteristics	30
18	Outer control loops in droop based control [58]	31
19	Full scheme of droop based converter with cascade control [19]	31
20	Inner control loops (a) Voltage controller (b) Current controller [19]	32
21	VSM control structure [66]	33
22	VSG control structure [66]	34
23	Synchronverter control scheme [72]	35
24	Diagram of phase-locked loop [20]	36
25	Linearized model of phase-locked loop [15]	37
26	DC voltage regulator [20]	39
27	Equivalent model of AC side of a VSC [20]	40
28	General control overview [13]	43
29	General scheme of wind turbine model	44
30	Wind turbine power model	45
31	Pitch angle controller	45
32	One mass model	46
33	DC bus schematic [38]	48
34	Grid side VSC control structure [20]	49
35	Designed PLL in Simulink	49
36	Park and Inverse park transform blocks	50
37	DC voltage regulator in Simulink	50
38	Implemented Q Loop in Simulink	50
39	Current regulator structure [20]	51
40	Machine angular and rotational speed measurement	52
41	Current reference computer	52
42	Machine-side current regulator	53
43	Wind turbine model in PSCAD	54
44	Pitch controller in PSCAD	55
45	Wind source block in PSCAD	55
46	Power circuit of Type IV wind turbine in PSCAD	56



47	DC-Chopper model in PSCAD	57
48	DC voltage support model in PSCAD	57
49	PLL designed model in PSCAD	58
50	DC voltage regulator in PSCAD	59
51	Grid-side current regulator in PSCAD	59
52	Inner loop controller of the GFOR converter in PSCAD	61
53	Active power controller of the GFOR converter in PSCAD	61
54	Reactive power controller of the GFOR converter in PSCAD	62
55	Rotational speed measurement in PSCAD	63
56	Machine-side current reference computer in PSCAD	63
57	Machine-side current regulator in PSCAD	64
58	The attributes of the Generator 1	67
59	IEEE 9-bus system [1]	67
60	IEEE 9-bus system in PSCAD	68
61	Synchronous machine in PSCAD	70
62	Wind speed, pitch angle and power variation	71
63	Variation of grid-side power, voltage, current	72
64	Relation of wind speed, pitch angle, and power coefficient	73
65	Wind speed, pitch angle and power variation in PSCAD (GFOL)	74
66	Variation of grid-side voltage and current and dc-link in PSCAD (GFOL)	74
67	Wind speed, pitch angle and power variation in PSCAD (GFOL) during the fault	75
68	Variation of grid-side voltage and current and dc-link in PSCAD (GFOL) during the fault	76
69	Variation of grid-side voltage and current, dc voltage, and chopped power in addition to converter power and PLL angular speed in PSCAD (GFOL) during the fault	77
70	Wind speed, pitch angle and power variation in PSCAD (GFOR)	78
71	Variation of grid-side voltage and current and dc-link plus the injected battery power and the droop rotational speed in PSCAD (GFOR)	79
72	Voltage, current, power, and angular speed of GFOL converter connected to an ideal grid	80
73	Voltage, current, power, and angular speed of GFOL converter connected to the grid with SCR=5	81
74	Voltage, current, power, and angular speed of GFOL converter connected to the grid with SCR=3	82
75	Voltage, current, power, and angular speed of GFOL converter connected to the grid with SCR=1	83
76	Voltage, current, power, and angular speed of GFOR converter connected to the grid with SCR=1	84
77	Voltage, current, power, and angular speed of GFOR converter connected to the grid with SCR=3	85
78	Voltage, current, power, and angular speed of GFOR converter connected to the grid with SCR=5	86
79	Voltage, current, power and angular speed of GFOR converter in island mode	87
80	IEEE 9-bus system with GFOL converter in normal operation	88
81	IEEE 9-bus system with GFOL converter with a symmetric fault	89
82	IEEE 9-bus system with GFOL converter with a symmetric fault (detailed view)	89
83	IEEE 9-bus system with GFOL converter with an added load	90
84	IEEE 9-bus system with GFOL converter with an added load (detailed view)	91



85	IEEE 9-bus system with GFOL converter and a generator disconnection condition	92
86	IEEE 9-bus system with GFOL and GFOR converters	93
87	IEEE 9-bus system with GFOL and GFOR converters with a symmetric fault . . .	94
88	IEEE 9-bus system with GFOL and GFOR converters with a symmetric fault (de- tailed view)	94
89	IEEE 9-bus system with GFOL and GFOR converters with an added load	95
90	Effects of different virtual inertia values on the system	96
91	IEEE 9-bus system with GFOL and GFOR converters and a generator disconnec- tion condition	97



List of Tables

1	Comparison between different Types of wind turbine [36]	22
2	Key differences between Grid-following and Grid-forming [66]	30
3	Wind turbine parameters [2]	44
4	Coefficient power parameters [2]	44
5	PMSG parameters [2]	47
6	VSC back-to-back [13]	47
7	AC grid [13]	47
8	Terminal conditions of IEEE 9-bus system	69
9	Transmission line characteristics of IEEE 9-bus system	69
10	Load characteristics of IEEE 9-bus system	69
11	Cost of the project	99
12	Environmental impact of the project	99



1 Introduction

1.1 Background

In Europe, fossil fuels account for around 70% of total energy consumption (22% gas and 43% oil), and electricity, which accounts for about 22% of total energy consumption [28], is also mostly produced using fossil fuels, primarily coal and gas. Gas usage has increased recently as a result of perceptions that it is a cleaner energy source than coal and oil and is more popular with the public than alternative power sources like nuclear. Concerning natural gas, the European economy is dependent on countries out of the EU, with conditions varying from nation to nation (with some, particularly in the Baltic's, receiving 100% of their demand) [7]. In addition, the EU has pledged to make new, ambitious climate change reduction goals legally enforceable. According to a new agreement reached by the EU Parliament and member states, the EU will reduce carbon emissions by at least 55% by 2030 compared to 1990 levels [46]. Transitioning to more sustainable renewable energy sources like wind and solar is therefore required to address issues like releasing from unfriendly energy providers and fulfilling carbon reduction targets.

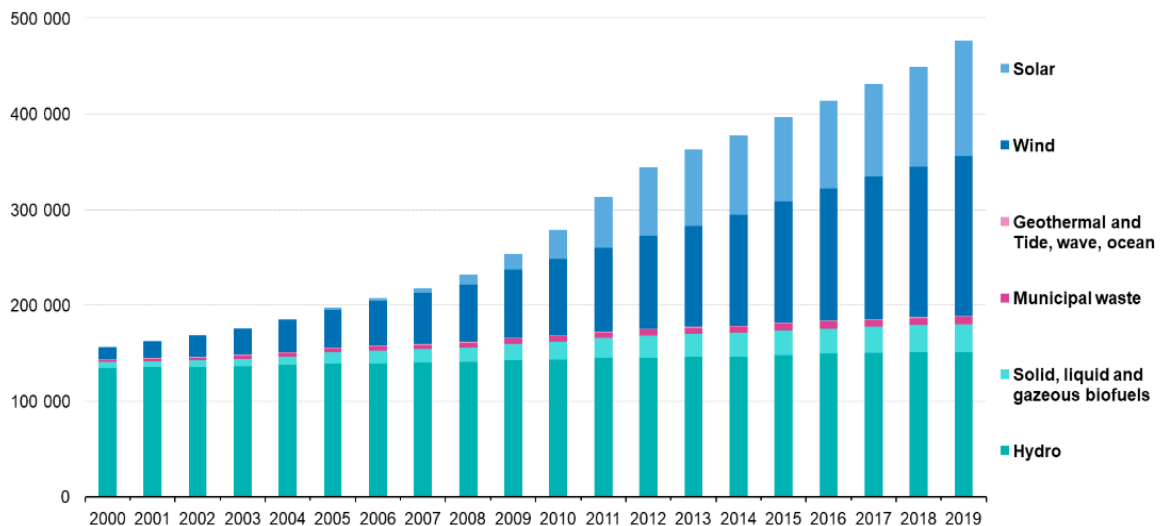


Figure 1: Evolution of installed renewables and renewable waste capacity (MW) in EU-27 [22]

As shown in Fig. 1, renewable installed capacity has expanded in recent years and will continue to do so. This transformation has altered the network from conventional centralized features to distributed generation and smarter grids, increasing system complexity. The system strength is more crucial when renewable sources, which employ fast converters, replace traditional generation. The fast reaction of reactive power injection from the converters into the grid, which results in un-damped voltage oscillations, may cause issues if the grid is weak and has a high voltage sensitivity. Therefore, the grid strength and converter speed will influence dynamic response and grid stability. New control mechanisms are needed to prevent the system from collapsing when power converter penetration increases [55].



1.2 Current state of wind energy production

The year 2020 was the strongest year for the wind energy sector, with a 53% year-over-year gain. Despite the interruptions caused by the pandemic, 93 GW of additional capacity was added to the network, demonstrating the wind power industry's resiliency [10]. Wind-generated almost 1600 TWh of power in 2020, accounting for more than 5% of global electricity and 2% of total energy consumption. With over 100 GW added in 2020, primarily in China, global installed wind power capacity surpassed 730 GW [32]. Analysts think it should increase far quicker - by more than 1% of power output each year - to help fulfill Paris Agreement commitments to reduce climate change [14]. However, as seen in Fig. 2, this goal has yet to be met, and growth is less than 1%.

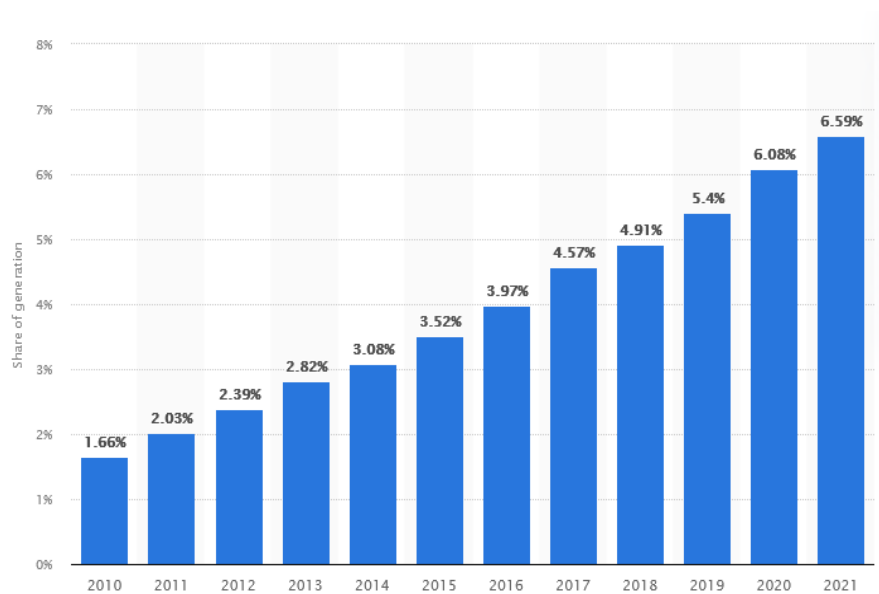


Figure 2: Global wind energy share in electricity mix 2021 [35]

It is important to note that onshore wind farms are now more common than offshore ones, although developed nations have a strong desire to expand offshore [70]. The constancy of the wind over the oceans and sea compared to onshore winds makes offshore wind farms more efficient in addition to the reason that these wind farms are far from humans so environmental concerns will be reduced significantly. The issue is offshore wind turbines are more expensive compared to onshore farms but by developing the technology and higher generation capacity of offshore turbines due to the abundance of wind over the sea, the economical barriers can be compensated and in the future offshore farms can be the most implemented wind farms [16].

Wind turbine Type IV is the most commonly used offshore wind turbine due to its capabilities, such as variable speed, high efficiency, and the absence of a gearbox and brushes in the case of a permanent magnet rotor, which minimizes maintenance, as well as the full-scale converter, which can completely decouple the machine from the grid. Because of the aforementioned reasons, wind turbine Type IV was investigated in this study.



1.3 Power system challenges with high penetration of renewable energy

Different future scenarios of electrical generation in Europe have been taken into consideration in the Ten-Year Network Development Plan of the European Network of Transmission System Operators for Electricity, or ENTSO-E. According to a 2018 assessment, renewable energy sources will likely provide 50% or possibly more of all demand until 2030 and up to 80% by 2040. It is noteworthy that they forecast that by 2030, installed wind capacity in Europe will double or triple from what it was in 2014 [57].

As further renewable with power converters join the network, various concerns arise owing to the nature of power converters vs synchronous generators, which are more focused on system stability. Some of these issues will be addressed.

- Frequency stability:

Replacing traditional synchronous generators with power converters entails swapping out massive rotating shafts for quick power electronics. Those heavy rotational rotors provide a high value of inertia, which greatly aids grid stability during faults or overload conditions [45]; even so, with power converters, this characteristic does not exist in real life; however, by adding virtual inertia or fast frequency response, the problem can be mitigated.

- Voltage stability:

Based on the ability to produce an angle while adjusting the voltage and injecting power, synchronous generators are typically regarded as PV buses in power system analyses. As power converter deployment increases, which they are expected to continue to do so, converters are regarded as PQ buses in power systems with grid-following control structures; hence, for conversion to PV bus characteristics, their control structure must be grid-forming. In grid-forming, the converter has the ability to generate its own voltage and angle, connect to weak grids or operate alone, and perform black-start, which is important [55].



1.4 Objectives

The objectives of this project are to comprehend the modeling of Type IV wind turbines, design and comprehend various control strategies, such as grid-following and grid-forming, research and model Type IV wind turbines with grid-following and grid-forming control, simulate and analyze Type IV wind turbine grid-following and grid-forming control in an IEEE 9-bus system, and build a Python tool that reads data from PSSE and sends it to PSCAD.

1.5 Scope of the project

- Investigating the Type IV wind turbine in detail.
- Analysis of the Grid-following and Grid-forming control structures.
- Performing simulation of the wind Type IV with Grid-following control in Simulink.
- Performing simulation of the wind Type IV with Grid-following and Grid-forming control in PSCAD.
- Analysis of the IEEE 9-bus system with Grid-following converter.
- Analysis of the IEEE 9-bus system with Grid-following and Grid-forming converters.



2 Wind energy technology

2.1 Wind origin

In its simplest form, the wind is just a large volume of air moving in one direction. It starts because of variations in air pressure and temperature. Sunlight is the reason for these variations. Some areas of the Earth's surface are heated by solar radiation more than others because of the way the planet spins. Hot regions cause air to lift and expand, creating low pressure underneath. High pressure is produced when the air cools and falls in cold locations. The wind is created when high-pressure air rushes into a low-pressure region [59].

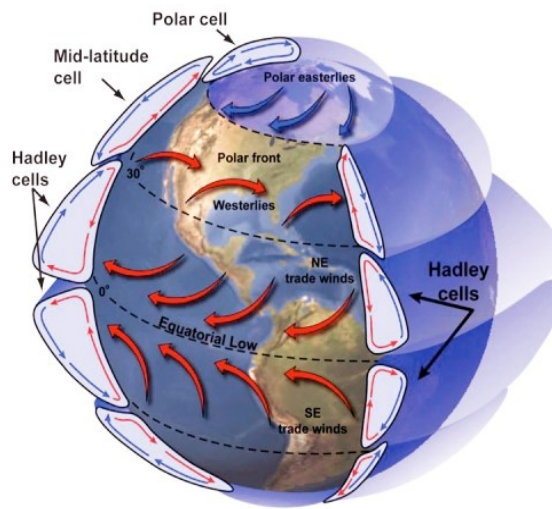


Figure 3: Global winds [24]

Climate-affecting global wind patterns are created by similar factors. The equator, for example, is usually hot. High above the ground, air rises here and spreads north and south. Air is drawn in from the north and south at a lower altitude. Because of the Coriolis effect, which is a result of the Earth's rotation, moving air masses curve, causing the winds that converge on the Equator to originate from the northeast in the Northern Hemisphere and the southeast in the Southern Hemisphere, respectively. These winds are termed the trade winds.

The surface winds attempt to blow toward the poles farther away from the equator, but the Coriolis force bends them in the other direction, producing westerlies. Cold surface winds attempt to blow toward the equator at latitudes higher than around 60°, but, like the trade winds, they are deflected by the Coriolis effect, creating polar easterlies [65].

2.2 Wind energy potential

Understanding the characteristics of the wind resource is essential for all aspects of utilizing wind energy, from finding suitable locations and determining the economic viability of wind farm projects to designing the wind turbines themselves and comprehending their impact on electricity distribution networks and consumers [12].



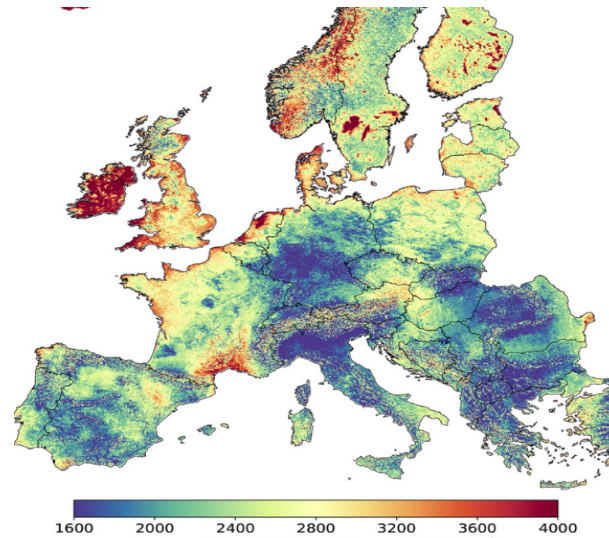


Figure 4: Onshore wind full load hours[kwh kw⁻¹][6]

Wind energy is the kinetic energy of air in motion. The total amount of wind energy passing over a hypothetical surface of size A at time t is [62]:

$$E = \frac{1}{2}mv^2 = \frac{1}{2}(A_{vt}\rho)v^2 = \frac{1}{2}At\rho v^3 \quad (1)$$

Where ρ is the density of air, v is the wind speed, A_{vt} is the volume of air flowing through A (which is assumed perpendicular to the wind direction), and $A_{vt}\rho$ is therefore the mass m flowing through A [62].

$$P = \frac{E}{t} = \frac{1}{2}A\rho v^3 \quad (2)$$

Thus, the available power rises eight times when the wind speed doubles. Wind power in an open airflow is related to the third power of the wind speed.

2.3 Wind turbine fundamentals

A wind turbine is a machine that uses the wind's kinetic energy to generate electricity. The wind must slow down by losing part of its kinetic energy, but only the air that passes through the rotor disc is impacted. A boundary surface can be drawn that contains the affected air mass, and this boundary can be extended upstream and downstream to form a long stream tube with a circular cross-section. This is presuming that the affected air mass remains distinct from the air that does not pass through the rotor disc and does not slow down. The mass flow rate of the air moving down the stream tube will be the same at all stream-wise points along the stream tube since there is no airflow over the boundary. The cross-sectional area of the stream tube must increase to make room for the slower-flowing air because the air inside the stream tube slows down without becoming squeezed as can be seen in Fig. 5.

A quick step change in velocity is not conceivable nor desired because of the large accelerations and forces it would need, even though kinetic energy is collected from the airflow. However, pressure energy may be extracted step-wise, and all wind turbines, regardless of their design, work this way. Upstream air is gradually slowed down by the turbine's presence such that by the time it reaches the rotor disc, its velocity has already fallen below that of the free-stream



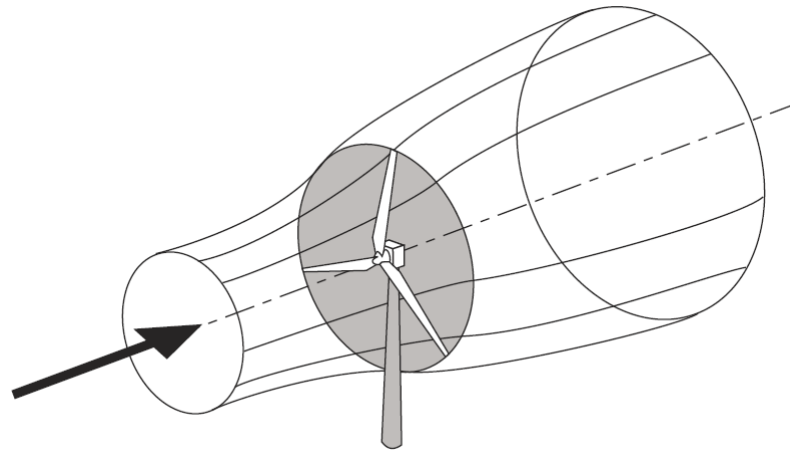


Figure 5: The energy extracting stream-tube of a wind turbine [12]

wind. Because the air has not yet been worked on or by the slowdown, its static pressure rises to soak up the loss of kinetic energy. The stream tube expands as a consequence of the slowing.

By design, there is a static pressure decrease as the air moves through the rotor disc, causing the air to exit below atmospheric pressure. After that, the air moves downstream at a slower, static pressure. For equilibrium to occur, the static pressure in the wake must eventually, far downstream, restore to atmospheric pressure. The increase in static pressure results in a loss of kinetic energy, which further slows the wind. As a result, there is no difference in static pressure between the far upstream and far wake situations, but there is a decrease in kinetic energy [12].

2.4 Power coefficient

The wind power sector frequently uses a metric of wind turbine efficiency called the Power Coefficient (C_p) is the ratio of a wind turbine's actual electric power output to the total wind power entering the turbine blades at a given wind speed. In this sense, the power coefficient refers to the efficiency of all the components that make up a wind power system, such as the generator, power electronics, shaft bearings, and turbine blades.

$$c_p = \frac{P_e}{P_w} \quad (3)$$

The c_p of a certain wind turbine changes depending on factors like wind speed, pitch angle, rotation speed, and other factors. It is a measurement of the total system effectiveness of a certain wind turbine. It should not be compared to or confused with the capacity factor for wind energy [62]. The expression that is used to compute c_p is [2]:

$$c_p(\lambda, \theta_{pitch}) = c_1 \left(\frac{c_2}{\Lambda} - c_3 \theta_{pitch} - c_4 \theta_{pitch}^{c_5} - c_6 \right) e^{-c_7 \frac{1}{\lambda}} \quad (4)$$

$$\Lambda = \left[\left(\frac{1}{\lambda + c_8 \theta} \right) - \left(\frac{c_9}{\theta^3 + 1} \right) \right]^{-1} \quad (5)$$



2.4.1 Betz's law

A wind turbine cannot convert more than 16/27 (59.3%) of the kinetic energy of the wind into mechanical energy spinning a rotor, according to German scientist Albert Betz, who came to this conclusion in 1919. This is still referred to as the Betz Limit or the Betz' Law and it can be deduced as follows:

According to (1) which illustrates the wind power based on kinetic energy [11],

$$\begin{aligned}
 P &= \frac{1}{2}m(v_1^2 - v_2^2) \\
 P &= \frac{1}{2}A\rho v(v_1^2 - v_2^2) \\
 P &= \frac{1}{4}A\rho(v_1 + v_2)(v_1^2 + v_2^2) \\
 P &= \frac{1}{4}A\rho v_1^3 \left(1 - \left(\frac{v_2}{v_1}\right)^2 + \left(\frac{v_2}{v_1}\right) - \left(\frac{v_2}{v_1}\right)^3\right)
 \end{aligned} \tag{6}$$

By obtaining the derivative of P respect to $\frac{v_2}{v_1}$ at a certain speed and area, it can be concluded that maximum power may be acquired when $\frac{v_2}{v_1} = \frac{1}{3}$, Then by substituting in (2) [11],

$$\begin{aligned}
 P_{max} &= \frac{16}{27} \frac{1}{2} A \rho v^3 \\
 P &= c_p \frac{1}{2} A \rho v^3
 \end{aligned} \tag{7}$$

This restriction stems from the inherent limitations of wind turbines rather than inefficiencies in the generator. A wind turbine would need to block 100% of the wind to be 100% efficient; but, in that case, the rotor would have to be a solid disk, which would prevent it from turning and prevent any kinetic energy from being transferred. On the other hand, in the case of a wind turbine with a single rotor blade, the majority of the wind flowing through the region the blade sweeps would totally miss the blade, allowing the wind to retain the kinetic energy.

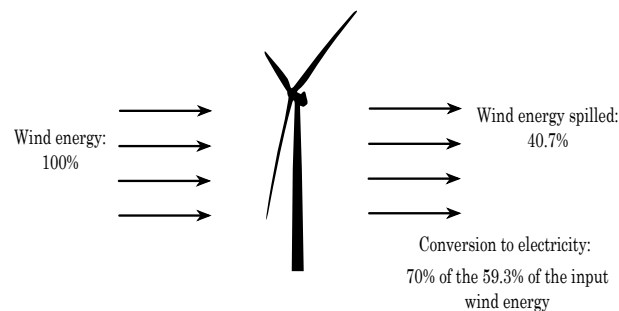


Figure 6: Betz limit [37]

The theoretical maximum power efficiency of any wind turbine design is 0.59, meaning that a wind turbine can only capture up to 59% of the energy delivered by the wind. The real-world limit is significantly below the Betz Limit after the engineering specifications for a wind turbine are taken into account, with values of 0.35 to 0.45 being typical even in the best-designed wind turbines. Only 10 to 30 percent of the wind's power is ever truly turned into usable energy when additional inefficiencies in the entire wind turbine system are taken into consideration, such as those in the generator, bearings, power transmission, and other components [37],[43].



2.4.2 Aerodynamic lift force

The force that defies gravity is called lift [29]. All wind speeds instantly provide lift force at the moment of wind impact, which also happens to be the moment the rotor begins to revolve. It is crucial to maximizing aerodynamic lift using suitable design since it is the force that determines how much power the turbine will produce [52]. According to the configuration of the rotational axis on the horizontal axis and vertical axis turbines, wind turbines that use aerodynamic lift may be classified as either working with lift force or drag force [5]. A response force known as thrust is produced by the lift produced at the rotating blades and it works to counteract the oncoming wind [21].

The forces acting on the turbine depend on both the local relative airspeed and the angle of attack of the turbine. The assumption is that the blades are stiff and quickly aroused by air to change the angle of attack. By changing angles normally to the wind direction, it is possible to create aerodynamic lift. The angle of attack (AoA) generates the most lift in this situation. The angle of attack is controlled by adjusting the blade pitch, which enhances the lift [18]. According to Betz's law, the relative speed at which air impacts a lift-driven rotor's blade (V) depends on the blade's speed at the radius in question and about two-thirds of the wind speed [52]. According to the (7), the lift force is also a function of dynamic pressure, surface area, and lift coefficient [12].

$$F_L = \left(\frac{1}{2}\rho A_L V^2\right)C_L \quad (8)$$

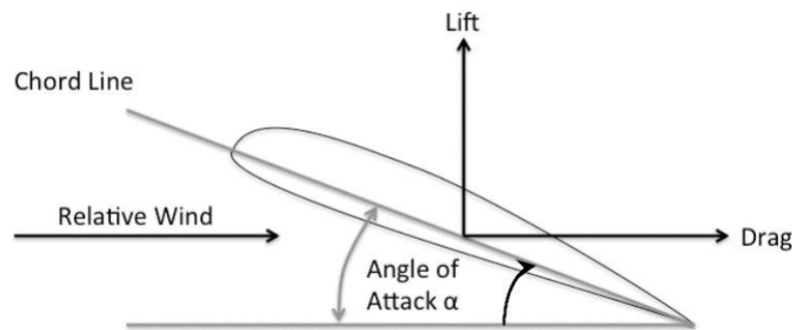


Figure 7: Lift and drag force of wind turbine [56]

Due to the fact that the blades absorb the wind's energy according to Bernoulli's principle in order to attain the lift because of the air pressure difference. The lift factor is stated as [12]:

$$C_L = \frac{F_L}{\frac{1}{2}\rho A_L V^2} \quad (9)$$

As the angle of attack on the rotor blade increases, lift forces will also rise. Beyond 2.2° , the angle of attack falls and the lift-drag ratio decreases [18] this implies that at every rotor speed, the relative wind velocity is unchanged [52]. That is to say, an increase in turbine speed results in an increase in the turbine's lift. On the other hand, a slower-moving turbine produces less lift.



2.4.3 Restrictions on power

Once wind speed exceeds the wind turbine's rated speed, the most popular method for changing the aerodynamic thrust is pitch angle control. Other controlling factors include wind speed, generator speed, and generator power. The efficiency of the turbine will be greatly improved in low wind speeds below the defined value if the speed controller is able to hold the tip speed ratio constant at the level that provides the greatest power coefficient.

When the rotating speed is maintained constant and the wind speed exceeds the rated velocity, pitch angle correction is necessary. Small adjustments to pitch angle can have a significant impact on power output [68]. The following might be used to explain the pitch angle control's objective:

- Optimizing the wind turbine's power production. For the greatest power, the pitch setting should be at its highest value when the wind speed is below the rating.
- Avoiding surpassing the design limitations with regard to input mechanical power. Pitch angle control offers a highly efficient way to manage the aerodynamic power and loads generated by the rotor over the rated wind speed.
- Reducing the mechanical component of the turbine's fatigue stresses. It is obvious that the stresses the turbine experiences may be significantly impacted by the way the control system behaves. The influence on loads must be considered in the controller's design, and the controller should make sure that the control action won't lead to excessive loads. Beyond this, it is feasible to explicitly include the reduction of certain fatigue loads as an extra target when designing the controller.

The Fig. 8 depicts the usual power control zones of a wind turbine. When the wind speed is greater than the cut-in wind speed, the turbine starts to rotate. With increased wind speed, the turbine can produce more electricity. The producing power reaches the rated power of the turbine at the predetermined wind speed. The generator output power remains constant at the design limit as long as the wind speed increases. The turbine is turned off for safety reasons when the wind speed exceeds the cut-out wind speed [68].

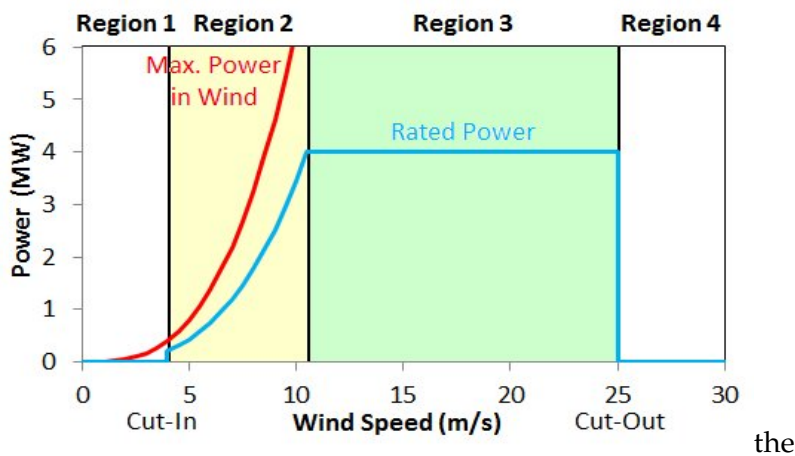


Figure 8: Power control regions of wind turbine [17]



2.5 Types of wind turbine

2.5.1 Wind turbine Type I

The fixed-speed wind turbine using a directly grid-coupled squirrel-cage induction generator (SCIG) is one of the wind turbine ideas, as depicted in the figure below. The rotor shafts of the high-speed induction generator and the low-speed wind turbine are connected by a gearbox. Only a small range of rotating speeds above the synchronous rotational velocity can be tolerated in this wind turbine design. These minuscule fluctuations in rotational speed are what lead this Type of wind turbine to be regarded as operating at a constant speed. Due to the reactive power consumption of the SCIG, compensating capacitors are typically used for reactive compensation and to enhance the power factor [50].

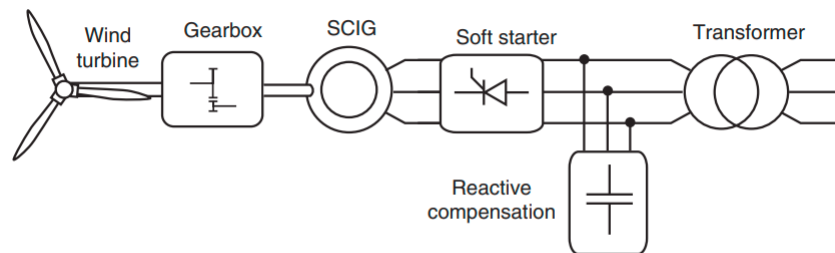


Figure 9: Wind turbine Type I [31]

Durability and ease of control are two main benefits of this Type of wind turbine, however since it must operate continuously at a constant speed, there will be considerable mechanical stress alongside the necessity of a soft starter, to mention it won't be able to sustain the grid during faults [25].

2.5.2 Wind turbine Type II

The wound rotor induction generator that powers the limited variable speed wind turbine, as seen in the following figure, is connected directly to the grid. A soft starting ensures a smooth grid connection, and certain capacitor banks offer reactive power adjustment. The rotor windings are also linked to a set of three-phase external resistors, a three-phase diode bridge, and an IGBT switch.

With this configuration, the generator speed may only vary by 0 to 10% above synchronous speed. As a result, the term "limited variable speed wind turbine" refers to a wind turbine with an induction generator and variable rotor resistance. By adjusting the IGBT switches, the effective value of the rotor resistance may be controlled. Then, by adjusting the rotor resistance, the rotor current and, consequently, the rotor speed, will be managed [51].



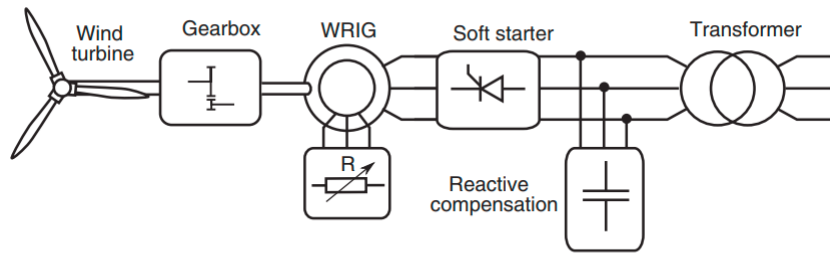


Figure 10: Wind turbine Type II [31]

2.5.3 Wind turbine Type III

According to Fig. 11, a Type III wind turbine uses doubly-fed induction generators (DFIGs), the stator windings of which are connected directly to the power grid, and the rotor windings, which are connected to the grid via a back-to-back voltage source converter (VSC) made up of a machine side converter (MSC) and grid side converter (GSC). By adjusting the rotor position, the MSC controls active and reactive power, while the GSC guarantees a steady voltage across the DC link. Due to its tiny size, the DC-link is often not utilized to absorb extra energy from the machine side or inject energy into the grid side to restore voltage levels. Instead, it is used to temporarily store energy for switching occasions. About 40% of the overall power output normally passes through the converter [69].

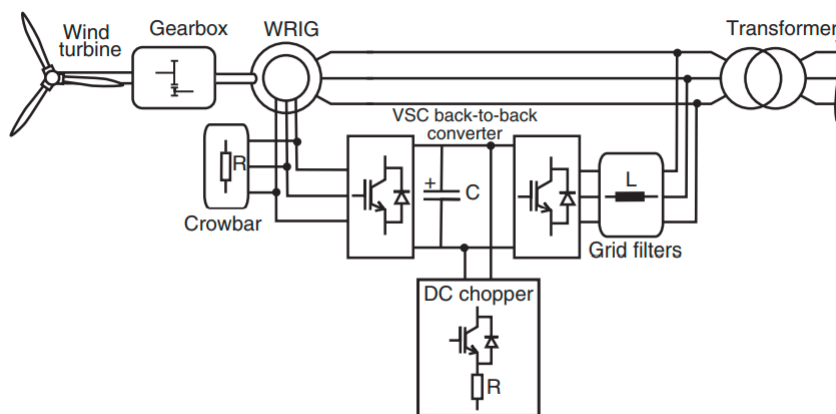


Figure 11: Wind turbine Type III [31]

2.5.4 Wind turbine Type IV

The Type IV wind turbine is the most sophisticated one, consisting of a generator (either an induction generator (IG) or a synchronous generator (SG)) linked to the grid through a full converter. It has superior fault ride-through capabilities than Type III since it is totally disconnected from the grid. However, losses will be greater with Type IV since all current flows through the



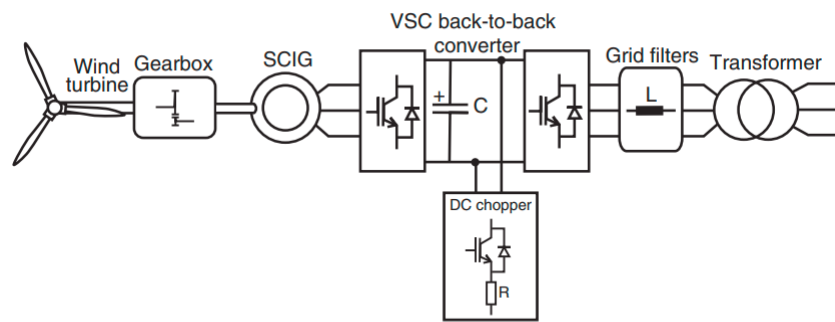


Figure 12: Wind turbine Type IV [31]

converter, necessitating higher ratings and hence larger switching and conduction losses. The MSC, like Type III, modulates the rotating speed, while the GSC attempts to minimize reactive power use while delivering active electricity to the grid. Currently, the SG may be implemented using either a wound rotor or a permanent-magnet configuration.

This Type is more widely utilized due to the capacity of permanent-magnet synchronous generators (PMSG) to self-excite, which results in a high power factor and efficiency. Another benefit is that the gearbox can be removed with a PMSG, allowing it to go from a gearbox-driven to a direct-driven WT. Because the gearbox is one of the components of a WT that needs frequent maintenance, this improves operational dependability. The primary disadvantage of a full-converter is that all current passes through it, which can be a concern in terms of protection if subjected to transients. It is also more expensive owing to the requirement of a full power converter [69]. Table 1 illustrates a brief comparison between different Types of wind turbines.



Table 1: Comparison between different Types of wind turbine [36]

<i>Indices</i>	TypeI	TypeII	TypeIII	TypeIV
WT concept	Fixed Speed	Limited Variable Speed	Variable Speed	Variable Speed
Generator	(SCIG)	(WRSG)	(DFIG)	WRSG PMSG
Grid connection	Direct, Soft starter and capacitor bank are required	Direct, Soft starter and capacitor bank are required	Partial scale converter	Full-scale converter
Drive train	Gearbox	Gearbox	Gearbox	Gearbox Gearless
Speed range	~2% Slip	~10% Slip	+30% -30% Slip	(0-1)Nrated
Blade angle control	Stall/Active Pitch control	Stall/Active Pitch control	Pitch control	Pitch control
Pros	Low cost Robustness Simple control	Low cost Better performance than TypeI	Ride-through capability, Active&reactive control	Gearless(PMSG) High efficiency
cons	Constant speed High stress No grid support	Slip rings Power loss No grid support	Slip rings Complex control	High cost Complex design

2.6 Grid stability

The short circuit ratio (SCR) or SCC is typically used to measure system strength. SCR measures how much power the system can supply during failures in relation to the associated element's rating, while SCC measures how much power it can supply overall, the SCR equation is as follows:

$$SCR = \frac{SCP}{P_n} \quad (10)$$

Where SCP in (10) is short circuit power and P_n is the nominal power. A high voltage level and a low Thevenin grid impedance are often correlated with a high fault current ratio compared to load current, or rather, a high SCR. If the grid's Thevenin impedance is low, a bigger change in grid current is required to change the voltage at the generation terminal. A highly powerful system normally has an SCR of 10, whereas a very weak system has an SCR of 1 [30].

2.7 The swing equation and inertia

The swing equation defines the dynamics of the machine's rotor during acceleration and deceleration. The inertial response is defined as the power exchange between the machine's rotor and the grid. The rotor motion is determined by the [26]:

$$J \frac{d^2 \theta_m}{dt} = T_m - T_e = T_a (N.m) \quad (11)$$



Where J is the total moment of inertia, θ_m is the angular position of the rotor, T_m and T_e are mechanical and electrical torque respectively and finally T_a is the total accelerating torque. It can be noted that when T_a is equal to zero electrical and mechanical torque have the same values and the machine is in a steady state. The angular rotor position θ_m in qd frame is [26]:

$$\theta_m = \omega_s t + \delta \quad (12)$$

Where ω_s is the machine synchronous speed and δ is the rotor's angle of variation from the reference axis that rotates synchronously, expressed in mechanical radians. The derivatives of (12) are [26]:

$$\frac{d\theta_m}{dt} = \omega_{sm} + \frac{d\delta_m}{dt} \quad (13)$$

$$\frac{d^2\theta_m}{dt^2} = \frac{d^2\delta_m}{dt^2} \quad (14)$$

Substituting (14) in (11), will provide [26]:

$$J \frac{d^2\delta_m}{dt^2} = T_a = T_m - T_e (N.m) \quad (15)$$

And by taking into consideration of machine rotational speed as [26]:

$$\omega_m = \frac{d\theta_m}{dt} \quad (16)$$

By taking into account, torque times machine rotational speed equals power, so the product of (15) and (16) will be [26]:

$$J \omega_m \frac{d^2\delta_m}{dt^2} = P_a = P_m - P_e (W) \quad (17)$$

where P_m and P_e representing mechanical and electrical power while P_a is the accelerating power of the machine. Following is the inertia constant [26]:

$$H = \frac{E}{M_p} = \frac{J \omega_s^2}{2 S_{rated}} \quad (18)$$

Where E represents the stored kinetic energy and M_p is the machine rating power. By substituting (18) into (15) following equation is obtained [26]:

$$2H \frac{S_{rated}}{\omega_s^2} \omega_r \frac{d^2\delta}{dt^2} = P_m - P_e = P_a \quad (19)$$

Further, by assuming steady-state conditions, ω_r may be replaced by ω_s because the machine's angular speed and synchronous speed are the same. So, the ultimate swing equation is as follows [26]:

$$\frac{2H}{\omega_s} \frac{d^2\delta}{dt^2} = P_m - P_e = P_a \quad (20)$$

The essential equation that controls the rotational dynamics of the synchronous machine in stability studies is (20), sometimes referred to as the swing equation of the machine.



2.8 Permanent magnet synchronous machine (PMSG)

The efficiency of the permanent-magnet machine (PMSG) is better compared to the induction machine since excitation is produced without any energy source. Because of their high efficiency and power factor, numerous studies have advised that this kind be employed in off-shore wind turbines; nevertheless, the materials used to build PMSG are costly. In addition, a full-scale converter is required in conjunction with the PMSG to adapt the frequency and voltage of generation to the point of grid connection, which is an additional expenditure, although the gearbox, which is one of the major causes of failures, can be eliminated and power can be injected at any speed [38]. The rotor of PMSGs is equipped with a permanent-magnet pole system and has a winding stator. It can also have salient poles or be cylindrical. Salient poles may be the most practical variant for a wind generator application since they are more prevalent in slow-speed machines. The PMSG's synchronous nature might lead to issues with voltage management, synchronization, and start-up. When there is an external short circuit or an unstable wind speed, the synchronous operation also results in highly stiff performance. The fact that magnetic materials are temperature-sensitive and can lose their magnetic properties at high temperatures is another drawback of PMSGs (e.g. during a fault). Therefore, a cooling system may be needed and the rotor temperature of a PMSG must be monitored [2].

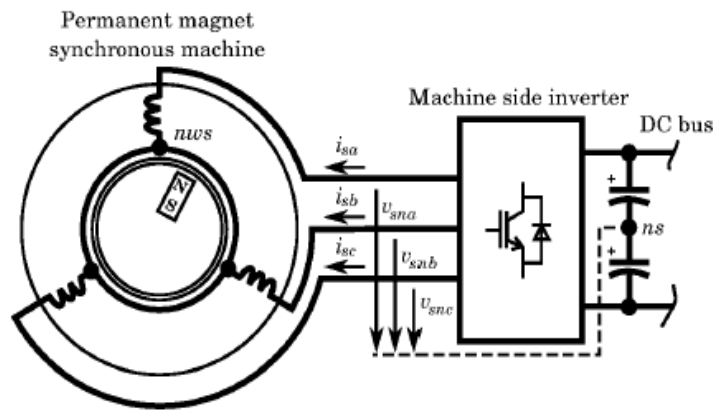


Figure 13: Details of PMSG connection for a Y configuration without neutral conductor [38]

Relation between voltage and current in PMSG can be written as [38]:

$$v_s^{abc} = r_s i_s^{abc} + \frac{d}{dt} \lambda_s^{abc} \quad (21)$$

Where v_s^{abc} is the stator voltage vector, i_s^{abc} is the stator current vector, λ_s^{abc} is the stator flux linkage vector and r_s is resistance of stator only for one phase. For sake of modeling the magnetic circuit, the saturation nonlinearities will be disregarded in this case. However, even while machines with surface-mounted magnets may also be thought of as having inductances that are independent of rotor position, a more general situation must be taken into account to accurately simulate the behavior of a machine with buried magnets. In such a model, the inductances are taken into account as the following function of the predicted rotor angle [38]:

$$\lambda_s^{abc} = ([L_1] + [L_2(\theta_r)]) i_s^{abc} + \lambda_m \begin{bmatrix} \sin(\theta_r) \\ \sin(\theta_r - \frac{2\pi}{3}) \\ \sin(\theta_r + \frac{2\pi}{3}) \end{bmatrix} \quad (22)$$



with:

$$[L_1] = \begin{bmatrix} L_{ls} + L_A & -\frac{1}{2}L_A & -\frac{1}{2}L_A \\ -\frac{1}{2}L_A & L_{ls} + L_A & -\frac{1}{2}L_A \\ -\frac{1}{2}L_A & -\frac{1}{2}L_A & L_{ls} + L_A \end{bmatrix} \quad (23)$$

and:

$$[L_{2\theta_r}] = -L_B \begin{bmatrix} \cos(2\theta_r) & \cos(2\theta_r - \frac{\pi}{3}) & \cos(2\theta_r + \frac{\pi}{3}) \\ \cos(2\theta_r - \frac{\pi}{3}) & \cos(2\theta_r + \frac{\pi}{3}) & \cos(2\theta_r) \\ \cos(2\theta_r + \frac{\pi}{3}) & \cos(2\theta_r) & \cos(2\theta_r - \frac{\pi}{3}) \end{bmatrix} \quad (24)$$

Where λ_m is machine flux linkage and L_A is an inductance quantity that is independent of the position of the rotor. L_B is the maximum inductance value for a condition whose value varies with rotor position. It should be noted that for salient pole magnets, L_B is about zero. The machine voltage can be rewritten as [38]:

$$v_s^{abc} = (r_s[I_3] + \omega_r \frac{d}{d\theta_r} [L_2(\theta_r)]) i_s^{abc} + ([L_1] + [L_2(\theta_r)] \frac{d}{dt}) i_s^{abc} + \lambda_m \omega_r \begin{bmatrix} \cos(\theta_r) \\ \cos(\theta_r - \frac{2\pi}{3}) \\ \cos(\theta_r + \frac{2\pi}{3}) \end{bmatrix} \quad (25)$$

Equation (25), which may be put in qd form to make equations easier to use and simplify calculations, calls for a park transformer, the result by decoupling the zero sequence will be [38]:

$$v_s^{qd} = \begin{bmatrix} r_s & \omega_r(L_{ls} + \frac{3}{2}(L_A + L_B)) \\ -\omega_r(L_{ls} + \frac{3}{2}(L_A + L_B)) & r_s \end{bmatrix} i_s^{qd} + \begin{bmatrix} L_{ls} + \frac{3}{2}(L_A - L_B) & 0 \\ 0 & L_{ls} + \frac{3}{2}(L_A + L_B) \end{bmatrix} + \frac{d}{dt} i_s^{qd} + \lambda_m \omega_r \begin{bmatrix} 1 \\ 0 \\ 0 \end{bmatrix} \quad (26)$$

Because there is no neutral conductor in this situation, the total of the abc currents is zero, hence there is no zero sequence current and just the qd subsystem equations must be addressed. The equation for the generator's torque, on the other hand, may be determined by computing the mechanical power of the generator, P_M , and dividing it by the mechanical speed. To calculate mechanical power, multiply the stator voltage (25) by the rotor voltage, and the terms that do not relate to joule effect losses and power stored in inductors are defined as [38]:

$$P_m = \omega_r \{i_s^{abc}\}^T \frac{d}{d\theta_r} [L_2(\theta_r)] i_s^{abc} + \lambda_m \omega_r \{i_s^{abc}\}^T \begin{bmatrix} \cos(\theta_r) \\ \cos(\theta_r - \frac{2\pi}{3}) \\ \cos(\theta_r + \frac{2\pi}{3}) \end{bmatrix} \quad (27)$$

By applying park transformation to this equation, in terms of the $qd0$ variables, it can be expressed as follows [38]:

$$P_m = \omega_r \{i_s^{abc}\}^T [T_{qd0}^{-1}(\theta)]^T \frac{d}{d\theta_r} [L_2(\theta_r)] [T_{qd0}^{-1}(\theta)] i_s^{qd0} + \lambda_m \omega_r \{i_s^{abc}\}^T [T_{qd0}^{-1}(\theta)]^T \begin{bmatrix} \cos(\theta_r) \\ \cos(\theta_r - \frac{2\pi}{3}) \\ \cos(\theta_r + \frac{2\pi}{3}) \end{bmatrix} \quad (28)$$



Then P_m will be [38]:

$$P_m = \omega_r \{i_s^{abc}\}^T \begin{bmatrix} \frac{3}{2} 3LB \cos 2(\theta_r - \theta - \frac{\pi}{2}) & \frac{3}{2} 3LB \cos 2(\theta_r - \theta) & 0 \\ \frac{3}{2} 3LB \cos 2(\theta_r - \theta) & -\frac{3}{2} 3LB \cos 2(\theta_r - \theta - \frac{\pi}{2}) & 0 \\ 0 & 0 & 0 \end{bmatrix} i_s^{qd0} + \lambda_m \omega_r \{i_s^{abc}\}^T \begin{bmatrix} \cos(\theta_r - \theta) \\ -\sin(\theta_r - \theta) \\ 0 \end{bmatrix} \quad (29)$$

This may be simplified further by defining the stator flux as [38]:

$$P_m = \frac{3}{2} \omega_r (\lambda_s i_{sq} - \lambda_s i_{sd}) \quad (30)$$

where :

$$\lambda_s^{qd0} = \begin{bmatrix} L_{ls} + \frac{3}{2} L_A - \frac{3}{2} L_B \cos 2(\theta_r - \theta) & \frac{3}{2} L_B \cos 2(\theta_r - \theta - \frac{\pi}{4}) & 0 \\ \frac{3}{2} L_B \cos 2(\theta_r - \theta - \frac{\pi}{4}) & L_{ls} + \frac{3}{2} L_A + \frac{3}{2} L_B \cos 2(\theta_r - \theta) & 0 \\ 0 & 0 & L_{ls} \end{bmatrix} i_s^{qd0} + \lambda_m \begin{bmatrix} \sin(\theta_r - \theta) \\ \cos(\theta_r - \theta) \\ 0 \end{bmatrix} \quad (31)$$

The torque equation is derived by multiplying this equation by the mechanical speed as [38]:

$$T_m = \frac{3}{2} P (\lambda_{sd} i_{sq} - \lambda_{sq} i_{sd}) \quad (32)$$



2.9 Power converters

The power converter circuit, which can adjust the generator's frequency and voltage to the grid, is necessary for some wind turbine types. Converter topologies have been devised in a variety of forms, and each one has advantages and disadvantages. To enhance power quality and increase voltage level, respectively, the majority of the suggested converters need line filters and transformers. The expense of installing and maintaining turbines as well as building towers is greatly increased by these large, heavy components. To reduce the size, weight, and price of power converters, novel structures for converters have been developed as a result of recent developments in power semiconductors and magnetic materials.

2.9.1 Diode rectifier based converter

A controlled inverter is used in this converter system to first convert a variable frequency and variable magnitude AC power from the wind turbine generator to DC power. The DC power is then converted back to AC power at a different frequency and voltage level. Power is transferred in a single direction, like from a generator to the grid, through a converter system based on a diode rectifier (uncontrolled rectifier). Instead of an induction generator, this kind of power converter is typically utilized in wind power production systems using wound rotor synchronous generators (WRSG) or permanent magnet synchronous generators (PMSG). The grid-side inverter in this converter system regulates the active and reactive electricity sent to the grid. This converter system normally produces voltages between 380 and 690 volts [33].

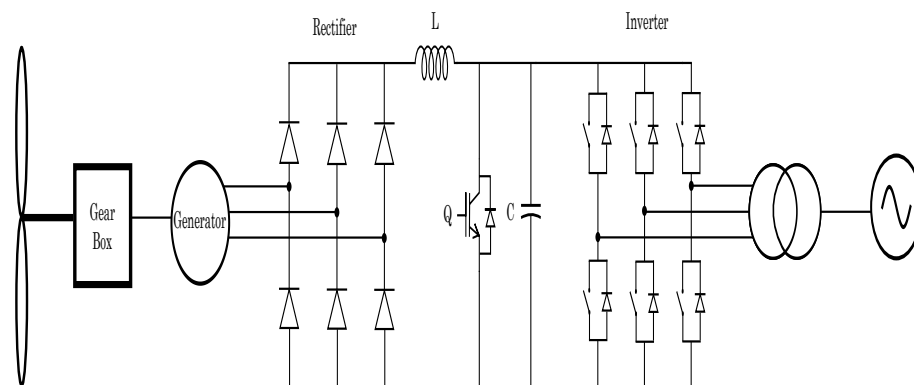


Figure 14: Diode rectifier based converter topology [33]

Advantages:

- Low cost
- Simple design and implementation

Disadvantages:

- Diode rectifiers generate a lot of harmonics which has a negative impact on the system
- Unidirectional power flow



2.9.2 Back to Back converter

Back-to-back converter, consisting of two conventional pulse width modulated (PWM) voltage source inverters, is the name given to the controlled rectifier and controlled inverter-based converter. For the rectification phase, where the controlled rectifier replaces the diode rectifier with a chopper circuit, it varies from the diode rectifier-based converter. The controlled rectifier allows for bidirectional power flow, which is not feasible in a power converter system based on diode rectifiers. Additionally, the controllable rectifier significantly lowers the harmonic losses and input current harmonics. In order to improve the output power quality by lowering total harmonic distortion, the grid side converter controls the active and reactive power flow to the grid and maintains a constant DC-link voltage. The generator side converter functions as a driver, adjusting the generator's optimum rotor speed and magnetization demand. The decoupling capacitor offers independent control capabilities for the two converters by separating the grid side converter from the generator side converter [33]. It may be noted that the average model based on a back-to-back converter was used for the methodology part of this study.

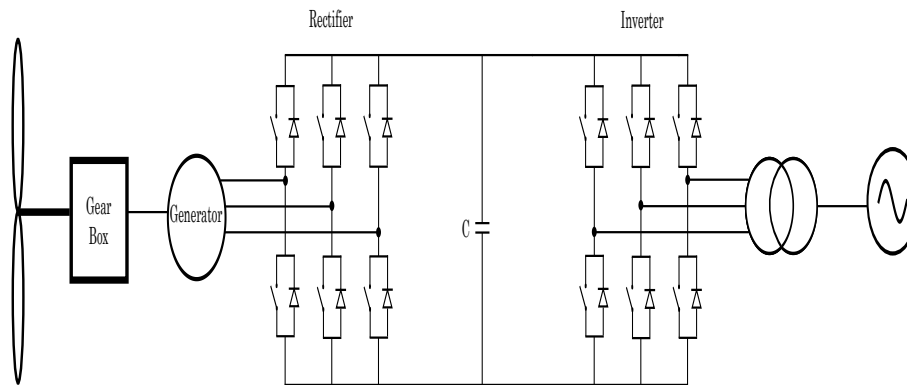


Figure 15: Back to Back converter topology [33]

Advantages:

- Bidirectional power flow
- Fair costs
- To gain full control of the grid current, the DC-link voltage can be increased to a level greater than the amplitude of the grid line-to-line voltage
- The capacitor between the inverter and the rectifier allows the control of the two inverters to be decoupled, allowing for asymmetry correction on both the generator and the grid sides.

Disadvantages:

- The presence of the large and massive DC-link capacitor raises the expenses and shortens the system's total lifetime
- Because the back-to-back converter has two inverters, the switching losses may be much more noticeable



2.10 Control systems of wind turbines

2.10.1 Grid-following versus Grid-forming

Normally, grid following control is used to integrate renewable energy sources into the grid. This kind of control structure works by determining the angle of the grid voltage at the connection point and then creating a current that supplies the appropriate amount of reactive and active power to maintain a stable operation [48]. A phase-locked loop (PLL) accomplishes the measurement and synchronization by locking the output signal to its input such that it matches the frequency and phase of the input signal [8].

In real terms, it means that these converters need "adequate assistance" to deliver a stable voltage to the grid, which is currently done by synchronous machines. Due to the frequency's close relationship to the rotor's rotational speed, synchronous generators are grid-forming apparatuses and may be utilized to supply a frequency reference to the grid under control. Grid-following converters would not work if all synchronous devices were eliminated since the grid would not have any frequency reference. Therefore, certain converters must be able to regulate the voltage. These converters, also known as grid-forming converters, guarantee the voltage waveform of the grid will remain stable even during extremely brief time intervals [3].

A comparison between the above-mentioned topologies are illustrated in Fig. 16. In the grid-following approach, the angle at the point of connection is determined using a PLL, together with active and reactive power, and then the values in the current regulator are compared with references, and the output is computed. In the grid-forming on the other hand, the active and reactive powers are still measured at the point of connection, but the angle is derived from the difference between the reference active power and the measured active power rather than being measured there. Reactive power controller data may be used to compute the voltage magnitude, and the computed angle can be used to determine the reference output voltage of the converter.

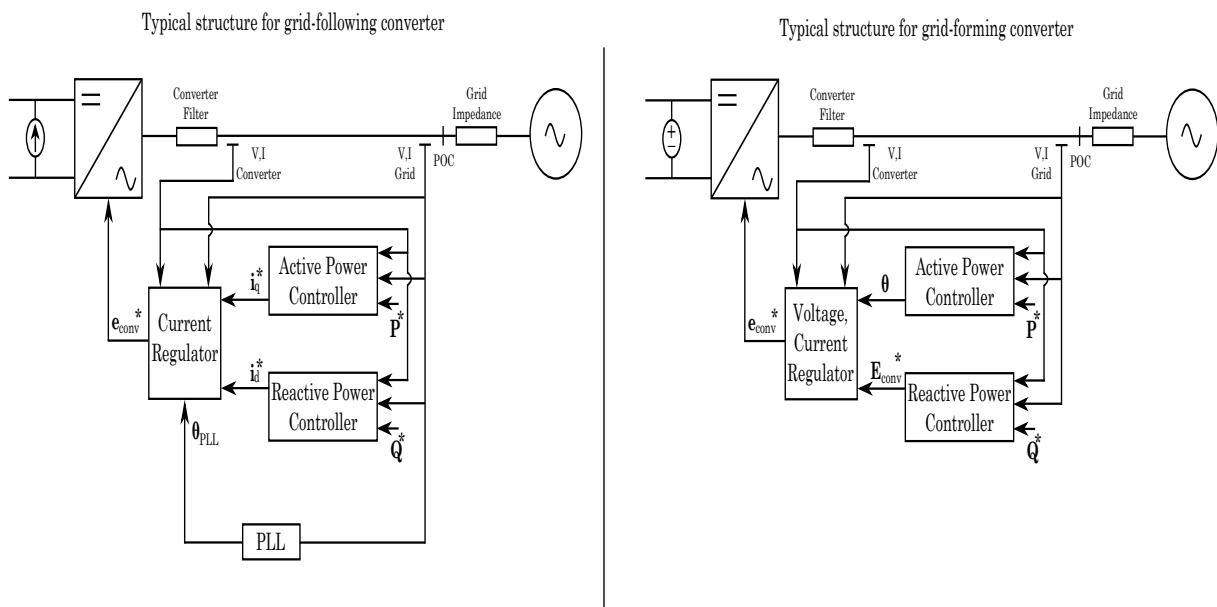


Figure 16: Grid-following (left) vs Grid-forming (right)



Table 2: Key differences between Grid-forming and Grid-following [66]

<i>Type</i>	Grid-forming	Grid-following
Function	Supporting the grid	Following the grid
Source behavior from grid view	Voltage source	Current source
Set grid voltage and frequency	Yes	No
Provide active and reactive power via voltage	Yes	Just P&Q
Response	Slow response due to large inertia	Fast response to the intermittent
Inertial response	Yes	No
Support weak grid operation	Yes	No
Islanding	Yes	No
Fault ride-through	To be improved	Yes

As previously indicated, the switch to grid-forming converters opens the door to new processes. However, grid-following control systems have been demonstrated to be effective for many years, making them superior for particular operational regions. Table 2 lists some of the two control approach features.

Active power must be transferred between the converter and the grid in order to provide virtual inertia in grid-forming. For this to work, the control system must provide enough energy to achieve the necessary inertia. The quantity of energy required depends on the characterization of the inertial response, however, an energy storage device is often necessary to provide adequate energy. Some grid-forming control structures are explained below.

2.10.2 Droop based with cascade control

The Fig. 17 shows the basic operating concept of the conventional power plants, which were mostly equipped with SGs. Quantities f_0 and U_0 are the voltage and frequency nominal values.

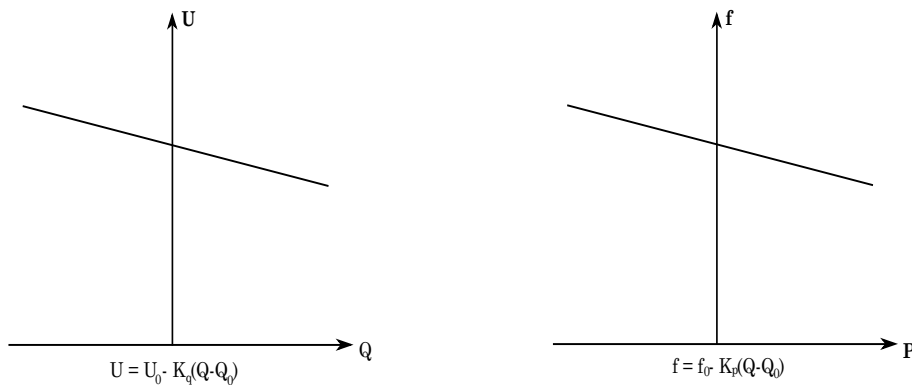


Figure 17: Droop characteristics



The Fig. 17 demonstrates that in synchronous generators, active power and frequency as well as reactive power and voltage have a direct relationship. For example, greater frequency calls for more active power, while higher voltage requires more reactive power. The frequency and Q loop of a grid-forming converter based on droop will attempt to emulate this behavior of an SG. The block diagrams for the frequency and Q loops which may be called outer loops are as follows in Fig. 18. In general, k_p and k_q which are the frequency and voltage drop will be set 5% and 10% respectively [58].

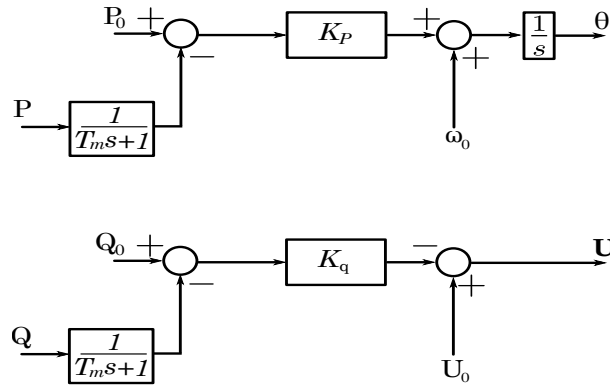


Figure 18: Outer control loops in droop based control [58]

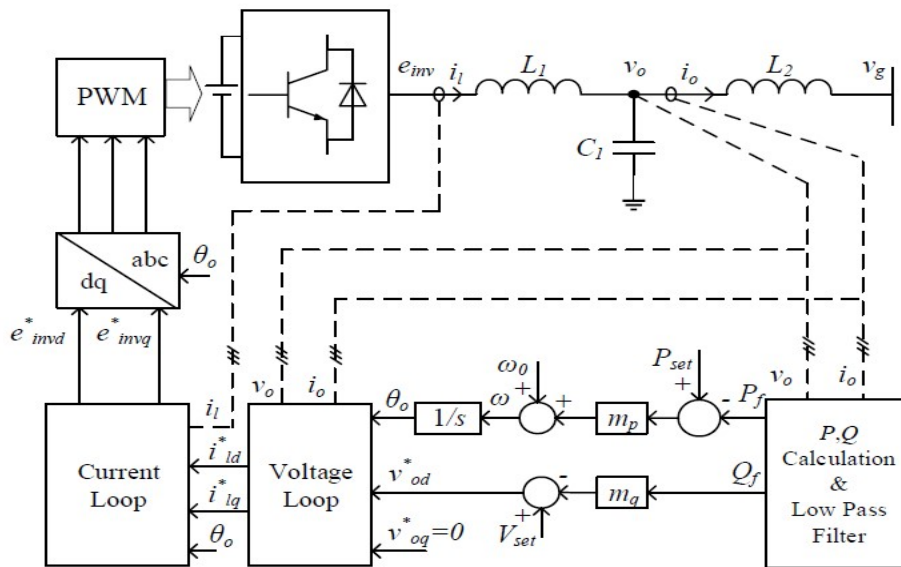


Figure 19: Full scheme of droop based converter with cascade control [19]

Considering Fig. 19, The frequency droop and Q loop, inner voltage control loop and inner current control loop all form a cascaded structure in the controller. Equations (33) and (34) describe how the controller calculates the instantaneous active power P and reactive power Q in the qd rotating reference frame as well as measuring the filter capacitor voltage v_o and output current i_o . Then, the Q loop will supply the voltage reference (v_{0d}^*) to the inner loop, and the output of the frequency droop will give the angle for all of the controller's park and inverse park



transformers [19].

$$P = v_{0d}i_{0d} + v_{0q}i_{0q} \quad (33)$$

$$Q = v_{0d}i_{0q} - v_{0q}i_{0d} \quad (34)$$

The current references in the qd frame for the current control loop are the outputs of the voltage control loop, i_{ld}^* and i_{lq}^* . The internal voltage reference in the qd frame for PWM control is provided by the outputs of the current control loop, e_{invd}^* and e_{invq}^* . Fast control of the inverter filter capacitor voltage is ensured by the inclusion of the extra inner voltage and current loops. If the voltage and current loop parameters are appropriately set, the filter capacitor voltage acts nearly as a controlled voltage source. As a result, the design principle of this control strategy is that it first approximates the inverter filter capacitor voltage to a controllable voltage source via well-tuned voltage and current control loops; then, it regulates the angular frequency and magnitude of the voltage based on the f and Q droops, respectively. The input references for the voltage loop are v_{0d}^* and v_{0q}^* , while the qd frame components of the filter capacitor voltage are v_{0d} and v_{0q} . The proportional and integral gains of the voltage control loop are k_{vp} and k_{vi} , respectively. The qd frame elements of the inner current are i_{ld} and i_{lq} . The proportional and integral gains of the present control loop are k_{ip} and k_{ii} . Fig. 20 shows the inner loop which contains inner voltage and current control loops.

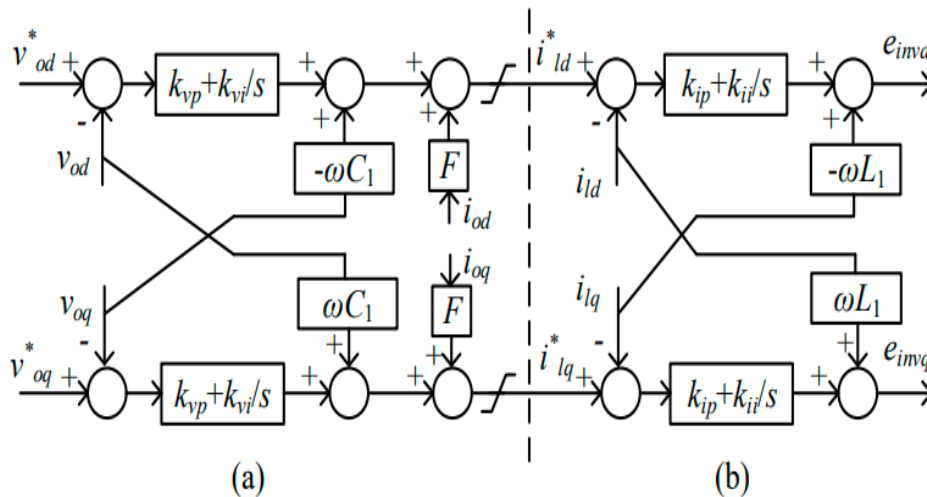


Figure 20: Inner control loops (a) Voltage controller (b) Current controller [19]

2.10.3 Virtual synchronous machine

The issues brought on by converter-connected sources are resolved by virtual inertia (VI)-based converters. VI-based converters go by a variety of names, including synchronverter, virtual synchronous machine, and virtual synchronous generator. Each idea originated from the SM's structure and mathematical model [66]. Although there are slight variations among them all, all of the control approaches promote the notion of running a converter similarly to a synchronous machine [61]. Both the DC-link voltage and the grid frequency may be compared, as well as the capacitance and the moment of inertia. Similar to the spinning inertia of SMs, the DC link capacitor acts as a storage capacity for transient active power fluctuations. As a consequence, when there is an imbalance between the AC power supplied to the network and the input power



from the machine side, the DC-link voltage changes. If there is sufficient energy in the DC-link capacitors, they can supply the short-term power required for inertia emulation. However, in all cases, the DC link balancing power must originate from the device side (wind turbine, battery, solar PV, supercapacitor, etc.) in order to maintain the DC link voltage within the operational ranges required for the converter to function properly. The basis for all VI-based converters is the swing equation (20). By regulating their output power during frequency disturbances, the VI-based converters enable renewable energy sources to take part in frequency regulation. A significant benefit over genuine SGs is the ability to select and modify the operating parameters (such as inertia, field inductance, mutual inductance, and friction coefficient). Three of the most prevalent topologies of VI-based converters will be briefly discussed.

- VSM

VSM is based on synchronous machine emulation, with some minor modifications. The VSM's goal is to enable grid forming using frequency droop and VI. A phase-locked loop (PLL) is commonly utilized for frequency estimation while driving the VI loop [39]. During normal operation, the usage of PLL is avoided. It is because, following PLL startup, VSM may synchronize with the grid based on power balance. Fig. 21 depicts the VSM control hierarchy.

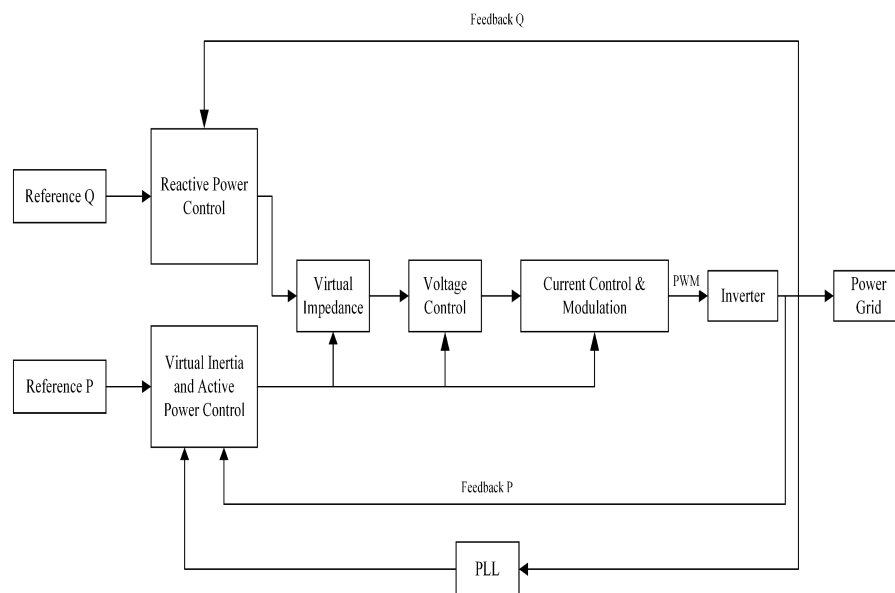


Figure 21: VSM control structure [66]

A mathematical model of an SG based on $qd0$ or synchronous reference frame is used in VSM. It employs the park transformation to change the abc frame into $qd0$ and the inverse park transformation to transform $qd0$ back into abc . In general, the park transformation makes the system more complicated and increases the total execution time. The VSM operation steps are as follows:

- 1-The phase currents of the VSM are computed by measuring the voltages at the point of connection (POC) with the grid.
- 2-The calculated currents are used to regulate a current-controlled converter.
- 3-The inverter is driven by the pulse width modulation (PWM) modulator.



Benefits of this structure include conceptual simplicity, suppression of grid disturbances, and use in stand-alone and micro-grid systems [66]. The PLL's usage, which increases complexity, and the park transformer's prolonged execution time are the drawbacks.

- Virtual synchronous generator

Virtual synchronous generator or VSG is largely built on normal inverter hardware with a controller that emulates an SG's inertial reaction to frequency changes. The VSG control method enables grid-connected converters to create VI [67]. The usage of VSG has gained a lot of interest since it has the same working mechanism as an SG and can provide a feasible scheme for grid-connected renewables [44]. The capacity of the microprocessor to alter VI during frequency change distinguishes VSG from SG. As a result, self-tuning algorithms are essential for varying the VI to reduce frequency fluctuation. Compared to a traditional droop controller that offers frequency regulation alone, VSG provides dynamic frequency control based on the derivative of the frequency measurement. Before establishing a connection to the grid, VSG needs pre-synchronization. Either a typical PLL or a phase angle regulator [41] can carry it out. The VSG control scheme is as Fig. 22.

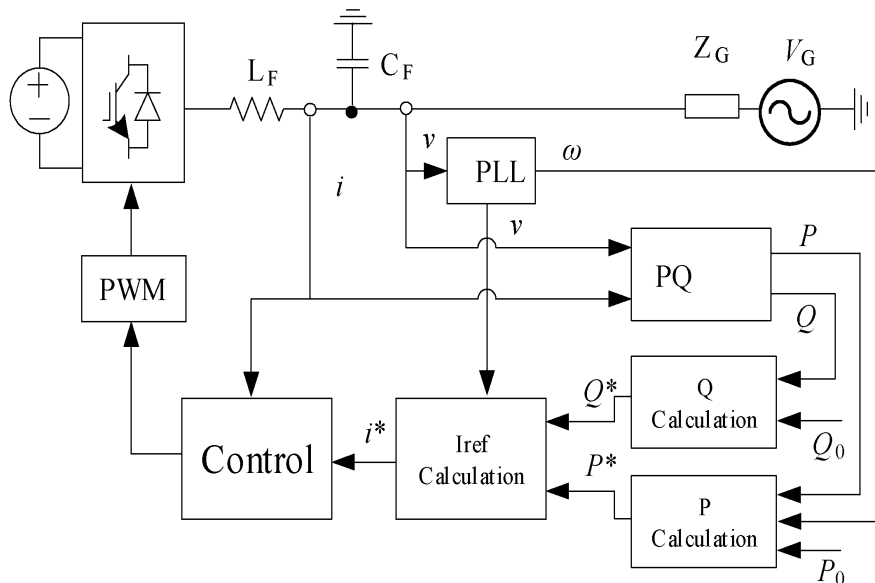


Figure 22: VSG control structure [66]

The general operations of a VSG are the following:

- 1-The processing unit that hosts the VSG algorithm collects a measurement of the grid voltage at the (POC) and sends it.
- 2-The processing unit calculates the stator current of the VSG by using a synchronous machine model.
- 3-Using the estimated reference current as a basis, the current controller sends the gate signal to the inverter (I_{ref}).

Fast reaction in tracking steady-state frequency is one of VSG's benefits. Eddy current losses and magnetic saturation are absent and the simplicity of implementation is as well. To mention a number of negative ones, due to Park Transformation, the execution takes a long time. PLL-



related instability, particularly in weak grids. Because it is not a grid-forming unit, it cannot be used in islanded mode.

- Synchronverter

Similar to VSM, synchronverters are another sort of control that tries to imitate the actions of an SG. This makes it simple to function as a grid-connected device inside the conventional system while providing the capabilities of distributed generation and renewable energy [71], due to the inverter's foundation in the intricate swing equation, the synchronverter has the advantage of inheriting all SG features. The inertia, friction coefficient, and field inductances are only a few of the parameters that may be manipulated freely since an SG is implemented virtually, even if some values are not possible to have in an SG. This increases the adaptability of the system [60].

A voltage controller is required in conjunction with the energy storage to maintain a constant DC-bus voltage. This may be achieved in one of two ways: by modifying the reference power of the synchronverter or by altering the power flow inside the energy storage [71]. There would be difficulties in maintaining stable operation if no energy storage and voltage controller is installed since there will be no physical means of either injecting or absorbing energy into the grid to maintain frequency and voltage [60]. Despite being an inverter, it may experience over-and-under excitation just as in the SG and will behave in the same way. The grid does not distinguish between the virtual and actual SGs, which makes the integration of these inverters less difficult. The technological maturity of the control since it is similar to SG and because PLL is not required are two advantages of this control technique. Additionally, without sufficient power reserves, it might become unstable [66].

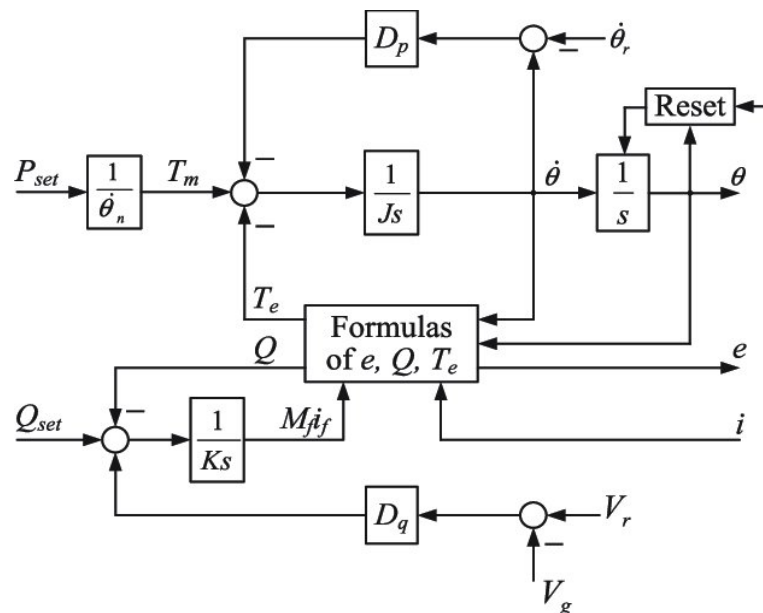


Figure 23: Synchronverter control scheme [72]



3 Converter's controller components

3.1 Park and inverse park transformation

The park transformation or synchronous reference frame is used to ease calculations and control of a three-phase AC rotating (abc frame) that needs to be converted to dc stable values ($qd0$ frame)[20]. The park transformation can be achieved by [20]:

$$[x_{qd0}] = [T_{qd0}][x_{abc}] \quad (35)$$

x_{abc} is a vector containing the three phase values in the abc frame, and x_{qd0} is a vector containing the converted quantities in the $qd0$ frame and the transformation matrix $T(\theta)$ is as following [20]:

$$T(\theta) = \frac{2}{3} \begin{bmatrix} \cos(\theta) & \cos(\theta - \frac{2\pi}{3}) & \cos(\theta + \frac{2\pi}{3}) \\ \sin(\theta) & \sin(\theta - \frac{2\pi}{3}) & \sin(\theta + \frac{2\pi}{3}) \\ \frac{1}{2} & \frac{1}{2} & \frac{1}{2} \end{bmatrix} \quad (36)$$

And the inverse park transformation and its matrix can be written as [20]:

$$[x_{abc}] = [T_{qd0}]^{-1}[x_{qd0}] \quad (37)$$

$$T^{-1}(\theta) = \begin{bmatrix} \cos(\theta) & \sin(\theta) & 1 \\ \cos(\theta - \frac{2\pi}{3}) & \sin(\theta - \frac{2\pi}{3}) & 1 \\ \cos(\theta + \frac{2\pi}{3}) & \sin(\theta + \frac{2\pi}{3}) & 1 \end{bmatrix} \quad (38)$$

3.2 Phase locked loop (PLL)

A phase-locked loop(PLL) is utilized to obtain the angle and rotational speed of the grid. A three-phase PLL is made up of a PI controller that controls the d-axis voltage component. The controller's output corresponds to the electrical grid's angular velocity ω_e , and the signal's integration corresponds to the grid angle θ_e . Fig. 24 is an example of a PLL arrangement.

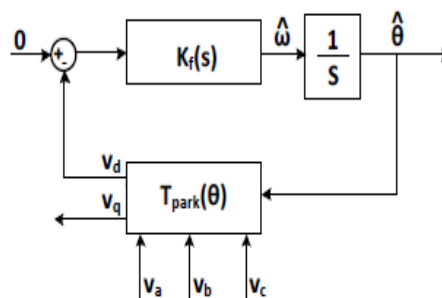


Figure 24: Diagram of phase-locked loop [20]



The linearized model of a phase-locked loop can be seen in Fig. 25. The transfer function of the mentioned system is as [15]:

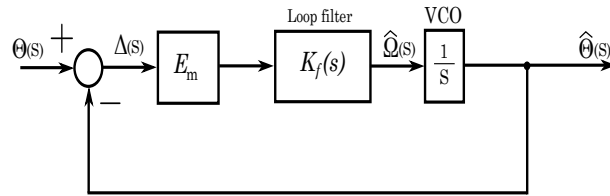


Figure 25: Linearized model of phase-locked loop [15]

$$H_c(s) = \frac{\hat{\Theta}(s)}{\Theta(s)} = \frac{K_f(s)E_m}{s + K_f(s)E_m} \quad (39)$$

$$H_\delta(s) = \frac{\Delta(s)}{\theta(s)} = \frac{s}{s + K_f(s)E_m} \quad (40)$$

$\Theta(s)$, $\hat{\Theta}(s)$ and $\Delta(s)$ are Laplace transform of θ , $\hat{\theta}$ and δ respectively. The loop filter may be designed using a variety of techniques. A popular method for balancing system stability with filter performance is the second-order loop [23]. The second-order loop's proportional-integral (PI) type filter can be expressed as follows [15]:

$$K_f(s) = K_p \left(\frac{1}{\tau_{PLL}} + s \right) \quad (41)$$

Where K_p and τ_{PLL} which is the time constant of the PLL, define the gains of the PI filter. By rewriting (39) and (40) in general form, they will be [15]:

$$H_c(s) = \frac{\hat{\theta}(s)}{\theta(s)} = \frac{2\xi\omega_n s + \omega_n^2}{s^2 + 2\xi\omega_n s + \omega_n^2} \quad (42)$$

$$H_\delta(s) = \frac{\Delta(s)}{\theta(s)} = \frac{s^2}{s^2 + 2\xi\omega_n s + \omega_n^2} \quad (43)$$

The control parameters of K_p (proportional gain), K_i (integral gain), and τ_{PLL} (PLL time constant) are defined using the formulas below to construct a PLL [15]:

$$\omega_n = \sqrt{\frac{K_p E_m}{\tau_{PLL}}} \quad (44)$$

$$\zeta = \frac{\sqrt{\tau_{PLL} K_p E_m}}{2} \quad (45)$$

$$K_i = \frac{K_p}{\tau_{PLL}} \quad (46)$$



3.3 Current reference computation

The current references, i_q^* and i_d^* , which are symbols for active and reactive power, are necessary for regulating and feeding the voltage modulation section. They may be deduced from the instantaneous power theory. To obtain power equations first is necessary to write three-phase voltages and current in qd form as follows [20]:

$$v_{qd} = \frac{v_q - jv_d}{\sqrt{2}} \quad (47)$$

$$i_{qd} = \frac{i_q - ji_d}{\sqrt{2}} \quad (48)$$

The power of a three-phase system can be expressed as [20]:

$$S = P + jQ = 3v_{qd}i_{qd}^* = 3\left(\frac{v_q - jv_d}{\sqrt{2}}\right)\left(\frac{i_q + ji_d}{\sqrt{2}}\right) \quad (49)$$

$$P = \frac{3}{2}(v_q i_q + v_d i_d) \quad (50)$$

$$Q = \frac{3}{2}(v_q i_d - v_d i_q) \quad (51)$$

Because the single frame PLL utilized in this study assures that v_d is zero, i_q and i_d may be represented as follows [20]:

$$i_q = \frac{2}{3} \frac{P}{v_q} \quad (52)$$

$$i_d = \frac{2}{3} \frac{Q}{v_d} \quad (53)$$

The estimated reference current has to be constrained in accordance with the converters' physical constraints. Depending on the relative importance of active and reactive power, the restriction might be applied differently:

- Granting priority to active power and supply reactive power when there is enough available current.
- Granting priority to reactive power and supply active power when there is enough available current.
- Keeping the angle between P and Q and decreasing them both equally.

3.4 DC voltage regulator

The existence of a DC voltage regulator is essential to maintain the voltage of the dc bus and guarantee the balance of produced and injected power. The DC voltage regulator's control scheme is as follows:

This control structure, as shown in Fig. 26, produces the i_q^* by comparing the E^{2*} and E^2 values, which represent the capacitor energy reference and actual value, and a feed-forward P_{DC} , which



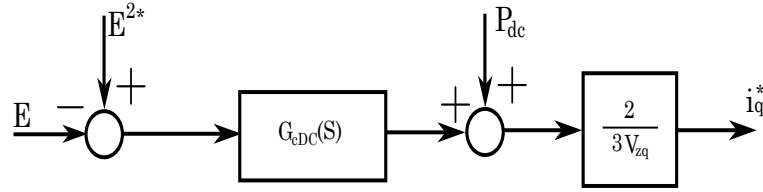


Figure 26: DC voltage regulator [20]

is the measured power before the capacitor. Overall reference converter power can be expressed as [20]:

$$P^* = P_c^* + P_{DC} \quad (54)$$

The DC voltage control may be designed using the control variable $W = E^2$. In the Laplace domain, the capacitor power P_C may be represented as follows [20]:

$$P_c(s) = \frac{1}{2} s C W(s) \quad (55)$$

For the $G_{cDC}(s)$ a PI controller can be utilised [20]:

$$G_{cDC}(s) = K_{pDC} + \frac{K_{iDC}}{s} \quad (56)$$

The closed-loop transfer function will be [20]:

$$\frac{W(s)}{W^*(s)} = \frac{s K_{pDC} + K_{iDC}}{\frac{1}{2} s^2 C + s K_{pDC} + K_{iDC}} \quad (57)$$

Which (57) is the form of:

$$\frac{W(s)}{W^*(s)} = \frac{2s\xi_E\omega_E + \omega_E^2}{s^2 + 2s\xi_E\omega_E + \omega_E^2} \quad (58)$$

Then PI controller gains will be [20]:

$$K_{pDC} = C\xi_E\omega_E \quad (59)$$

$$K_{iDC} = \frac{C\omega_E^2}{2} \quad (60)$$

where ξ_E is the intended DC voltage loop damping ratio and ω_E is the desired voltage loop angular velocity. It is significant to note that in order to guarantee steady system response, the DC voltage loop must be substantially slower than the inner current controller.



3.5 Current regulator (Grid-side)

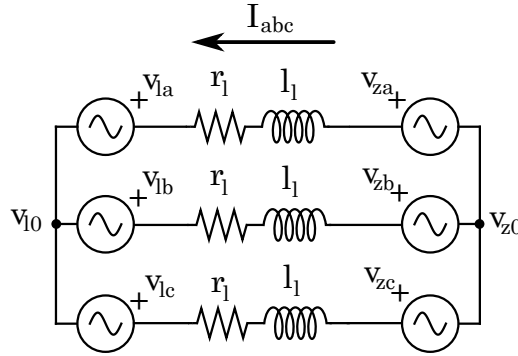


Figure 27: Equivalent model of AC side of a VSC [20]

The equivalent voltage equation of Fig. 27 can be written as [20]:

$$\begin{bmatrix} v_{za} \\ v_{zb} \\ v_{zc} \end{bmatrix} - \begin{bmatrix} v_{la} \\ v_{lb} \\ v_{lc} \end{bmatrix} - (v_{l0} - v_{z0}) \begin{bmatrix} 1 \\ 1 \\ 1 \end{bmatrix} = \begin{bmatrix} r_l & 0 & 0 \\ 0 & r_l & 0 \\ 0 & 0 & r_l \end{bmatrix} \begin{bmatrix} i_a \\ i_b \\ i_c \end{bmatrix} + \begin{bmatrix} l_l & 0 & 0 \\ 0 & l_l & 0 \\ 0 & 0 & l_l \end{bmatrix} \frac{d}{dt} \begin{bmatrix} i_a \\ i_b \\ i_c \end{bmatrix} \quad (61)$$

Where v_{za} , v_{zb} , v_{zc} are the grid voltages in abc frame, v_{la} , v_{lb} , v_{lc} are the converter voltages in abc frame, i_a , i_b , i_c are the instantaneous currents in abc frame. r_l is the inductance equivalent resistance and l_l is the inductance value. The voltage difference between the converter and the grid neutral is given by $v_{l0} - v_{z0}$ and in a three-phase balanced system, $v_{l0} - v_{z0}$ can be considered as zero. By applying park transform to equation (61) and by taking into account $v_{zd} = 0$ by PLL, voltage equation will be [20]:

$$\begin{bmatrix} v_{zq} \\ 0 \end{bmatrix} - \begin{bmatrix} v_{lq} \\ v_{ld} \end{bmatrix} = \begin{bmatrix} r_l & l_l \omega_e \\ -l_l \omega_e & r_l \end{bmatrix} \begin{bmatrix} i_q \\ i_d \end{bmatrix} + \begin{bmatrix} l_l & 0 \\ 0 & l_l \end{bmatrix} \frac{d}{dt} \begin{bmatrix} i_q \\ i_d \end{bmatrix} \quad (62)$$

As demonstrated in equation(62) there is a coupling between voltage and current qd components. There are essentially two principal control strategies to manage i_q and i_d :

- Multi-variable control, using a single two-dimensional controller to control both the d and q components.
- Decoupling, controlling d and q independently which in this study is chosen to proceed.

In order to decouple q and d [20]:

$$\begin{bmatrix} v_{lq} \\ v_{ld} \end{bmatrix} = \begin{bmatrix} -\hat{v}_{lq} + v_{zq} - l_l \omega_e i_d \\ -\hat{v}_{ld} + l_l \omega_e i_q \end{bmatrix} \quad (63)$$

\hat{v}_{lq} and \hat{v}_{ld} are the results of the current controller and v_{lq} and v_{ld} are the voltages that the converter will deliver. By swapping (63) into (62) and isolating \hat{v}_{lq} and \hat{v}_{ld} there will be [20]:

$$\begin{bmatrix} \hat{v}_{lq} \\ \hat{v}_{ld} \end{bmatrix} = \begin{bmatrix} r_l & 0 \\ 0 & r_l \end{bmatrix} \begin{bmatrix} i_q \\ i_d \end{bmatrix} + \begin{bmatrix} l_l & 0 \\ 0 & l_l \end{bmatrix} \frac{d}{dt} \begin{bmatrix} i_q \\ i_d \end{bmatrix} \quad (64)$$



The transfer function between the controller voltages and converter currents may be obtained using the Laplace transformation as follows [20]:

$$\frac{\hat{v}_{lq}(s)}{i_q(s)} = \frac{1}{l_{ls} + r_l} \quad (65)$$

$$\frac{\hat{v}_{ld}(s)}{i_d(s)} = \frac{1}{l_{ls} + r_l} \quad (66)$$

Based on Internal Model Control technique the controller can be designed as [20]:

$$G_{ciq}(s) = G_{cid}(s) = \frac{K_p s + K_i}{s} \quad (67)$$

And the constants are:

$$K_p = \frac{l_l}{\tau} \quad (68)$$

$$K_i = \frac{r_l}{\tau} \quad (69)$$

where τ is the electrical system's closed-loop time constant. This constant must be determined with the physical constraints of the converter in mind. It is standard procedure to define it ten times quicker than the converter switching frequency.

3.6 Current regulator (Machine-side)

In a permanent magnet synchronous machine, the relationship between the voltage and the current is expressed in equation (26). The q and d variables are connected in these equations, and the dynamic response of the current is dependent on the mechanical speed of the machine. To simplify the design of the current controller, a decoupling feedback is utilized, which both decouples the q and d components and eliminates the dependent on the mechanical speed of the machine, hence removing nonlinear dynamics [53]. To do this, a voltage is given to the machine's stator, which compensates for the coupling terms. This voltage can be expressed as [38]:

$$\begin{bmatrix} v_{sq} \\ v_{sd} \end{bmatrix} = \begin{bmatrix} \hat{v}_{sq} + \omega_r L_d i_{sd} + \lambda_m \omega_r \\ \hat{v}_{sd} - \omega_r L_q i_{sq} \end{bmatrix} \quad (70)$$

Where \hat{v}_{sq} and \hat{v}_{sd} are the linear current regulator output. By considering ideal compensation, dynamics are [38]:

$$\hat{v}_s^{qd} = \begin{bmatrix} r_s & 0 \\ 0 & r_s \end{bmatrix} i_s^{qd} + \begin{bmatrix} L_q & 0 \\ 0 & L_q \end{bmatrix} \frac{d}{dt} i_s^{qd} \quad (71)$$

It should be highlighted that these equations are decoupled and no longer depend on mechanical speed. As a result, they may be divided into two separate systems for q and d. These may be transformed using the Laplace transform to produce the following transfer functions [38]:

$$\frac{i_{sq}(s)}{\hat{v}_{sq}(s)} = \frac{1}{L_q s + r_s} \quad (72)$$

$$\frac{i_{sd}(s)}{\hat{v}_{sd}(s)} = \frac{1}{L_d s + r_s} \quad (73)$$



By using the internal model control technique, the transfer function can be designed. So that the steady-state error for step reference inputs is zero and the controller is causal, the pole of the system is suppressed in this case by adding a matching zero to the controller transfer function plus an integrator. The result of the closed-loop transfer function is [38]:

$$\begin{bmatrix} i_{sq}(s) \\ i_{sd}(s) \end{bmatrix} = \begin{bmatrix} \frac{1}{\frac{1}{\alpha}s+1} & 0 \\ 0 & \frac{1}{\frac{1}{\alpha}s+1} \end{bmatrix} \begin{bmatrix} i_{sq}^*(s) \\ i_{sd}^*(s) \end{bmatrix} \quad (74)$$

The controller transfer function is equivalent to that of a PI controller with the following transfer function [38]:

$$K(s) = \frac{K_p s + K_i}{s} \quad (75)$$

$$K_p = \alpha L_q \quad (76)$$

$$K_i = \alpha r_s \quad (77)$$

where α is a design parameter proportional to the system's bandwidth. A broad bandwidth produces a rapid reaction, which is desired, but it also makes the system more sensitive to feedback measurement noise and necessitates a greater bandwidth of the control action [38].



4 Methodology

The implementation of the grid-connected voltage source converter and wind turbine and its components, as well as other aspects of this study, should be done in Matlab Simulink alongside PSCAD and other tools, with the findings described. The purpose of employing diverse software is to observe and analyze the system's behavior in different software. Both Simulink and PSCAD are EMT simulation tools, however, the differences in fine details will be visible in this study. To accomplish so, the intended circuit was developed by mentioned tools; the following is a description of the procedure from the beginning to the end. To clarify, after consulting with the supervisor, it was chosen to begin with the grid side and move on to the machine side in subsequent phases.

4.1 Simulation in MATLAB/Simulink

An interactive, graphical platform is provided for modeling, simulating, and evaluating dynamic systems by Simulink, a MATLAB add-on product. It makes it possible to quickly build virtual prototypes to quickly explore design concepts at any degree of detail. Simulink offers a graphical user interface (GUI) for modeling that allows models to be built as block diagrams. It features a vast library of prefabricated building components that may be assembled graphically using drag-and-drop mouse actions. Instead of spending hours building a model in a lab setting, the user is able to create one that is "up and running." It supports continuous-time, sampled-time, and hybrid models of linear and nonlinear systems [63].

The alleged circuit is made up of two parts: a power circuit and a control circuit; according to Fig. 28 a permanent magnet machine is linked to the machine side VSC, and the output of the machine side VSC is connected to the DC bus, which is connected to the grid side VSC via a capacitor. On the other hand, the grid side VSC is connected to the grid via filters. The two controllers for regulating the converters are the control components; the following is a detailed explanation of the entire model in Simulink.

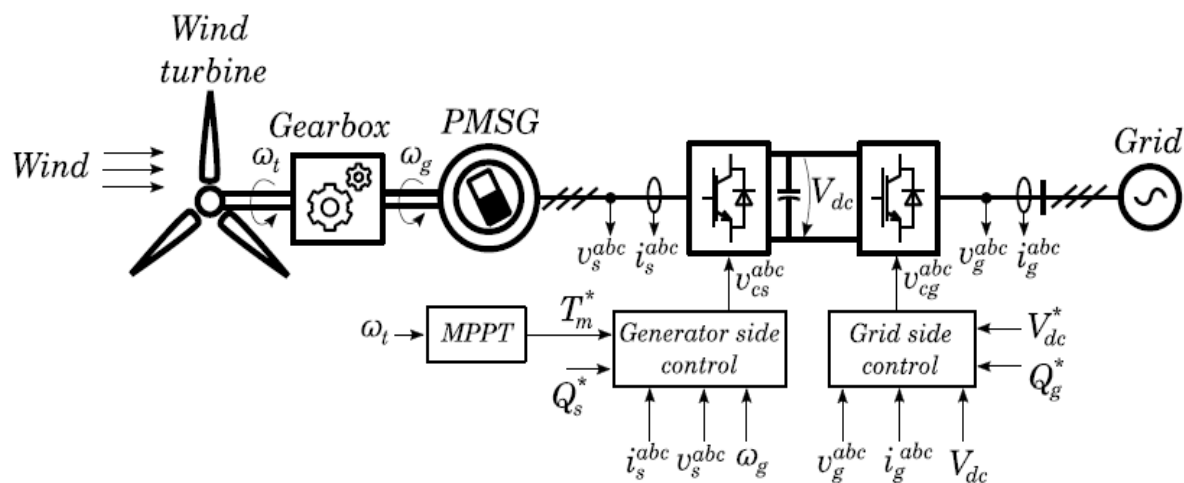


Figure 28: General control overview [13]



4.2 Wind Turbine Model

The wind turbine model consists of a wind turbine power model that reflects the power equation of the wind turbine, alongside a pitch controller and a mechanical model known as the one-mass model that reflects the turbine and generator shaft plus the inertia in the simulation, and an MPPT that tracks the optimal load alongside with a permanent magnet synchronous generator which is connected to the turbine shaft through a gearbox. Fig. 29 illustrates a general scheme of the wind turbine model to be implemented in Simulink.

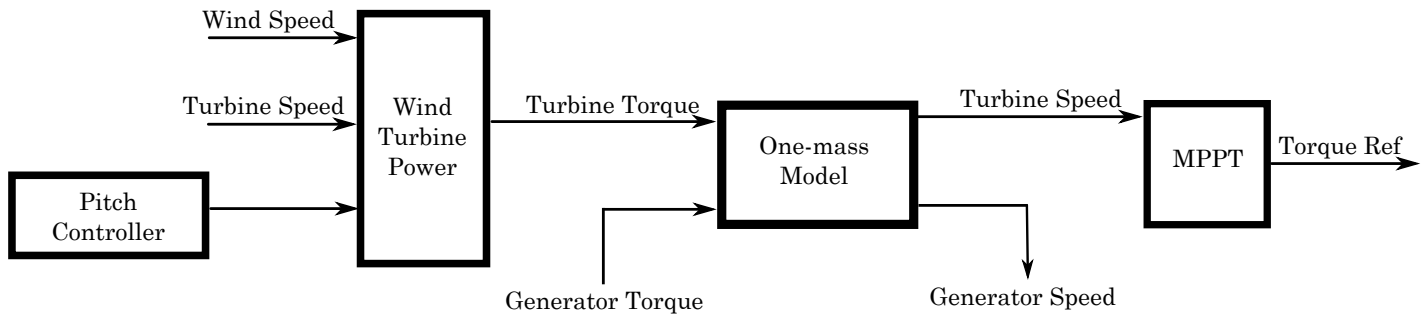


Figure 29: General scheme of wind turbine model

Table 3 provides the wind turbine's needed parameters, which will be implemented using the script.

Table 3: Wind turbine parameters [2]

Parameter	Value
Nominal power, P_n	5 MW
Nominal wind speed V_{wn}	14 m/s
Diameter, D_t	88 m
Transmission ratio of gearbox, N	80
Aggregated inertia, J_{tot}	$9 \cdot 10^4 \text{ kgm}^2$

Table 4: Coefficient power parameters [2]

Parameter	Value
c1	0.73
c2	151
c3	0.58
c4	0.002
c5	2.14
c6	13.2
c7	18.4
c8	-0.02
c9	-0.003



4.2.1 Wind Turbine Power Model

A wind turbine power model is created based on (7). Where variables, v wind speed, A area swept by blades, ρ air density, and power coefficient as presented in Table 4 are taken into account as inputs, and the output is the amount of power that the wind turbine will produce. The following is the wind turbine power model structure to be implemented in Simulink.

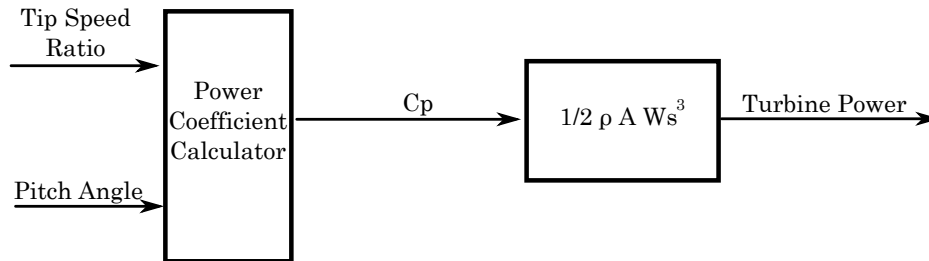


Figure 30: Wind turbine power model

4.2.2 Pitch Angle Controller Model

The pitch angle controller is only activated when the wind speed is higher than certain values. In certain cases, increasing the produced power will overwhelm the generator and/or the converter, making it impossible to manage the rotor speed. This keeps the rotor speed from rising too high and causing mechanical damage. The ideal angle increases progressively with increasing wind speed after the rated wind speed, the influence of the pitch angle on the power coefficient is calculated using (4) and (5). The resultant number may be used to compute the mechanical power collected from the wind using equation (7)[2].

The designed pitch angle controller is depicted in Fig. 31. It should be noticed that the pitch angle does not change instantly, but rather at a limited rate, which may be rather low due to the size of the rotor blades in current wind turbines. The highest rate of change of the pitch angle is around 10 degrees per second [9] which is also considered in this study.

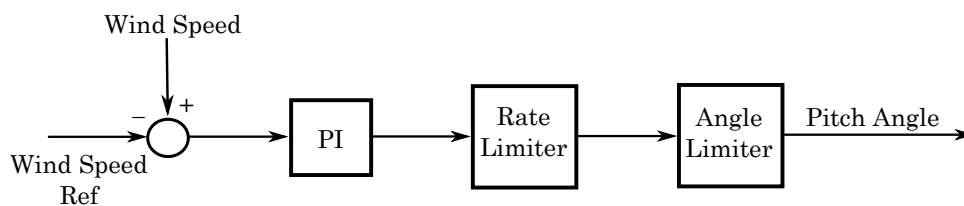


Figure 31: Pitch angle controller



4.2.3 Shaft Model

The equation (11) should be used to determine a one-mass model for a wind turbine assuming a completely stiff shaft, as has been stated in Section (2.7) the total accelerating torque is the difference of mechanical turbine torque and the electrical generator torque. Simulink's implemented model of the one mass model is as Fig. 32. Bear in mind the total inertia value is shown in Table 3.

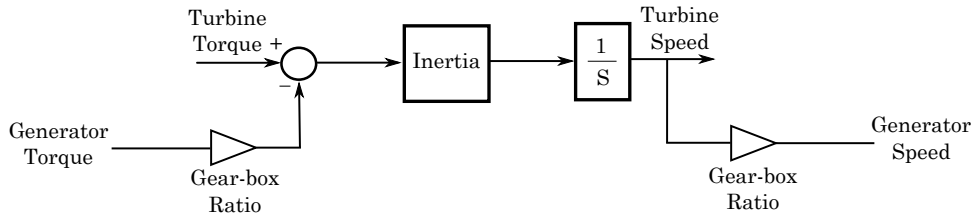


Figure 32: One mass model

It is important to rigorously remember that the integrator's starting condition in the Simulink One mass model must be different from zero for the model to function in the following phases. This is because the setup of the model makes the assumption that the turbine shaft is rotating at the beginning of the simulation.

4.2.4 MPPT

According to the wind power equation (7), it is demonstrated that the speed of the turbine must coincide with a certain value that relies on the speed of the wind in order to harvest the greatest amount of power from the wind [38]. Due to local fluctuations in speed and distortions brought on by the functioning of the wind turbine, measuring the wind speed precisely is a challenging task. Owing to this, a variety of alternative control algorithms have been proposed in the past to optimize energy extraction by performing the so-called maximum power point tracking (MPPT) without the requirement of a wind speed measurement. The most basic and well-known of these strategies, known as constant tip speed ratio control, is commonly used for modeling speed control behavior in wind turbine power quality simulations. The constant tip speed ratio control action may be determined as can be seen in equations below [13]:

$$T_{max} = \frac{K_{cp}}{N} \omega t^2 \quad (78)$$

$$K_{cp} = \frac{1}{2} \rho A r^3 \frac{c_1 (c_2 + c_6 c_7)^3 e^{-\frac{c_2 + c_6 c_7}{c_2}}}{c_2^2 c_7^4} \quad (79)$$

The maximum torque may be obtained using the quadratic relationship of the turbine speed, therefore the maximum torque obtained using the aforementioned equation (78) will serve as the reference torque while also demonstrating the amount of active power reference to the VSC controller in the machine side VSC.



4.2.5 Permanent Magnet Synchronous Generator

The generator used for this study is a synchronous generator with a permanent magnet rotor, according to the concept explained in Section (2.8). It is a three-phase machine with a rounded rotor and constant magnetic flux, more necessary specifications are shown in Table 5.

Table 5: PMSG parameters [2]

Parameter	Value
Synchronous nominal speed, ω_n	$2\pi 50$
Pairs of poles P	2
Stator resistance, R_s	0.01 Ω
d-component inductance, L_d	0.159 mH
q-component inductance, L_q	0.159 mH

4.3 Voltage source converter (VSC)

The chosen voltage source converter is a Simulink universal bridge block. It is a three-level VSC with a DC voltage on one side and a three-phase alternate voltage on the other, the characteristics are demonstrated in Table 6:

Table 6: VSC back-to-back [13]

Parameter	Value
Nominal power S_{cn}	5MVA
Nominal AC voltage U_{cn}	690V
Nominal DC voltage $V_{dc,n}$	1200V
Inductance of grid side VSC L_c	30.31 μH
Resistance of grid side VSC R_c	0.95m Ω
Capacitor of DC bus C_{dc}	278mF

In the PMSG block in Simulink there is a reference port that has to be linked to a fictitious reference; this port will be triggered by the controller which will be implemented and provide control over the VSC. Consider the fact that, to make this block function properly, it must receive the control signal in p.u to provide the requisite voltage level at the output.

4.4 AC Voltage source

In order to perform the role of the grid in the circuit, a three-phase source block from Simulink's library was chosen. The characteristics are shown in Table 7.

Table 7: AC grid [13]

Parameter	Value
Base power	5 MVA
Grid AC voltage, U_g	690 V
Grid frequency, f_g	50 Hz
Short circuit ratio	5



4.5 Converter's grid coupling filter

A RL filter was used in this study since it is necessary for power flow and decoupling in the current regulator. The values of resistance and inductance are shown in Table 6 and they will often be a ratio of the base impedance when designing a coupling filter. Resistance here is 1% of Z_{base} , while inductance is 10% of X_{base} [38]. The filter calculation is as follows:

$$\begin{aligned} Z_{base} &= \frac{V_c^2}{S_c} \\ X_{base} &= \frac{Z_{base}}{\omega_{base}} \\ R_c &= (1\%)Z_{base} \\ L_c &= (10\%)X_{base} \end{aligned} \quad (80)$$

4.6 DC bus

As depicted in Fig. 33, the buffer between the machine side and the grid side VSC is the DC link. The DC capacitor is the sole component that is present in this area.

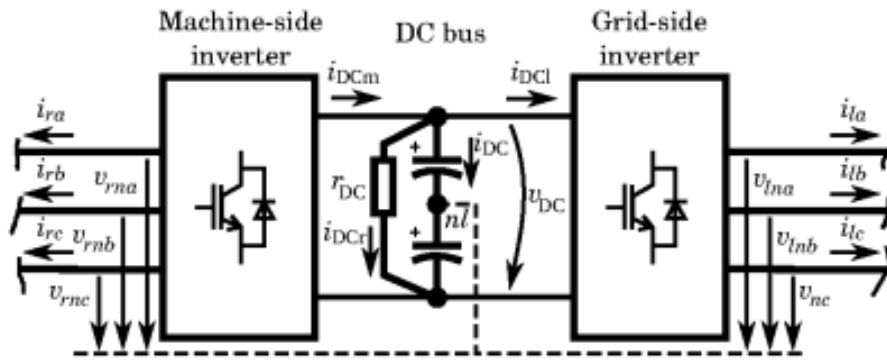


Figure 33: DC bus schematic [38]

The DC link capacitor is vital for controlling the power flow balance from the generator side converter to the grid side converter; according to the (81), the transferred active power from the DC-link to the AC grid has a direct relationship with the capacitor voltage [20].

$$C_{DC} = \frac{2\tau_c S_{cn}}{(V_{dc}^*)^2} \quad (81)$$

According to Table 6, V_{dc}^* is set to 1.2 kV and the nominal power of converter S_{cn} is 5 MVA, to perform a proper response from the capacitor the time response τ_c is set to 0.04 s. It is important to keep in mind that the capacitor must be initialized with the voltage reference value required to execute the simulation.

4.7 Grid side VSC controller

The grid side VSC controller maintains the DC-link voltage and guarantees the balance between power generation and power injection [73]. In this approach, the grid-side VSC is responsible for active and reactive power while holding the dc voltage reference. The control structure of the grid side VSC is as follows:



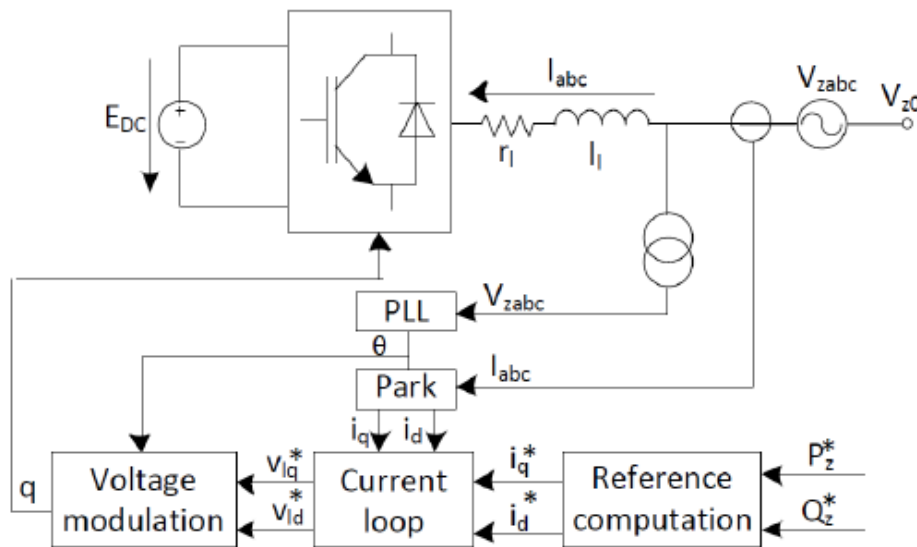


Figure 34: Grid side VSC control structure [20]

Grid-forming and grid-following inverters are two types of control methods used to integrate renewable energy resources into power grids. They have certain commonalities but also have some significant variances, making their relationship highly delicate and often opaque [40]. A grid-following converter regulates the ac-side current and, using a phase-locked loop (PLL), follows the phase angle of the existing grid voltage [61]. The control structure for grid-side VSC for the simulation in Simulink is chosen to be grid-following.

The grid-side VSC control consists of the following components: PLL, park and inverse park transforms, Q loop, Vdc loop, and current regulator, which all will be briefly presented next.

4.7.1 Phase Locked Loop

As mentioned in Section (3.2), a phase-locked loop (PLL) is used to calculate the angle and angular rotational speed of the grid. Fig. 35 depicts the implemented PLL in Simulink. In this case, the PLL will attempt to maintain $v_d = 0$, and the error will be regulated in a PI controller designed according to (44), (45) and (46) and will be added with the grid’s nominal angular rotational speed, which has been determined up to this point, and integration of this value will provide the angle.

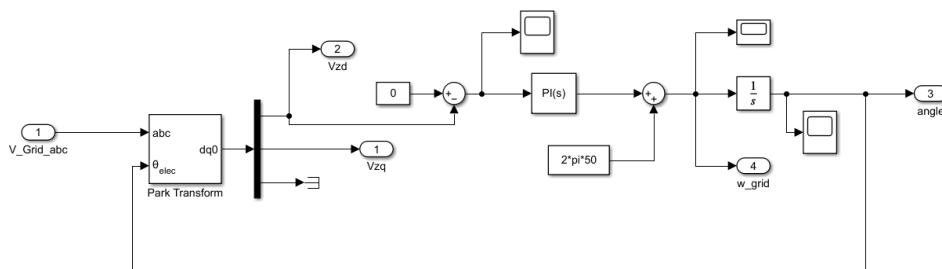


Figure 35: Designed PLL in Simulink



4.7.2 Park Transformation

The park transform and inverse park transform features have been detailed in Section (3.1). Park and inverse park blocks were chosen to accomplish the above statement in Simulink. According to Fig. 36, the input for park transform is voltage or current plus their angular speed ϑ , and the outcome is the input in $qd0$ frame. In this modeling, the voltage and current are received through grid-side voltage and current measurements, and the angular speed from the PLL feeds the input, resulting in a $qd0$ frame intake. In the case of the inverse park transform, the input is a $qd0$ frame of voltage or current, and the output is an abc frame.

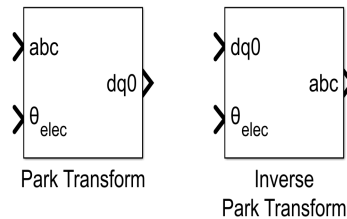


Figure 36: Park and Inverse park transform blocks

4.7.3 DC Voltage regulator

The dc voltage regulator, as specified in Section (3.4), maintains the dc bus voltage while ensuring power flow; the structure to be implemented in Simulink is shown in Fig. 37. Worth to mention, the speed of the PI controller of the dc voltage regulator must be at least 10 times slower than the speed of the current loop to avoid interactions.

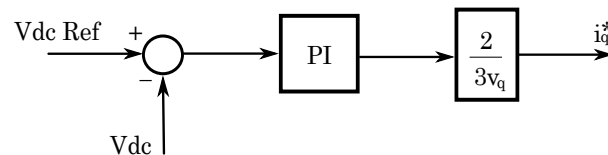


Figure 37: DC voltage regulator in Simulink

4.7.4 Q Loop

The purpose of the Q loop is to produce a reference i_d^* value that is representative of the reactive power in the control structure. To achieve so, according to the (53) and (51) i_d^* will be determined as illustrated in Fig. 38.

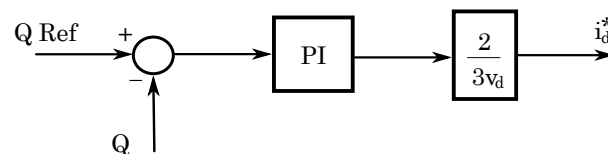


Figure 38: Implemented Q Loop in Simulink



4.7.5 Current regulator

The presence of a current regulator is due to voltage modulation and decoupling of the grid and converter voltages as expressed in Section (3.5), which is made feasible by (63). The current regulator will be made according to the structure as depicted in Fig. 39. It is possible to determine the values of proportional and integral gains using (68) and (69).

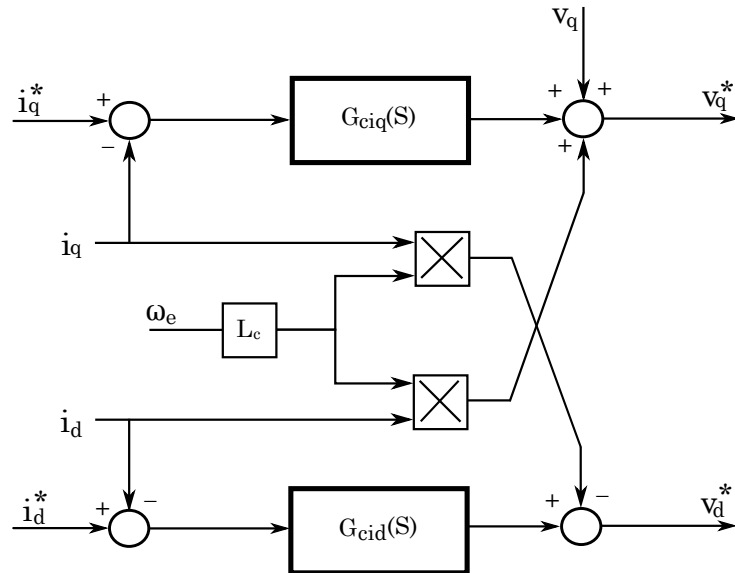


Figure 39: Current regulator structure [20]



4.8 Machine side VSC controller

In basic terms, the machine-side VSC is responsible for managing the injected active power to the system; to do so, a control structure proportional to the machine's power must be designed and implemented. To construct the machine-side current controller, reference parameters such as i_{sq}^* and i_{sd}^* must be determined in addition to the rotor speed and its position, and eventually, real values of the machine's current and voltage will be delivered to the converter after performing the park transform.

This controller contains similar components to the grid-side controller, such as park and inverse-park transforms and Qloop, but the main difference is that in the grid-side controller, the angle and rotational speed are determined by the PLL, whereas on the machine side, these values must be obtained from the machine. Park and inverse park transformers will function normally if the rotational speed and angle values are met.

4.8.1 Angular and rotational speed measurement

The mechanical speed will be received from the machine, and because the machine has two pair poles, the synchronous speed in the stator will equal the product of the mechanical speed and the pair poles. Setting an integrator to synchronous speed will be enough to obtain the machine's angle.

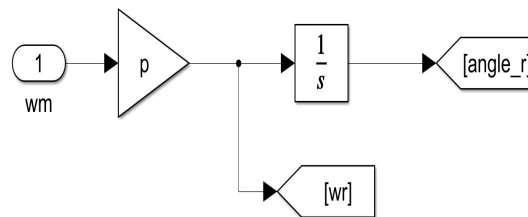


Figure 40: Machine angular and rotational speed measurement

4.8.2 Current reference calculation

To identify the current references, similarly to the grid-side, the d component of the current will be derived from the Q-loop, but the q component, which will be representative of the machine's actual power, must be determined from the torque reference. The generator torque equation (32) has been deduced by calculating the generator's mechanical power and dividing it by the mechanical speed in Section (2.8). In this simulation, the optimal torque value is sent from the MPPT, and by taking into consideration the (32) i_q^* can be calculated. To derive i_q^* from the (32), i_q must be isolated in that equation since machine torque has a direct relationship with flux (λ) and pole pairs (P). This is done by Simulink blocks as shown in Fig. 41:

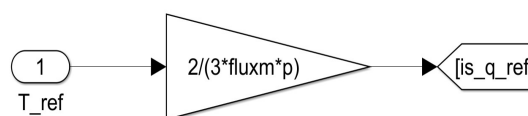


Figure 41: Current reference computer



4.8.3 Current regulator (Machine-side)

The machine-side voltage modulation and decoupling are carried out via the machine-side current regulator. The machine side current regulator, which is based on (70) and demonstrates how voltage qd components are decoupled, is described in Section (3.6). Although there won't be a filter between the machine's side VSC and the actual machine, internal machine characteristics like stator resistance and stator inductance are crucial for controller design. The current regulator for the machine side controller is as follows:

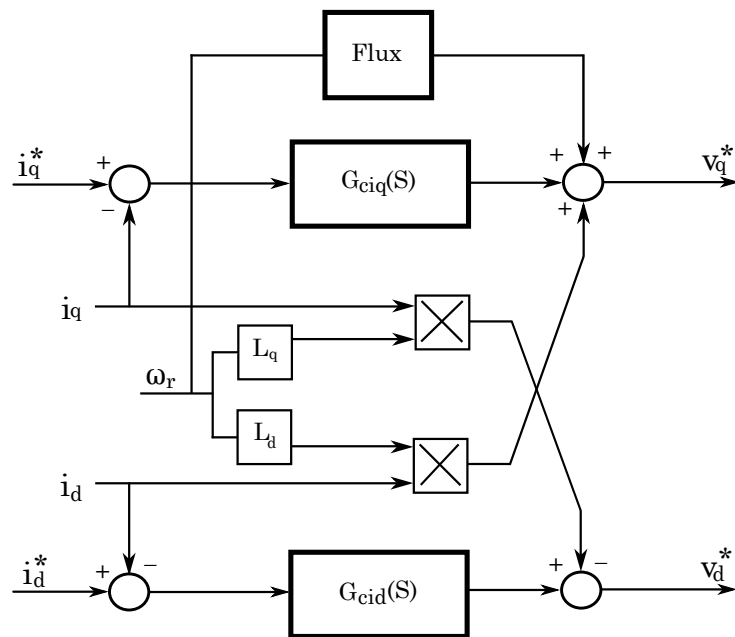


Figure 42: Machine-side current regulator



4.9 Simulation in PSCAD

One goal of this study is to analyze the implemented system in multiple software, one of which is PSCAD, which is commonly used these days. Time domain simulation software called PSCAD (Power Systems Computer Aided Design) is used to study transients in electrical networks. It is a set of applications that provide electromagnetic transients software with a graphical, Unix-based user interface (EMTP). It also is referred to as PSCAD/EMTDC. Since its first development in 1976, EMTDC (Electromagnetic Transients with DC Analysis) has undergone continuous scope and capability expansion. It is a crucial component of PSCAD since it establishes the simulation software that comes with PSCAD with its library of power system component models and processes. Together, they offer a quick, adaptable, and precise answer for the time-domain program that is effective for modeling a range of electrical power system transients and control networks. The power system's and its controllers' differential equations are solved in the time domain by PSCAD. The findings are computed as instantaneous values in time, but the real RMS meters and/or FFT spectrum analyzers may transform these to phasor magnitudes and angles [49].

The same process as with the Simulink model has been used to simulate the wind turbine Type IV in PSCAD, but with consideration for the variations between the two programs. The blocks' implementation will be developed in accordance with the differences between the master libraries' blocks in PSCAD and Simulink. Similar to the Simulink model, this model consists of a power circuit, a control structure, and a model of a wind turbine. Each of these components is described.

4.10 Wind turbine model in PSCAD

The PSCAD master library is where the wind turbine model for this part was obtained from. In addition, power coefficient values are attained from Table 4 along with the wind turbine data in Table 3. The wind turbine block in PSCAD offers two settings for the block's existing power coefficient, but it also takes external C_p values based on user preference, and in this study, the external input option is used. C_p values according to Table 4 were given by building components in the PSCAD area. Furthermore, as this wind turbine employs p.u values, similar to the majority of the PSCAD master library, multiplications and divisions are needed in order to per-unitize or convert the numbers to SI units.

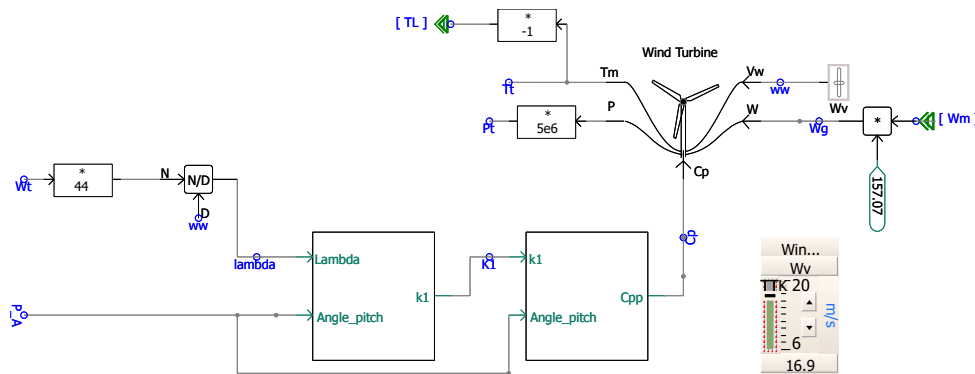


Figure 43: Wind turbine model in PSCAD



The pitch angle controller is identical to Simulink and is as follows:

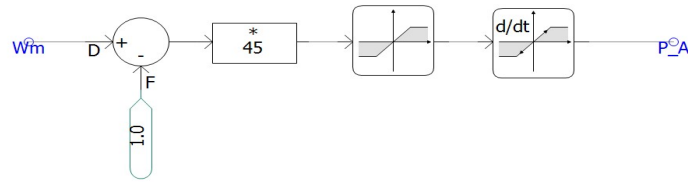


Figure 44: Pitch controller in PSCAD

To provide more realistic conditions for the wind turbine model, a wind source block from PSCAD's Master library is selected, as illustrated in Fig. 45. This block simulates the wind speed that would usually blow in nature. It is made up of four parts and is described by the (82); further data can be found in [4].

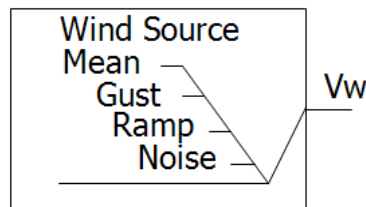


Figure 45: Wind source block in PSCAD

$$V_W = V_{WB} + V_{WG} + V_{WR} + V_{WN} \quad (82)$$

Where:

V_{WB} = base wind velocity

V_{WG} = gust wind component

V_{WR} = ramp wind component

V_{WN} = noise wind component

4.11 Power circuit in PSCAD

Similar to Simulink, PSCAD's power circuit consists of a PMSG, voltage source converter's machine side and the grid side, as well as a dc link connecting them, a converter coupling filter, and the grid but the contrasts are:

- The permanent magnet synchronous machine in PSCAD is different from the Simulink block by characteristics, hence the equal behavior and outcomes cannot be taken into account.
- Since there is no way to establish the initial value for the capacitor block in PSCAD, the capacitor is charged shortly using a dc voltage source.



- Although PSCAD's master library contains a three-phase source block, the author chose to use the grid Thevenin equivalent. To point out that the grid following model operates properly with both grid blocks, indicating that the control is effective.
- Due to the requirement to simulate faults, a chopper with a breaking resistor has been placed in the dc-link in this model.

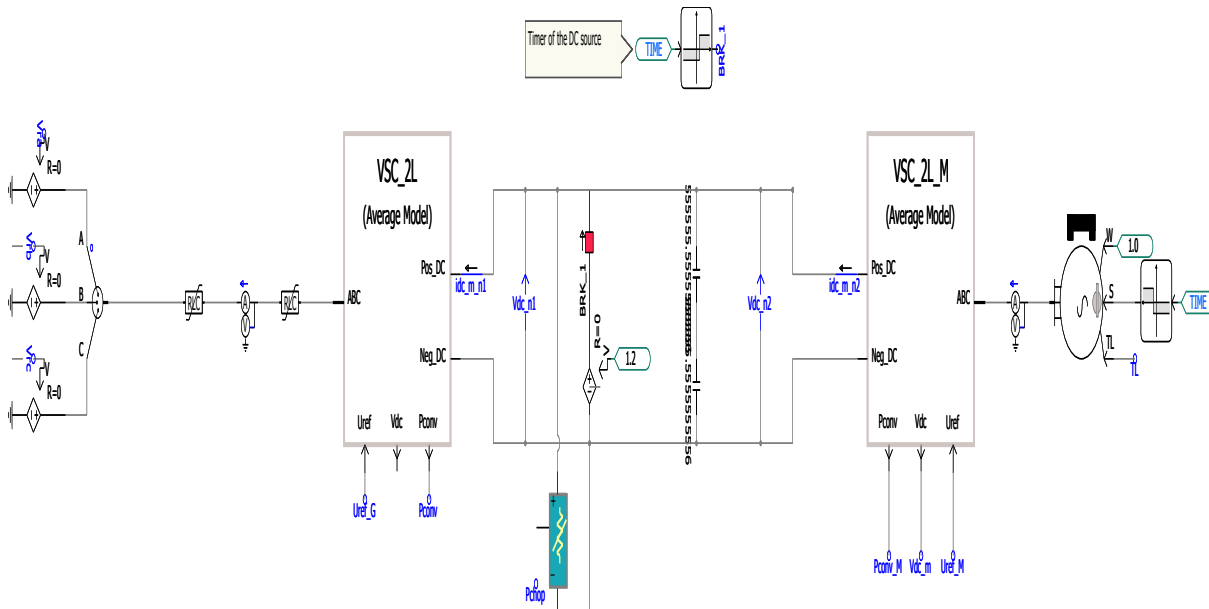


Figure 46: Power circuit of Type IV wind turbine in PSCAD

The PMSG is connected to the grid through a full-scale converter, as is seen in Fig. 46. In PSCAD, the PMSG can be set up at startup so that it runs as an ideal source for a predetermined period, then switches to a machine whose torque value is derived from a wind turbine immediately after. This is the rationale for the timer that is seen on the right side of Fig. 46. As previously stated, the existence of the timer up to the dc link is to count the time until the dc source breaker is disconnected from the circuit.

The PMSG machine first acts as a voltage source for two seconds, at which point it begins to inject wind power into the capacitor, which is ready to raise its voltage, via the dc link. However, the grid-side converter instead absorbs that power and injects it into the grid. The controllers on both sides are responsible for carrying out this operation.

4.12 DC-Chopper

A DC-chopper is a resistance circuit coupled in parallel with a DC-link capacitor between the grid-side converter and machine-side converter. By absorbing transitory stator over current, a breaking resistor is employed to sustain the DC-link voltage [27]. The DC chopper circuit's insertion and discharge times are controlled by the insulated gate bipolar transistor (IGBT), which is connected in series with resistors. Every time there is a grid fault, the stator current will quickly increase, charging the DC-link capacitor and causing the DC-link to over voltage. The IGBT should be closed to short the connection using breaking resistors when the DC-link voltage surpasses the threshold value [47]. Therefore, the DC-link voltage may be changed to a suitable value.

The IGBT switch is activated as illustrated in Fig. 47 when the dc-link voltage exceeds the nom-



inal value and remains on until the dc-link voltage is equal to or dips below the nominal value. It is important to note that the resistor value varies depending on the amount of power being wasted and the dc voltage.

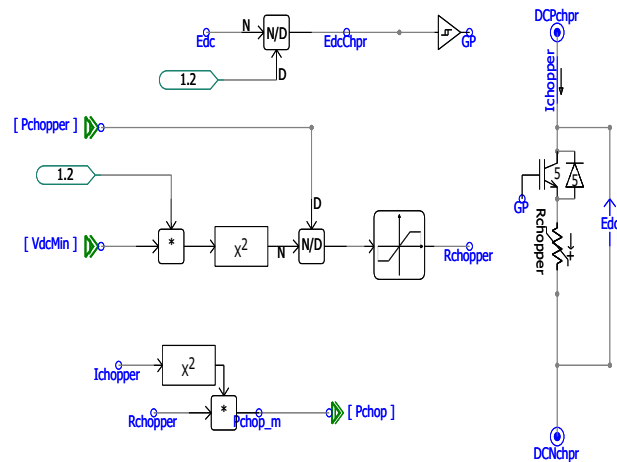


Figure 47: DC-Chopper model in PSCAD

4.13 DC voltage support

To keep the dc-link voltage in the range, it is important to employ a support dc voltage in GFOR control. This is because there is no controller to regulate the dc voltage, so the voltage of the dc bus might vary and be unstable. An ideal dc source is considered in this research to support the dc-link, but it will not be permanently linked; instead, a system similar to the chopper is considered, and instead of connecting when the voltage increases, it will connect when the voltage tends to decrease less than the nominal value. Fig. 48 shows the dc voltage support.

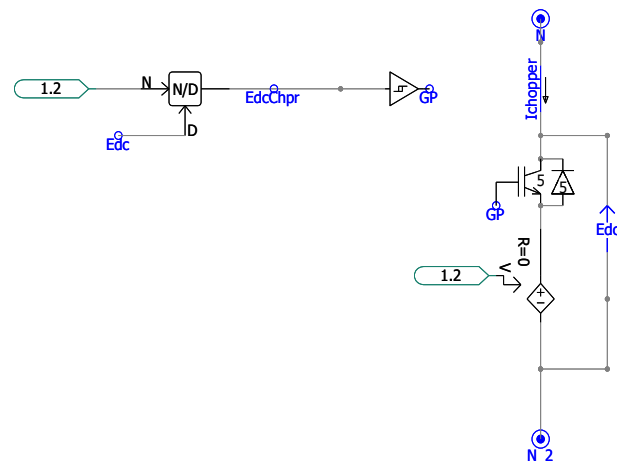


Figure 48: DC voltage support model in PSCAD



4.14 Grid-side controller in PSCAD (GFOL)

The grid-side controller in PSCAD follows the same procedures as the Simulink model and is composed of the current loop, PLL, Qloop, DC voltage regulator, and park and inverse park transformers. Park and inverse park transformers, Qloop, and the values provided for their structures and functions in the Simulink model will not be duplicated here; however, PLL, the DC voltage regulator, and the current loop have certain modifications specific to the PSCAD software that will be discussed.

4.14.1 PLL model in PSCAD

Although the master library contains a PLL block, the author opted to create PLL using blocks as illustrated in Fig. 49. To highlight, the control computations are the same as the model in Simulink.

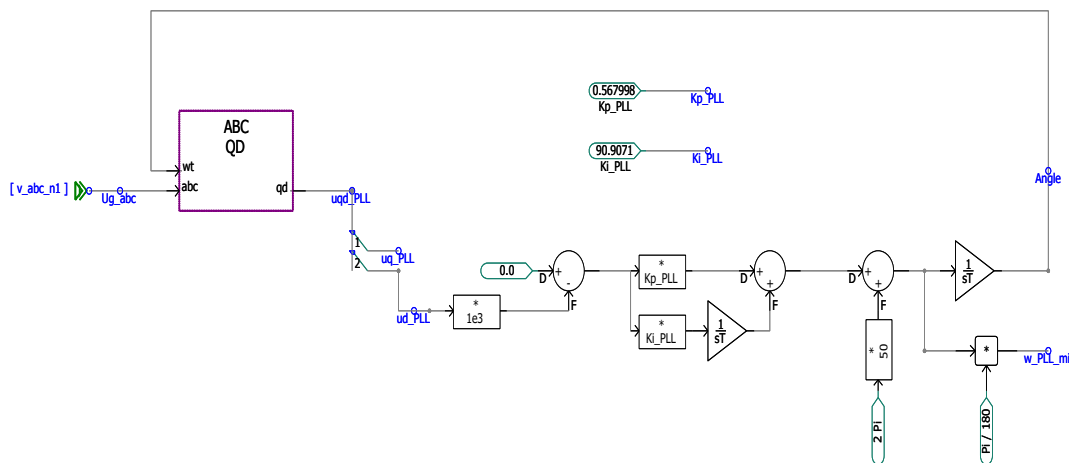


Figure 49: PLL designed model in PSCAD

4.14.2 DC voltage regulator in PSCAD

As previously mentioned, the dc voltage regulator controls the dc bus voltage to guarantee that the injected power from the machine side controller is delivered to the grid properly by providing the i_q^* reference [20]. The difference between the PSCAD dc voltage regulator and Simulink relates to the dc link capacitor block, which has been reported as having no initial voltage value setting options unlike the capacitor in Simulink. To solve this, a dc voltage source was established for 0.3 seconds. The timing before the PI controller is set to 0.3 seconds, as can be seen in Fig. 50, to guarantee that the capacitor will charge appropriately. Values of proportional and integral gains for the PI controller are equal to the Simulink model.



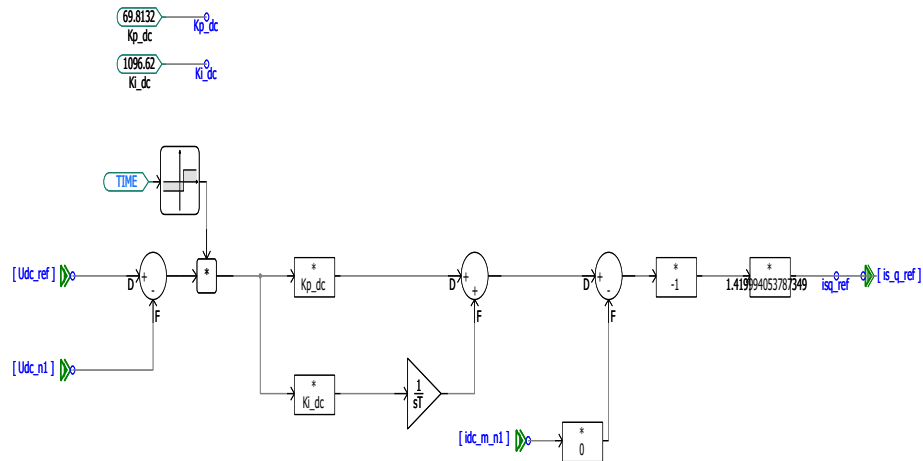


Figure 50: DC voltage regulator in PSCAD

4.14.3 Grid-side current regulator in PSCAD

The following is how the grid-side current regulator, which is in charge of decoupling the grid voltage, is built in the PSCAD, to mention it is made by taking into consideration (63).

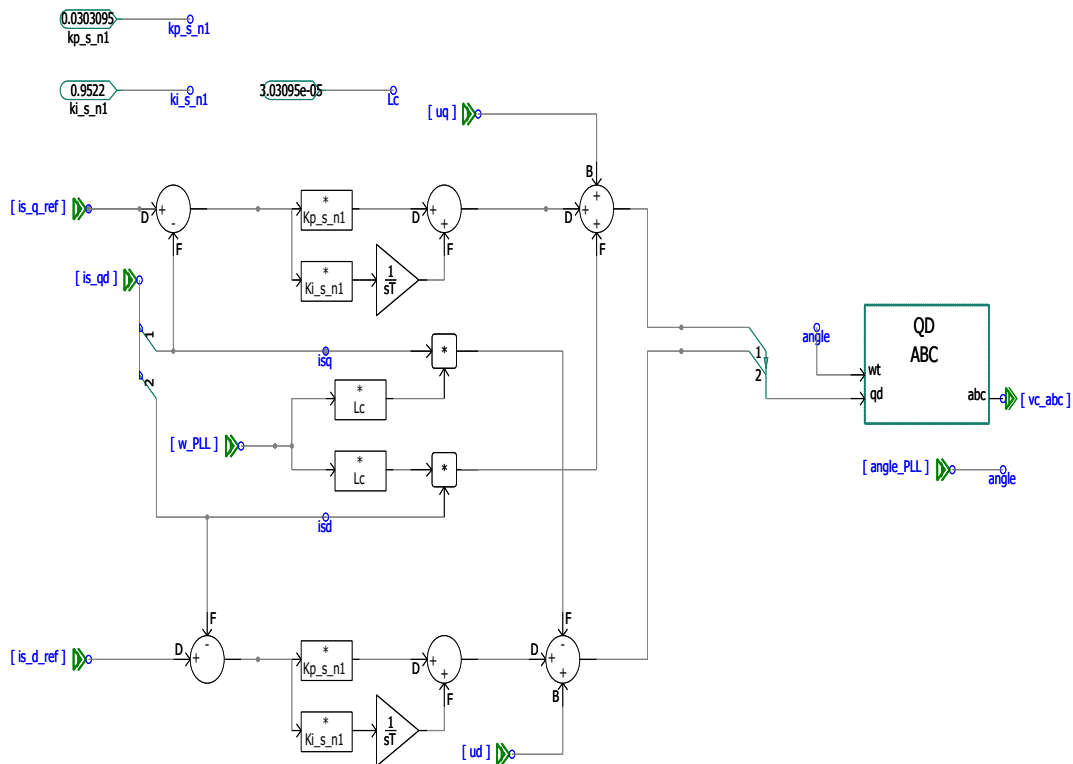


Figure 51: Grid-side current regulator in PSCAD



4.15 Grid-side controller in PSCAD (GFOR)

The grid-forming control for the converter's grid side will be detailed in this Section. A voltage controller, a current controller, a frequency or active power droop, and a voltage droop or reactive power droop comprise the grid-forming control based on cascaded control in addition to an LCL filter as stated in Section (2.10.2). Each will be discussed further below.

4.15.1 LCL filter

The LCL filter, which consists of an inductor, a capacitor, and a transformer, was chosen for the grid-forming simulation controller in this simulation. LCL filters are typically used in systems with low voltage magnitudes and 2-level or 3-level VSCs. The capacitor's presence is intended to decrease harmonic injection. The considered values for the filter are as follows:

$$\begin{aligned} Z_{base} &= \frac{V_c^2}{S_c} \\ R(pu) &= (1\%)Z_{base} \\ X(pu) &= (15\%)Z_{base} \\ C(pu) &= (15\%)Z_{base} \end{aligned} \tag{83}$$

4.15.2 Voltage controller

The fundamental objective of this controller, which regulates grid voltage in the qd frame, is to repel disturbances. Large disruptions like a shift in power or the disconnecting of a generator might have an impact on the system. If these conditions occur, the grid-forming control should operate as a voltage source. The control must therefore reduce the fluctuations. The method of calculating controller values is as follows:

$$\begin{aligned} K_p(v) &= 5.5 \frac{I_n}{V_{base}} \\ K_i(v) &= 200 \frac{I_n}{V_{base}} \end{aligned} \tag{84}$$

4.15.3 Current controller

The current controller's control approach in a cascaded control is the internal model control (IMC), which uses two PI controllers plus a decoupling loop to track the current in a time set. It is analogous to the grid-following current regulator. Equations (68) and (69) may be used to determine the proportional and integral constants of the PI controller while $\tau = 1ms$, however, in this case, new filter values must be taken into account. A full scheme of the inner controller of the grid-forming controller is illustrated in Fig. 52.



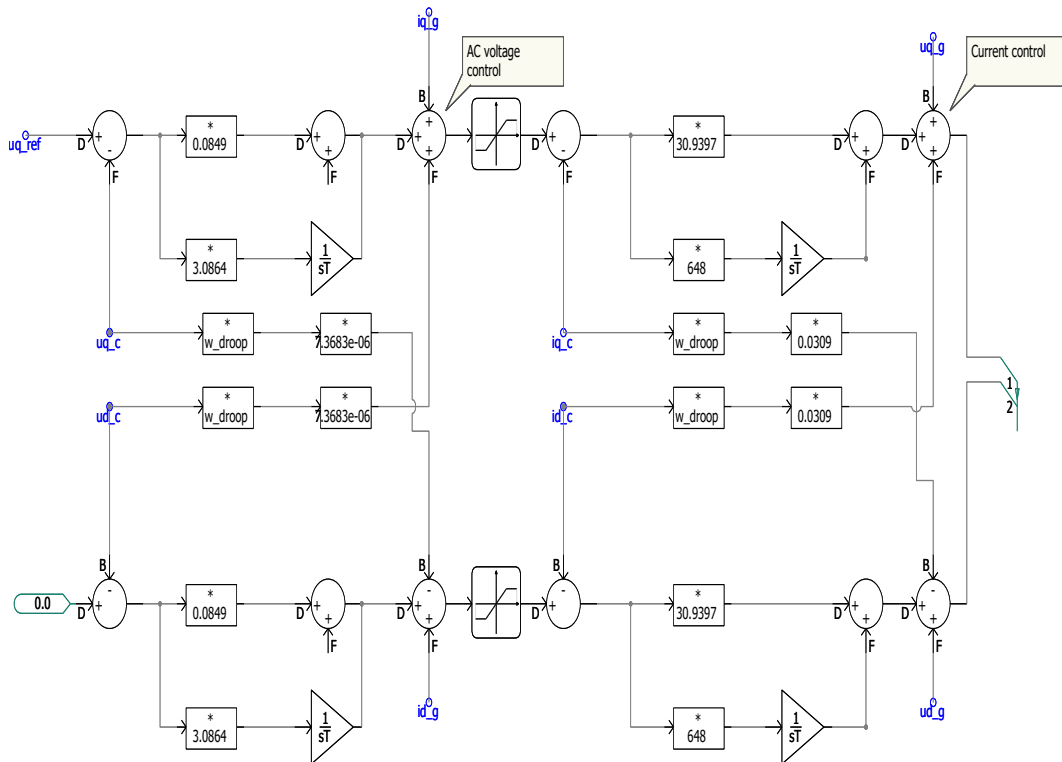


Figure 52: Inner loop controller of the GFOR converter in PSCAD

4.15.4 Active power droop

The converter’s phase and the power exchanged are controlled by the active power droop. The swing equation or a power frequency droop can be used for this control. This control includes virtual inertia, which enables the injection of instantaneous power when there is a change in the frequency or phase of the grid. The implemented active power droop in PSCAD is illustrated in Fig. 53. It should be highlighted that it works by comparing the converter’s output power to the reference value while the transfer function block represents the virtual inertia, multiplying the error by droop gain, and increasing or decreasing the converter’s frequency.

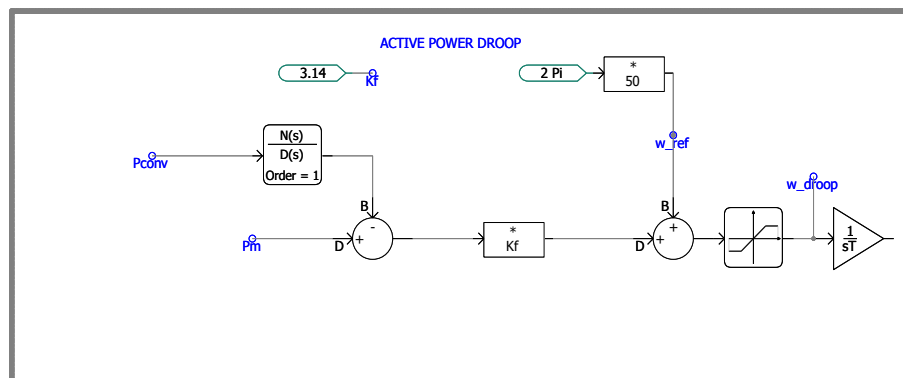


Figure 53: Active power controller of the GFOR converter in PSCAD



4.15.5 Reactive power droop

The reactive power droop serves as a voltage reference provider for the voltage controller in that the difference between the converter's measured output reactive power and the reactive power reference is multiplied by the droop gain, which causes the voltage reference to be increased or decreased.

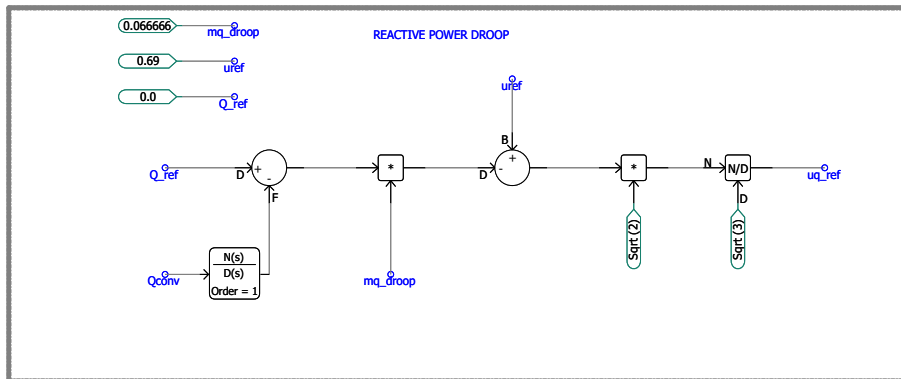


Figure 54: Reactive power controller of the GFOR converter in PSCAD



4.16 Machine-side controller in PSCAD

The Machine-side controller's control structure in PSCAD is created using the Simulink model that is currently in use. It consists of a current reference computer, Qloop, a park, an inverse park transformer, and rotational speed measurement. The author chose to synchronize the machine model first before implementing the controller since creating this controller is quite challenging due to the difference between the permanent magnet machine in PSCAD versus Simulink.

4.16.1 Rotational speed measurement in PSCAD

Since the PSCAD permanent magnet machine delivers speed in p.u., conversion is required. As demonstrated below, the machine's output speed measurement will multiply by the generator's nominal speed before being multiplied in pair poles to produce the machine's synchronous speed. To mention that the park and inverse park transformers will receive the rotor's angle directly from the machine output, so no conversion is required there.

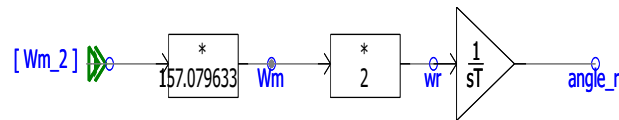


Figure 55: Rotational speed measurement in PSCAD

4.16.2 Current reference calculation in PSCAD

The active and reactive current reference i_q^* and i_d^* computer in PSCAD is implemented similarly to Section (4.8.3) and it sketched in Fig. 56. Since PSCAD functions with values such as kV and kA so obtained i_q^* must be in kA as well.

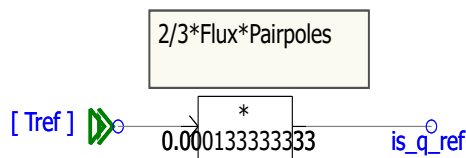


Figure 56: Machine-side current reference computer in PSCAD



4.16.3 Machine-side current regulator in PSCAD

The machine-side current regulator decouples the voltage qd values as stated in Section (2.8) and to build that model in PSCAD, similar steps as Section (4.8) were taken into consideration. It is demonstrated in Fig. 57.

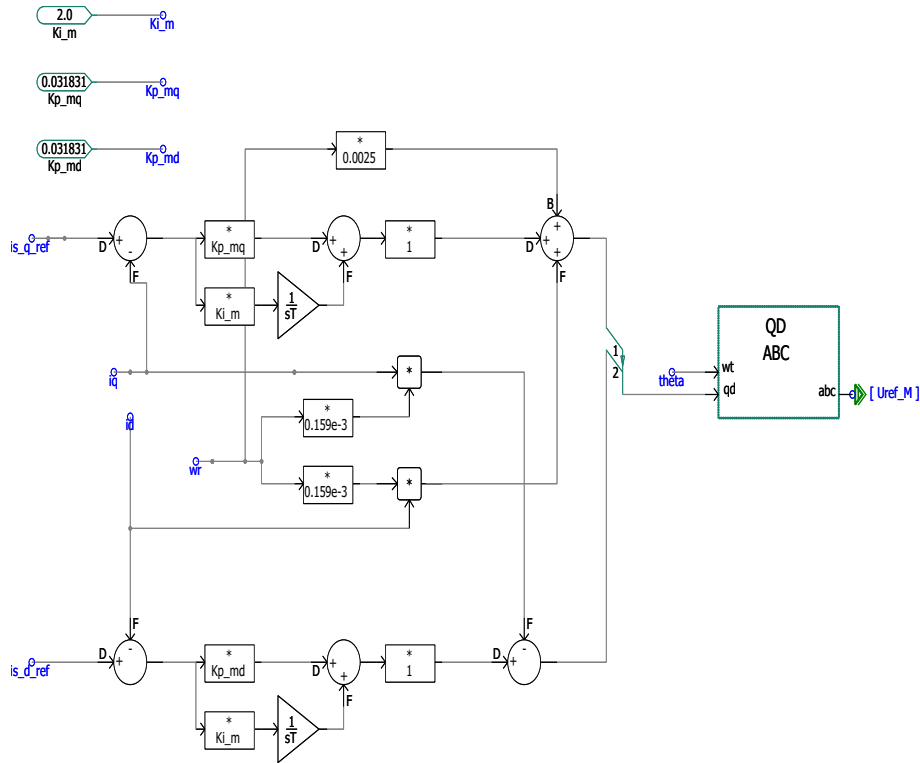


Figure 57: Machine-side current regulator in PSCAD



4.17 Automatic initialization in PSCAD

In MATLAB/Simulink, all that is needed to run and simulate the model is to deliver the data in the workspace and read those data in the Simulink area; however, in PSCAD, this must be done using Python, a programming language that is frequently used nowadays which can receive data and send them to PSCAD.

The main objective of the automatic initialization of wind turbine Type4 is to prepare all of the data in the Python area and then, by pressing the run button, all of the data will be sent to PSCAD and the simulation will begin to run and give the results. However, in the case of IEEE 9-bus, in addition to providing data for a wind turbine, the Python code must also be able to read data from PSSE raw files or any results from any other power flow software and send those data to PSCAD.

4.17.1 Providing wind turbine model's data

For the wind turbine model, PSCAD requires the following parameters: wind turbine characteristics, PMSG, grid, dc-link, converter, and its control. The parameters of a wind turbine to show as an instance, such as air density, turbine power, blade diameter, and others, are presented, as can be seen in the example below.

```
#Defining parameters of the Wind turbine
rho=1.225           #Air density in (kg\m^3)
Pn=5               #WT nominal power in (MVA)
rt=44             #WT diameter in (m)
wrat=314.1592     #WT nominal mechanical speed in (rad\sec)
A=math.pi*rt**2  #Rotor area in (m^2)
Gr=80.1          #Gearbox ratio
Ge=1             #Gearbox efficiency in (pu)
```

4.17.2 Reading the data from power flow results

PSSE, Digsilent, Matpower, and other software can be used to perform power flow. In this study, it was chosen to utilize PSSE raw file format, which can be created by PSSE software and also retrieved with the same format via Matpower, which is used in this case because of the ease of access to MATLAB as compared to PSSE.

The method is to execute the power flow code in MATLAB, which will produce the power flow results of the IEEE 9-bus as "case9," and then store the results in PSSE raw file format, which can be utilized by Python code to apply into PSCAD. After saving the data in raw format, the data for each component may be acquired and assigned using Python's "grg pssedata" package, which reads and splits the raw file data. An example code for dividing and assigning raw file data in Python is displayed below.

```
#Defining Generators parameters from raw file
vt1=(data.buses[0].vm)           #Initial voltage magnitude of G1
vt2=(data.buses[1].vm)           #Initial voltage magnitude of G2
vt3=(data.buses[2].vm)           #Initial voltage magnitude of G3
ph1=(data.buses[0].va)           #Initial phase angle of G1 in (radians)
ph2=((data.buses[1].va)*0.0174533) #Initial phase angle of G2 in (radians)
ph3=((data.buses[2].va)*0.0174533) #Initial phase angle of G3 in (radians)
```



```

pg1=(data.generators[0].pg)           #Initial active power of the G1
pg2=(data.generators[1].pg)           #Initial active power of the G2
pg3=(data.generators[2].pg)           #Initial active power of the G3
qg1=(data.generators[0].qg)           #Initial reactive power of the G1
qg2=(data.generators[1].qg)           #Initial reactive power of the G2
qg3=(data.generators[2].qg)           #Initial reactive power of the G3

```

As can be seen from the code above, the "grg pssedata" package names each column of data before printing the data required by calling the appropriate row number. The voltage of the generator, for instance, is available in the bus data section and the generator data section of the raw file. The voltage column is then given the name "vm" by the mentioned package, and all that is left to do is to write the number of the row, which in this case is 0 and denotes the first row of data.

4.17.3 Sending the data to PSCAD model

Once all of the necessary data has been prepared, it can be sent to PSCAD. The Type IV wind turbine model alone and the Type IV wind turbine model coupled to the IEEE 9-bus system were the two models in this study that were initialized using the same technique. Due to the solo wind turbine model's inclusion in the IEEE 9-bus example, the wind turbine Type IV initialization will also be addressed while discussing the IEEE 9-bus case.

The library *mhi.pscad*, which is compatible with PSCAD version 5.0.1, is utilized in conjunction with Python version 3.7 for this study. It is necessary to manually get each component's id in the PSCAD area in order to be able to send data to PSCAD components. In order to achieve this, Python will collect the data from the PSCAD model's primary canvas using the Canvas function, and after assigning the data as described in Section (4.15.2), the data will be sent to PSCAD. Here is an illustration of how Python combines the elements and the data.

```

# Get the "Main" canvas
main = project.canvas('Main')

#Getting Generators Datas
G1 =project.component(148919121)
G2 =project.component(1869282479)
G3 =project.component(1614675867)
# Sending Generators datas
G1.parameters(VT=vt1,Pheta=ph1,P0=pg1,Q0=qg1)
G2.parameters(VT=vt2,Pheta=ph2,P0=pg2,Q0=qg2)
G3.parameters(VT=vt3,Pheta=ph3,P0=pg3,Q0=qg3)

```

To demonstrate how to retrieve manually the component id, Fig. 58 illustrates the G1 id, which is also used in the code above. To obtain the attribute of each component, simply right-click on the component icon and choose attributes.



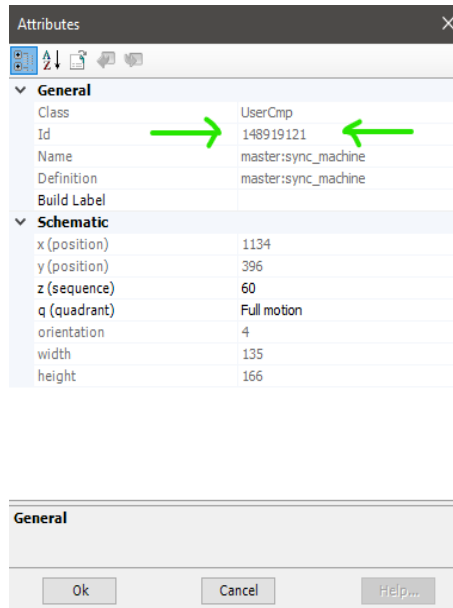


Figure 58: The attributes of the Generator 1

4.18 IEEE 9-bus system

The IEEE 9-bus system is chosen in order to assess the behavior of the system by connecting the built wind turbine to it while the wind turbine Type IV is linked to the network. Fig. 59 shows the IEEE 9-bus schematic.

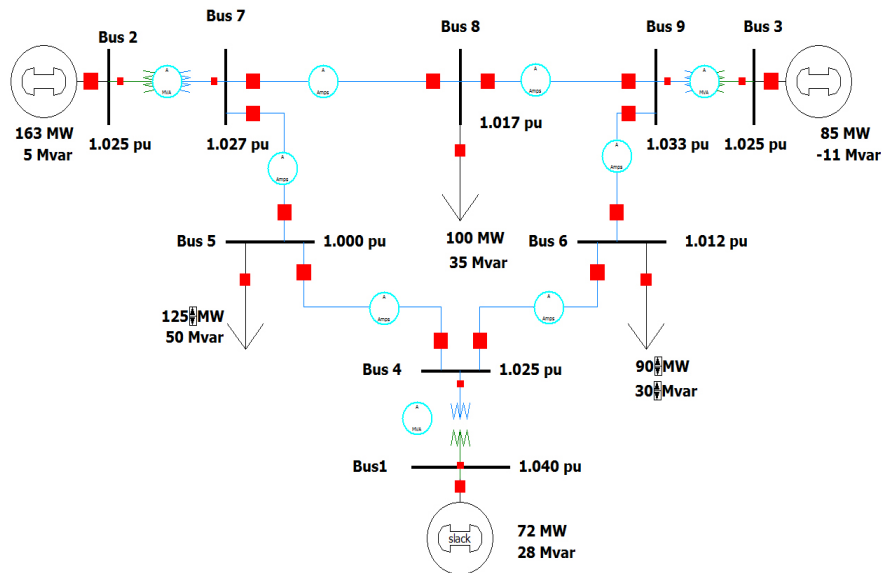


Figure 59: IEEE 9-bus system [1]

In a power system, there are three types of buses, Slack, PV, PQ. Each will be briefly explained.



- Slack bus

The purpose of the slack bus is to balance the active and reactive power in the system. It is also referred to as the Reference Bus or the Swing Bus. The slack bus, which its angle is considered at zero degrees, will act as an angle reference for all other buses in the system. At the slack bus, the voltage magnitude is similarly assumed to be 1 p.u. Due to the fact that active and reactive power won't be known for sure until the final solution is determined, the slack bus supplies or absorbs active and reactive power to and from the transmission line to compensate for losses. The only bus for which the system reference phase angle is known is the slack bus. A generator bus with the highest active power serves as the slack bus if a slack bus is not specified [54].

- PV Bus

The active power and voltage magnitude are defined in this type of bus which is commonly referred to as a Generator Bus. For buses that are generators, the active power and voltage are indicated. These buses feature a continuous power production that is regulated by a prime mover, as well as a constant bus voltage [54].

- PQ Bus

Real power and reactive power for PQ or load buses are known, but bus voltage magnitude and phase angle are unknown. The bus voltage should be determined using power flow analysis. The voltage at the load bus may vary approximately to 5% [42].

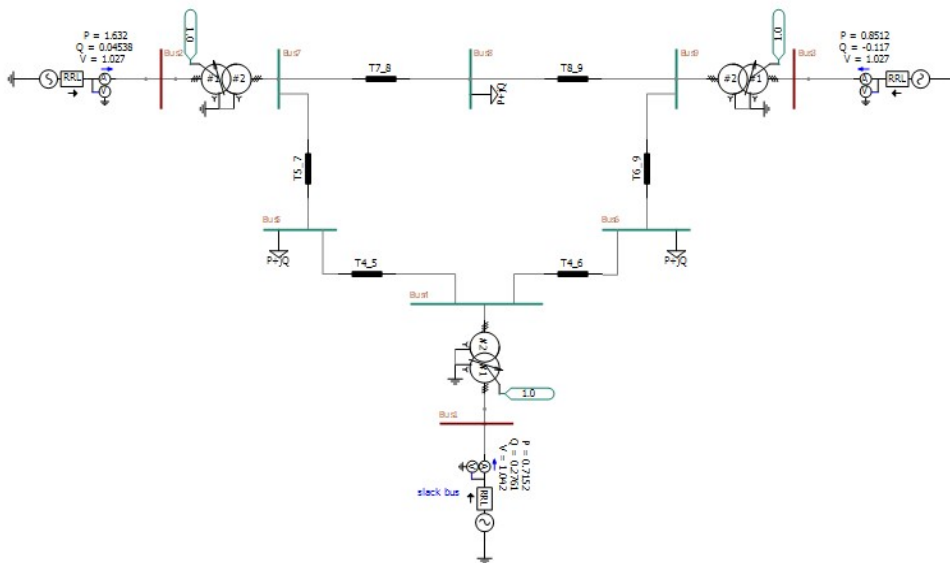


Figure 60: IEEE 9-bus system in PSCAD

As can be seen in Fig. 60, the IEEE 9-bus system consists of 3 generators, 3 loads, 6 power lines, 3 transformers, and 9 buses. Normally after running the power flow, the results must be compared with results in software such as PSSE, Matpower and etc in order to be sure about the model



Table 8: Terminal conditions of IEEE 9-bus system

BUS	V[pu]	D[deg]	P[pu]	Q[pu]
1	1.04	0	0.7163	0.2791
2	1.025	9.3507	1.63	0.049
3	1.025	5.142	0.85	-0.1145

Table 9: Transmission line characteristics of IEEE 9-bus system

From Bus	To Bus	R[pu\m]	X[pu\m]	B[pu\m]
4	5	0.01	0.0680	0.176
4	6	0.017	0.092	0.158
5	7	0.032	0.1610	0.306
6	9	0.039	0.1738	0.358
7	8	0.0085	0.0576	0.149
8	9	0.0119	0.1008	0.209

Table 10: Load characteristics of IEEE 9-bus system

BUS	P[pu]	Q[pu]
5	1.25	0.5
6	0.9	0.3
8	1	0.35

has been built properly. The required parameters are illustrated in Tables 8, 9, and 10.

In the IEEE 9-bus benchmark model, as shown in Fig. 60, the generators are configured as voltage sources rather than synchronous generators. To achieve more realistic results, it has been decided to replace the voltage sources with synchronous generators, the characteristics of which will be discussed.

- Synchronous Machine in PSCAD

The selected synchronous machine in PSCAD is demonstrated in Fig. 61. It is constituted of a generator, steam turbine, exciter, and governor. The exciter controls voltage in synchronous machines, whereas the governor controls the frequency. Additionally, the steam turbine and governor are selected from the master library and connected to the synchronous machine.

- Exciter

In a generator, the exciter's primary function is to supply a stationary spinning magnetic field that is used to generate a voltage in the armature coil. Therefore, the exciter which is just a coil receives DC power and generates a magnetic field. A revolving magnetic field that cuts the stationary armature coils and induces a voltage in the stationary armature coil will be available if a mechanical supply is provided to the exciter. The exciter is a tiny generator that is positioned on the same shaft as the main generator and generates DC power for the field winding of the main generator. There are many different types of exciters, but the brushless exciter is currently the most common. An IEEE standard exciter which is referred to as DC1C with a regulator value of 50 is chosen from the PSCAD master library for this simulation [64].



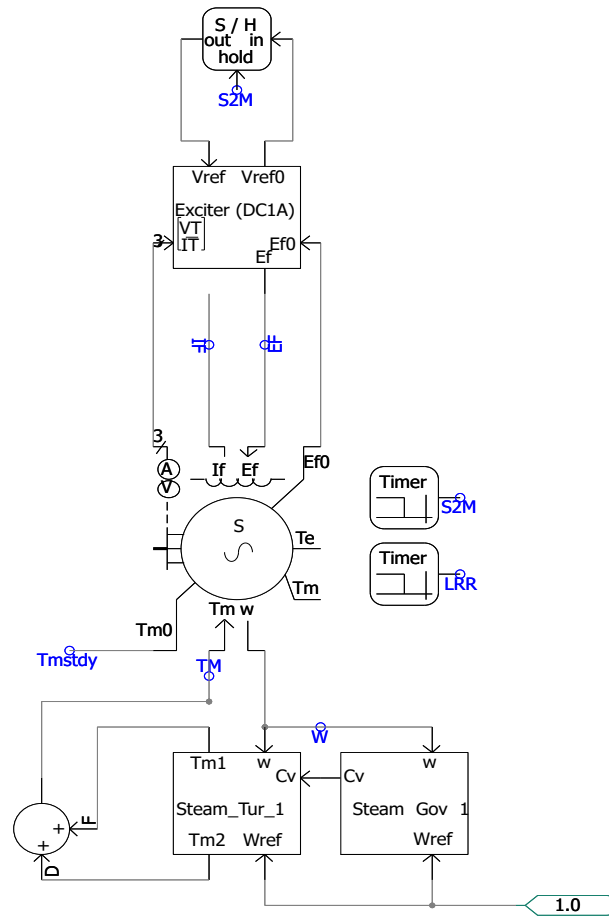


Figure 61: Synchronous machine in PSCAD

- Steam governor

The process of managing the steam flow rate to a steam turbine in order to keep its rotational speed constant is known as steam turbine governance. A steam turbine’s performance may be greatly impacted by changes in load while it is in operation. There is always a significant deviation from the desired performance of the turbine in a practical setting because the load regularly deviates from the designed or economic load. Maintaining a consistent rotational speed when operating a steam turbine is the key goal, regardless of how the load changes. It is possible to do this by controlling a steam turbine [34].



5 Results and discussion

5.1 Simplified models results

5.1.1 Results of wind turbine model in Simulink (GFOL)

In this section, the findings of the wind turbine Type IV model which was built in Simulink will be illustrated and explained. Firstly, the variation of wind speed and pitch angle and power are depicted in Fig. 62.

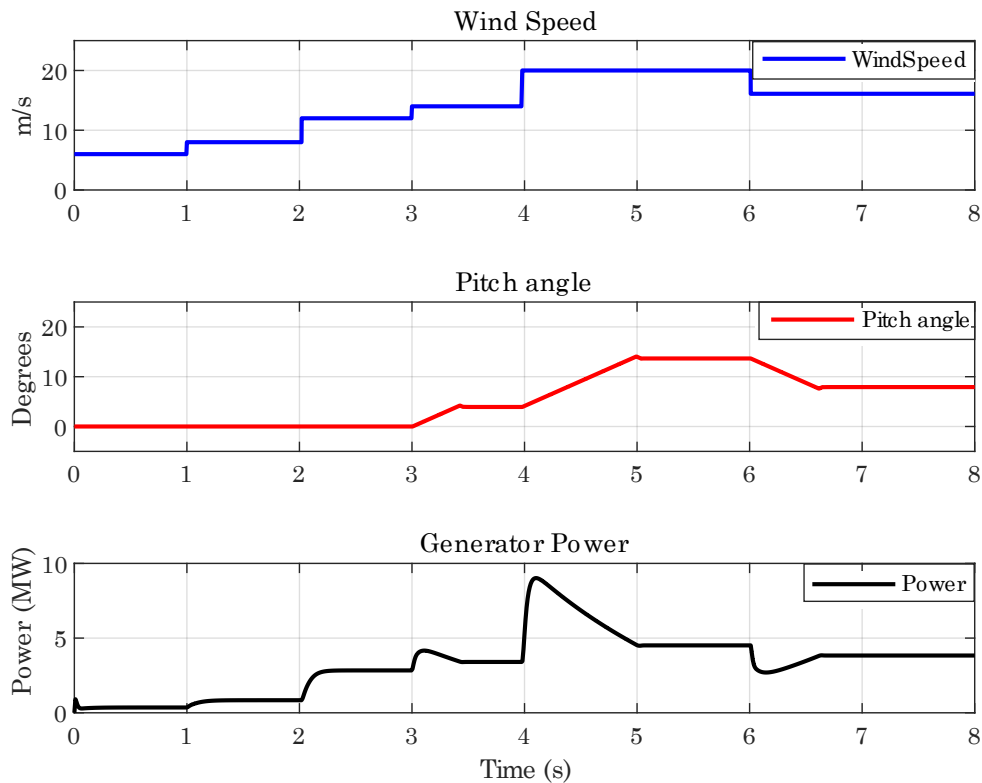


Figure 62: Wind speed, pitch angle and power variation

As shown in Fig. 62, the wind speed is increased from 6 m/s to 20 m/s and then decreased to 16 m/s in order to examine the performance of the wind turbine. While the turbine injects active power properly during the first three seconds, the pitch angle is zero, which means there is no power curtailment. However, in the second three, when the wind speed increases to 14 m/s, the pitch angle activates and controls the power in order to keep the machine operating at its nominal levels. The pitch angle increases to about 15 degrees between four to six seconds when the wind speed is at 20 m/s, which that is relatively a high value compared to the nominal wind speed. It is important to note, even so, that when the wind speed rises to 20 m/s, the pitch angle reaction is much slower than the wind speed spike, so power can exceed the nominal value in less than a second. This problem can be resolved by the presence of a current limit in the dc link which in this model is not considered. It is clear from focusing on 5 to 6 seconds that the pitch angle retains power below 5 MW, which is the desired behavior. The wind speed then decreases by 16 m/s, causing the pitch controller to ease off by 8 degrees, so reducing the power curtailment.



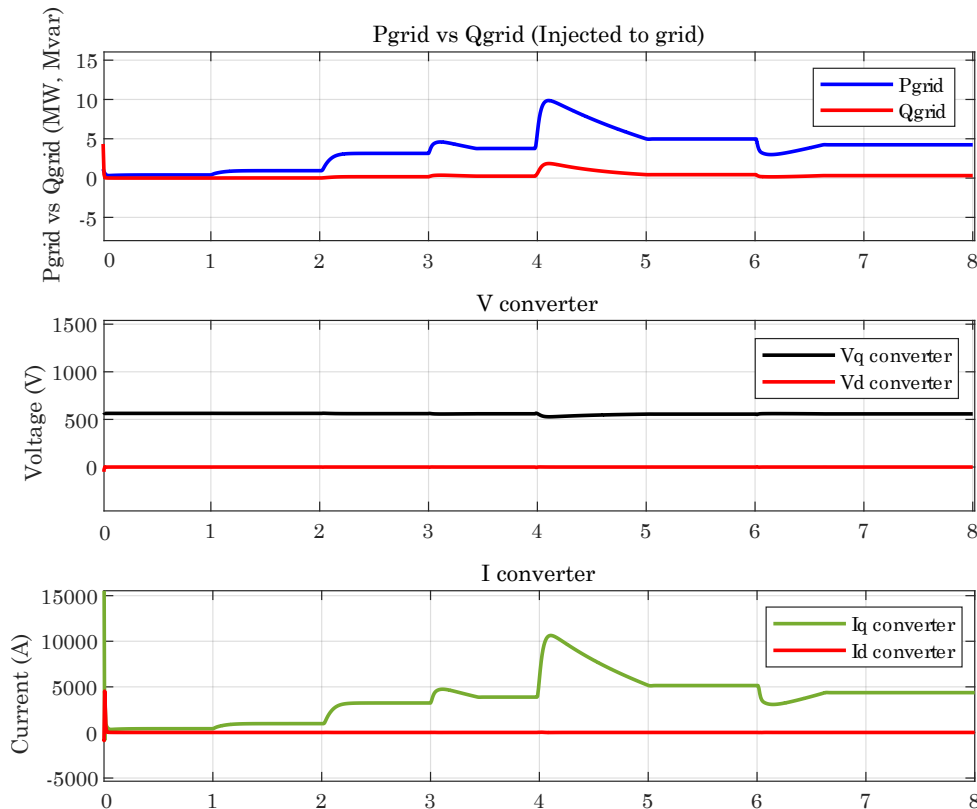


Figure 63: Variation of grid-side power, voltage, current

According to Sections (3.3) and (3.4), the dc voltage regulator is responsible for injecting active power, and Q-loop is in charge of injecting reactive power. Although the reference value for reactive power in this simulation is set to zero, some reactive power will still be injected during the active power exchanges, which is acceptable. The active injected power is significantly reliant on wind power, as can be observed in Fig. 63, and its variation demonstrates this. As previously stated, the control framework for this simulation is grid-following, therefore this wind turbine will operate similarly to a PQ bus and only inject its active and reactive power. As a result, it cannot impose its own voltage. As observed in the converter voltage graph, the PLL keeps the voltage level at the grid level while the only variable is the current in line with the machine side's active power generation.

The relationship between wind speed, pitch angle, and power coefficient in a wind turbine is depicted in Fig. 64. Equation (7) states that power and wind speed has a cubic relationship; hence, when wind speeds are below nominal power, the power coefficient is about at its maximum, and vice versa for pitch angle. According to (4) and (5), the power coefficient decreases as the pitch angle rises as the wind speed increases and exceeds the nominal wind speed. The greater the pitch angle rises, the smaller the power coefficient will be.



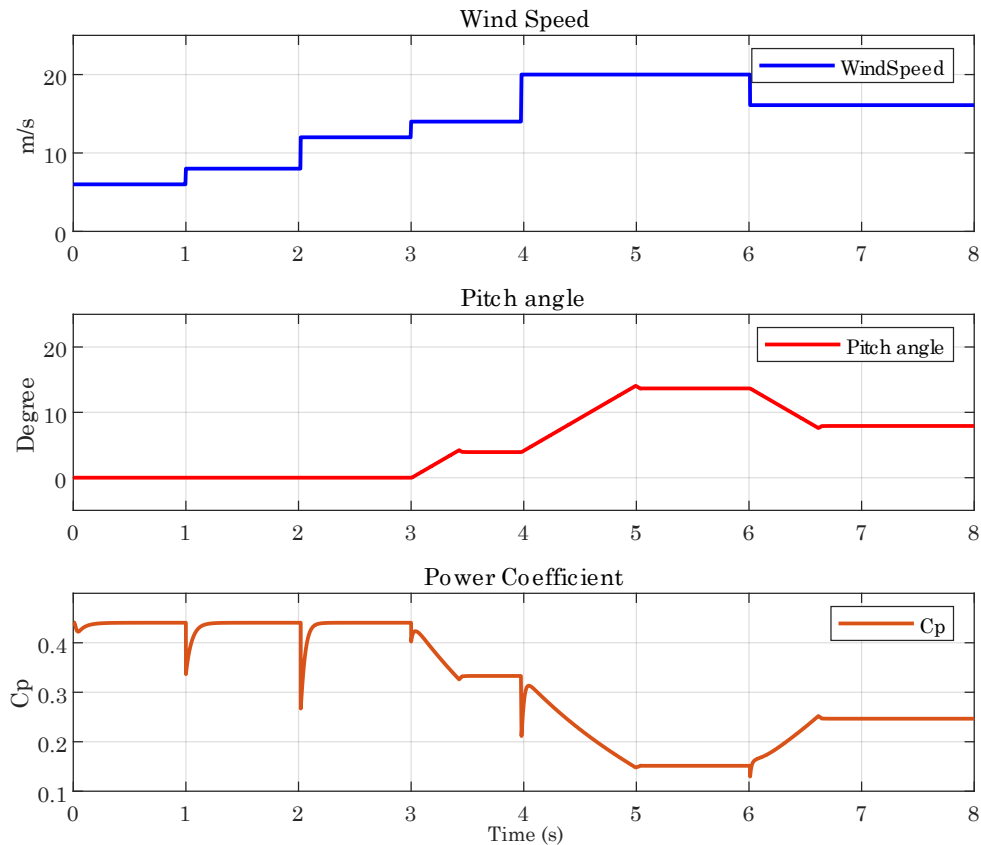


Figure 64: Relation of wind speed, pitch angle, and power coefficient

5.1.2 Results of wind turbine model in PSCAD (GFOL)

In this part, the model which is built in PSCAD software will be investigated. To analyze the model in a realistic condition a wind speed data set that is similar to the actual wind blowing characteristics is provided and given to the wind turbine as it is shown in Fig. 65. The range of the wind speed is between 6–16 m/s, although the change over time is rapid, which is caused by the wind's recognizable gusts and noises. By concentrating on pitch angle variation and generated power, it is evident that pitch angle controls excess power that might hurt the machine while also taming abrupt changes in wind speed.

The grid-side voltage and current are displayed in qd form in Fig. 65, for convenience. The grid's control structure is designed to inject both active and reactive power, as was stated in the Section before, and voltage is steady because of PLL. While the current varies as the wind speed varies, the grid-side voltage is nearly constant and the dc regulator maintains the dc-link voltage constant as well, as can be seen in Fig. 66. Because this is the predicted behavior, the model may inject power by maintaining the voltage in accordance with the reference.



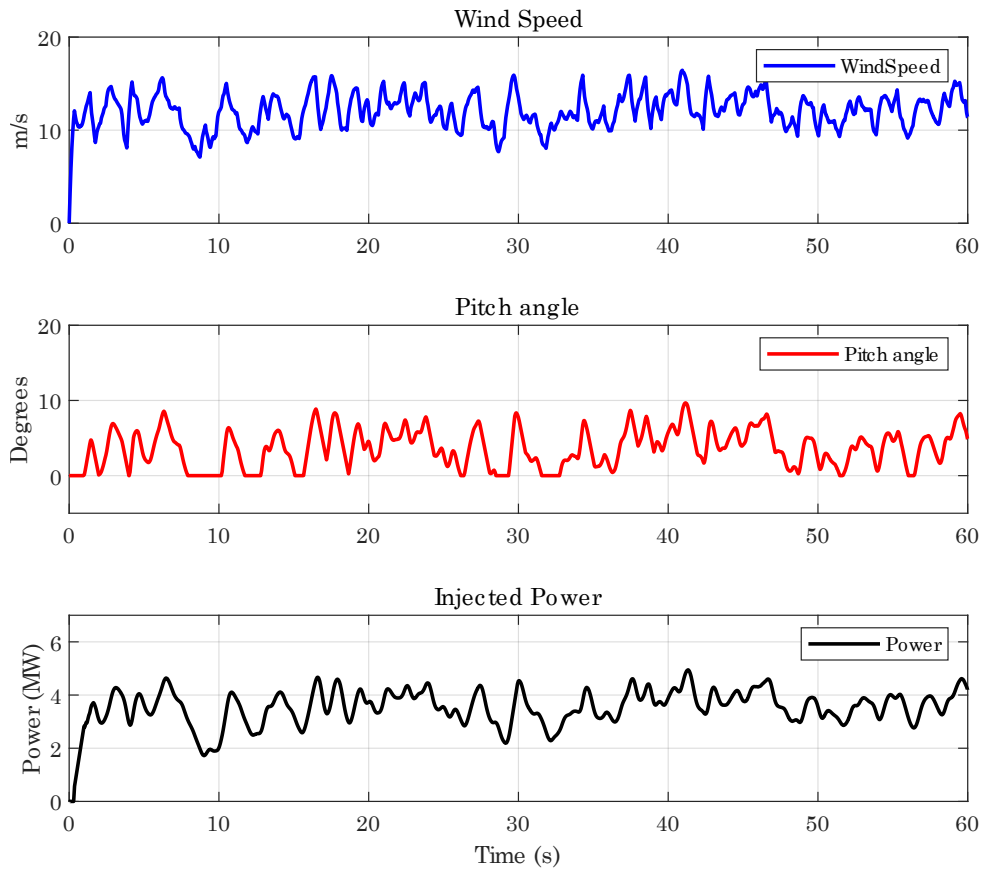


Figure 65: Wind speed, pitch angle and power variation in PSCAD (GFOL)

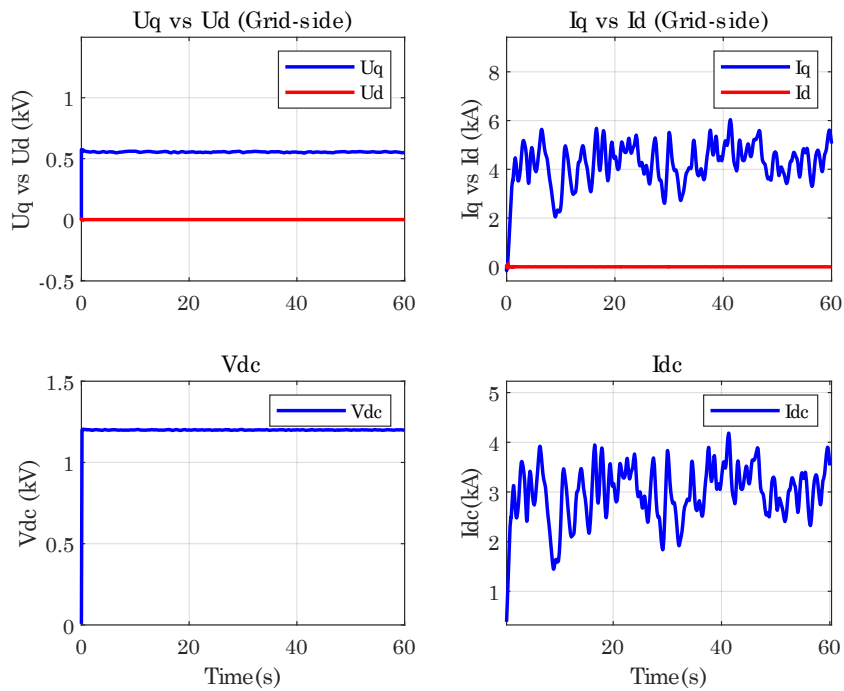


Figure 66: Variation of grid-side voltage and current and dc-link in PSCAD (GFOL)



To assess the control response of the Type IV wind turbine model in PSCAD to a symmetric fault, a 0.01Ω during 50 ms has been embedded to the point of connection of the wind turbine with grid, the fault is enabled at 30 seconds. Fig. 67 demonstrates that the power injected at the time of the fault leaps, but because of the embedded limits and dc chopper, the controller prevents the system from spinning out of control. Fig. 68 also shows how the fault affected the system and the system could recover. In Fig. 69 When a fault occurs at 30 seconds, the converter voltage drops while the current tends to increase to a significant value, but this is controlled by limits, and by focusing on the converter power graph, it can be deduced that the fault mostly requires reactive power, which is why reactive power increases while active power reduces. When a failure occurs and the converter is unable to inject active power, the remaining active power in the dc-link tends to increase the dc voltage, as shown in Fig. 69, but the embedded dc chopper connected to the dc-link dissipates that power in order to keep the dc voltage within an acceptable range.

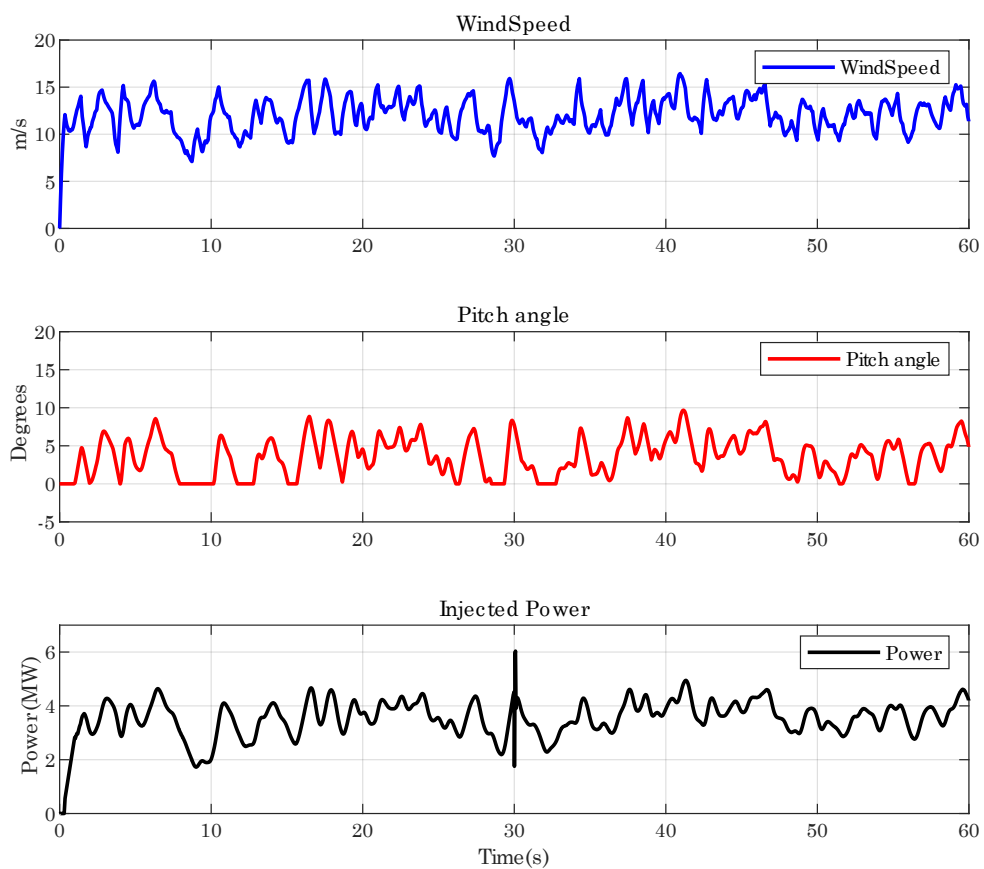


Figure 67: Wind speed, pitch angle and power variation in PSCAD (GFOL) during the fault



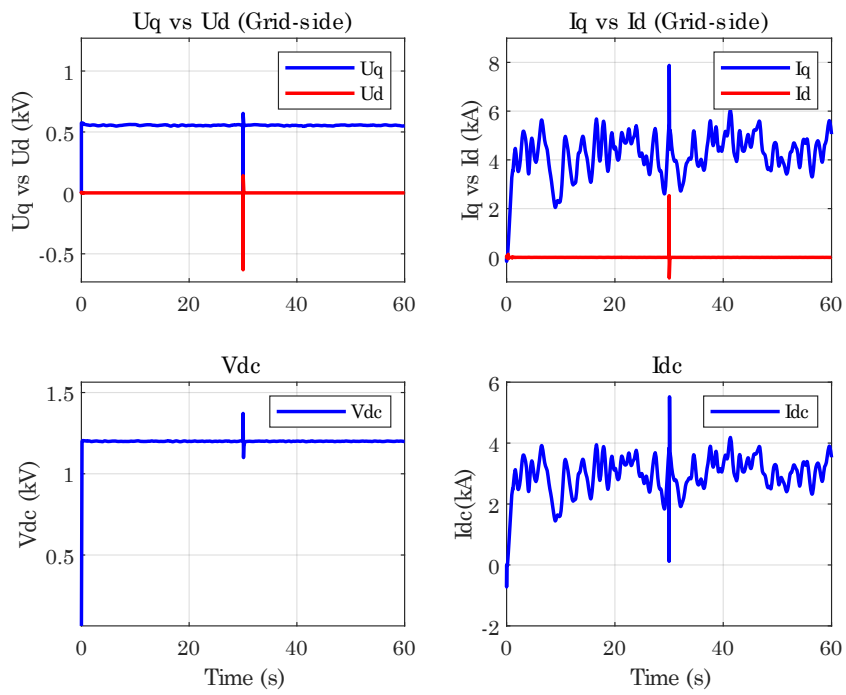


Figure 68: Variation of grid-side voltage and current and dc-link in PSCAD (GFOL) during the fault



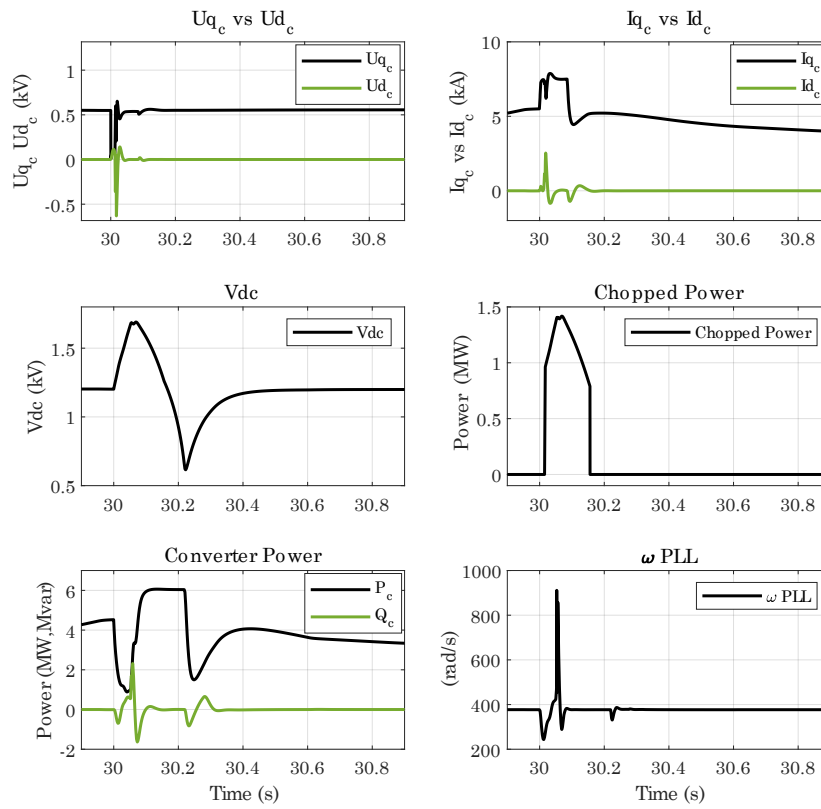


Figure 69: Variation of grid-side voltage and current, dc voltage, and chopped power in addition to converter power and PLL angular speed in PSCAD (GFOL) during the fault



5.1.3 Results of wind turbine model in PSCAD (GFOR)

The wind turbine model which is created in PSCAD will be investigated using a GFOR control based on droop based with cascade control at the grid-side VSC. The identical circumstances as in Section (5.1.2) are applied and results will be displayed and discussed. In GFOR control, the dc-bus voltage will be regulated with a dc voltage source which is a key difference compared to GFOL control where the dc-bus voltage is controlled by the grid-side controller.

According to Fig. 71, a wind turbine with GFOR control may inject power similarly to a GFOL control, but there are changes due to the influence of virtual inertia, which causes the capacitor at the dc-link to serve as a deposit, which is why the Vdc voltage increases at intervals. When the dc-link voltage rises, there is an unbalance between the injected and generated power, so the capacitor voltage increases and absorbs that energy, but only to a limited extent (no more than 30% of the capacitor voltage), and when the demand rises, the dc voltage source or a battery might cover the voltage drop in the dc-link.

Another distinction is the droop rotating speed, which, unlike in GFOL control, where the PLL rotational speed is the same as the grid, it is not constant in GFOR control. The rotating speed of the GFOR converter depends on the fluctuation of the generating power and the magnitude of the virtual inertia on which the converter imposes its angle. As can be noted in injected power graph in Fig. 70, there is power fluctuation at the beginning but after a few seconds it disappears, the reason is the nature of the GFOR control which is sensitive to the grid strength, the effect of different SCR values on GFOR control is in subsequent.

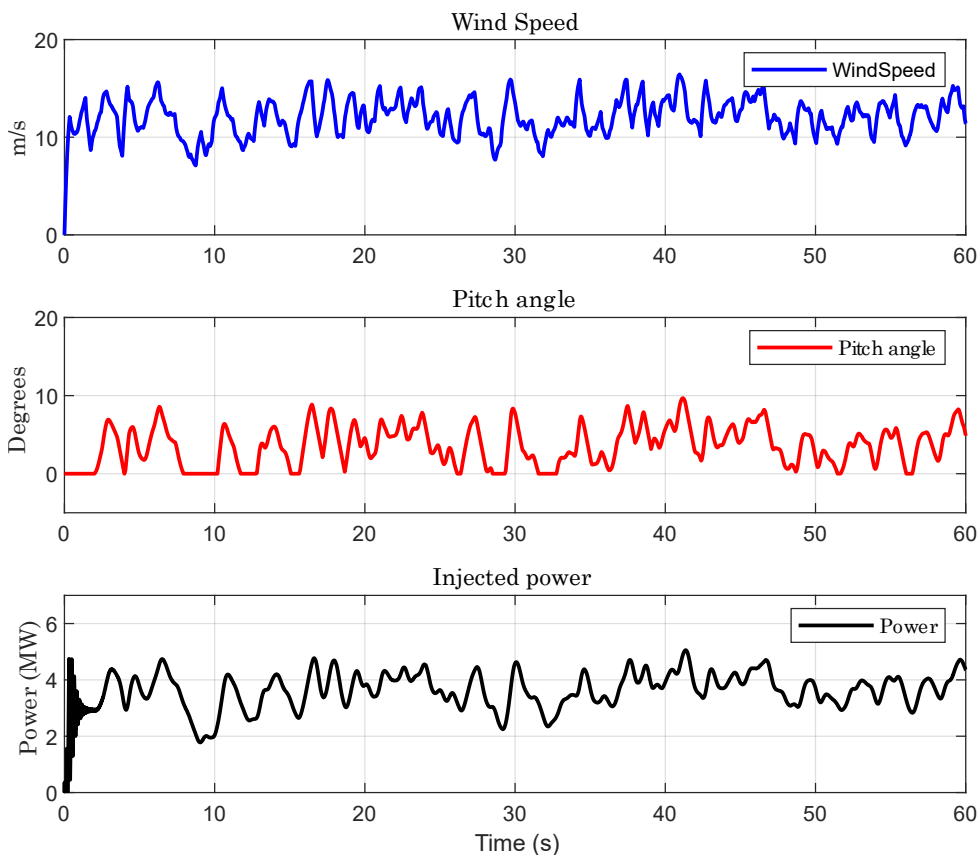


Figure 70: Wind speed, pitch angle and power variation in PSCAD (GFOR)



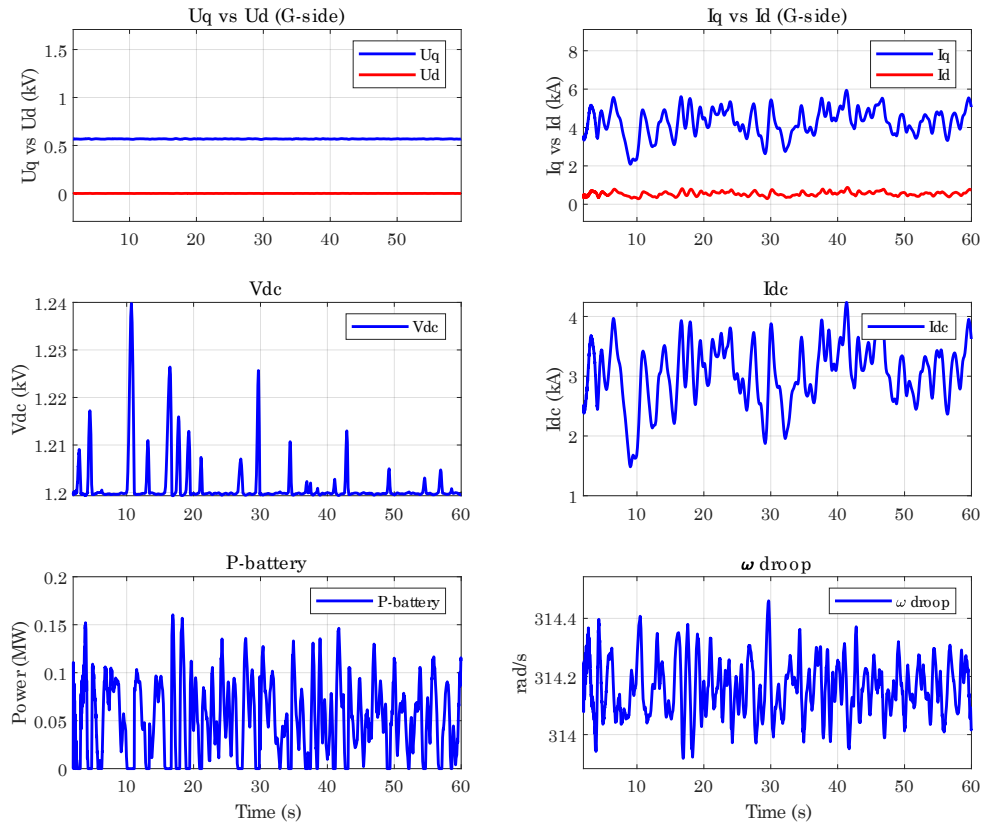


Figure 71: Variation of grid-side voltage and current and dc-link plus the injected battery power and the droop rotational speed in PSCAD (GFOR)

5.1.4 Results of simplified GFOL converter model with different grid strength

The behavior of a grid-following converter connected to the grid with various SCR ratios will be evaluated here. To mimic a real behavior of a detached machine, a regulated current source with an adequate current to meet the voltage drop need will be connected to the dc-side of the converter. It is designed to take 1 second to attain a steady state, after which the results will be shown.

- Ideal grid

Fig. 72 illustrates the results of a grid-following converter connected to an ideal grid with zero impedance. It can be noted that the converter is able to inject power without any problem. The power reaches the maximum value of 5 MW at 1 second while the PLL maintains the voltage and ω constant in accordance with the grid.



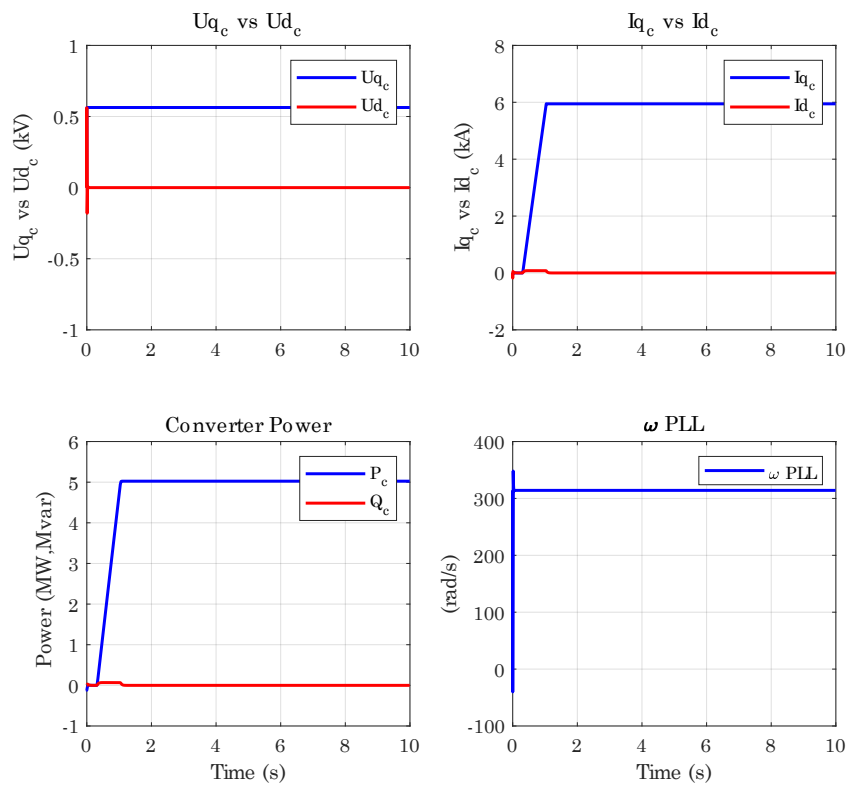


Figure 72: Voltage, current, power, and angular speed of GFOL converter connected to an ideal grid

- SCR=5

Fig. 73 reveals that there is no statistically significant difference between the ideal grid results and the grid with SCR=5, which is because a grid with SCR=5 is regarded a strong grid.



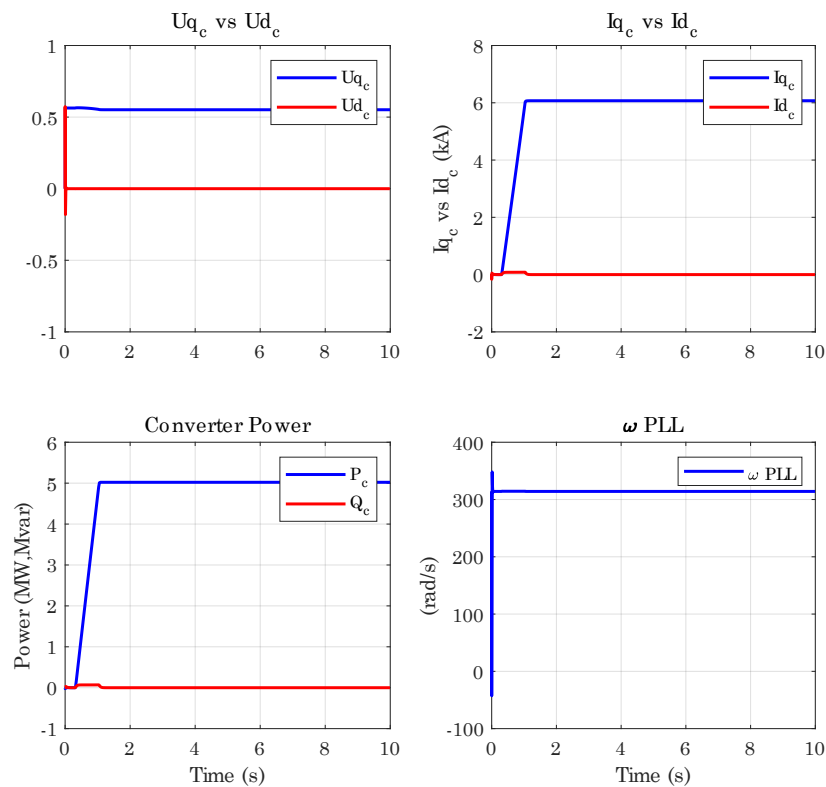


Figure 73: Voltage, current, power, and angular speed of GFOL converter connected to the grid with SCR=5

- SCR=3

By comparing the results of Fig. 73 and Fig.74 with Fig. 72 it should be observed that the greater grid impedance causes the voltage loss to rising as the grid becomes weaker and the SCR value decreases. Although there is no voltage loss when connected to an ideal grid, when connected to a grid with SCRs of 5 or 3, there is a slight voltage drop, which explains why the current in the Fig. 74 is a little greater.



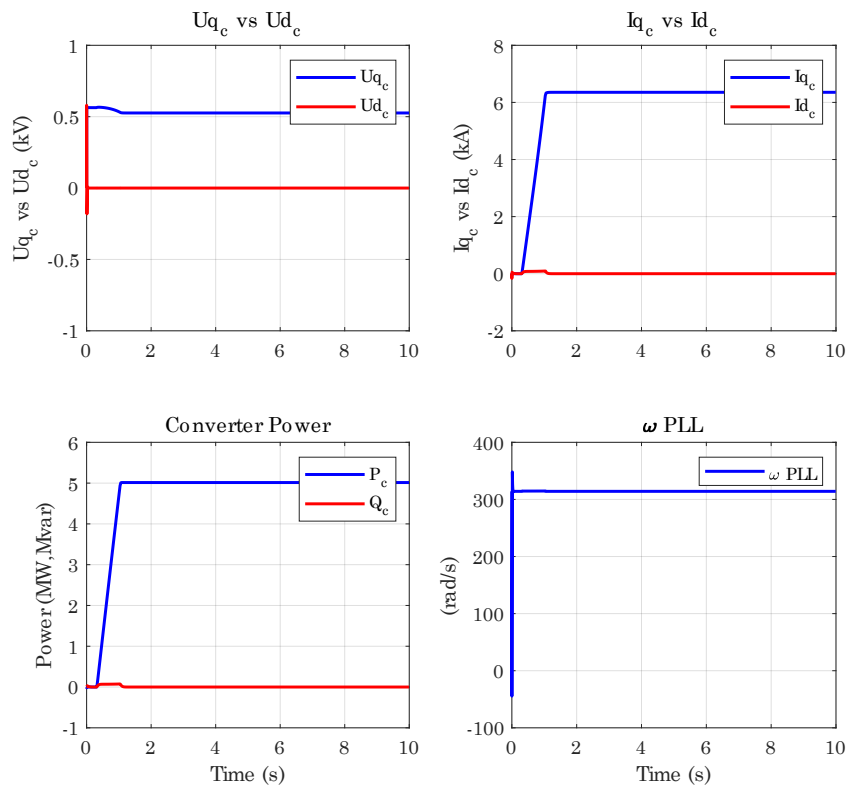


Figure 74: Voltage, current, power, and angular speed of GFOL converter connected to the grid with SCR=3

- SCR=1

Fig. 75 demonstrates why it is undesirable to use grid-following converters in weak grid conditions, such as SCR=1 or below. As depicted in Fig. 75, PLL is the primary cause of stability loss because it is unable to inject power and follow the grid when it encounters high impedance and that deters the PLL of tracking grid's angle. Therefore, this justifies the need for a grid-forming converter when dealing with weak grids.



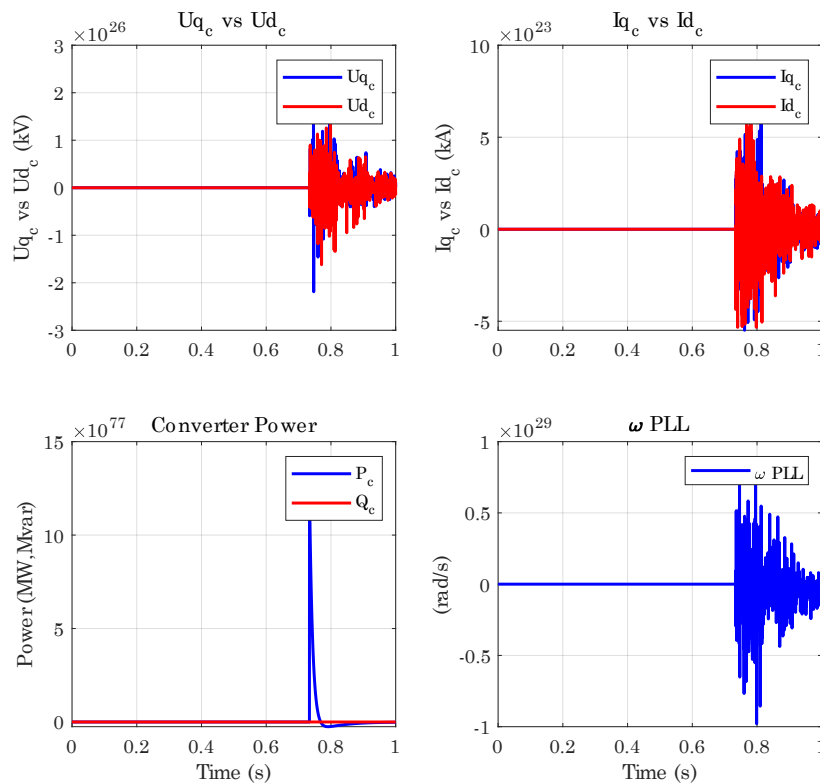


Figure 75: Voltage, current, power, and angular speed of GFOR converter connected to the grid with SCR=1

5.1.5 Results of simplified GFOR converter model with different grid strength

As per Section (2.10), the grid-forming structure is suitable in weaker grids, island mode, or even black start since grid-following converters are unable to supply power in those situations. A grid-forming converter was developed in PSCAD and linked to grids with SCR ratios of 1, 3, 5, and in addition to island mode analysis in order to explore the behavior of the converter under various grid strength situations. The findings of each experiment will be presented and analyzed separately. The converter and grid characteristics are the same as the wind turbine model just by taking into consideration $X/R = 10$ different SCR values will be calculated.

- SCR=1

SCR=1 is recognized as a very weak grid in which grid-following converters never operate in such a grid strength but as can be seen in Fig. 76 grid-forming converter can inject power while imposing its voltage without any problem.



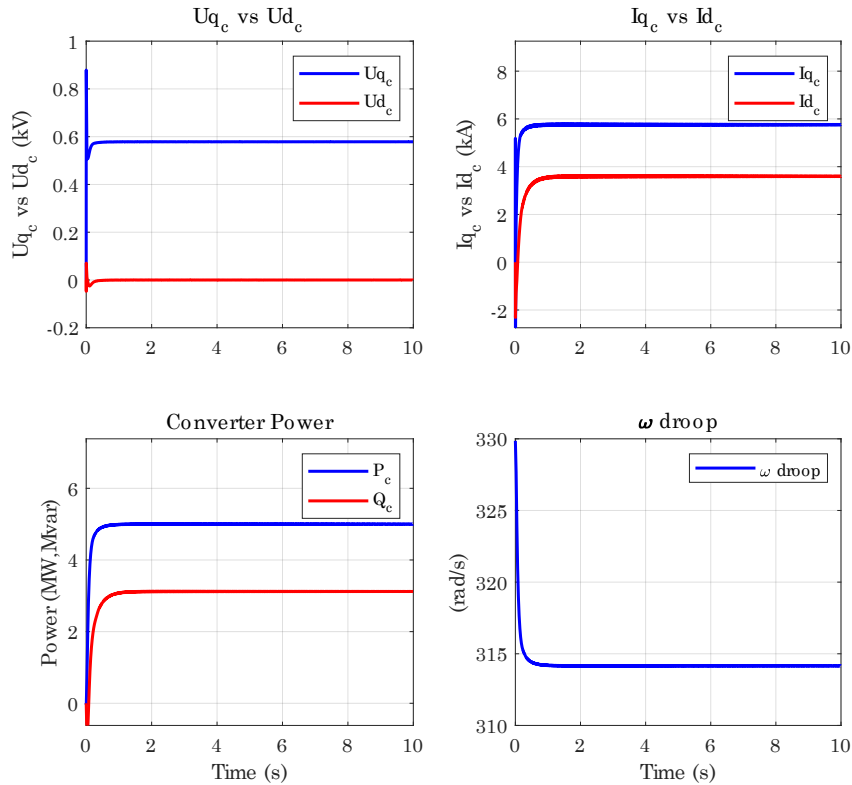


Figure 76: Voltage, current, power, and angular speed of GFOR converter connected to the grid with SCR=1

- SCR=3

Although a grid with a short circuit ratio equal to 3 is not considered a very weak grid but still not considered a strong grid neither however grid-following converters are able to work with this grid strength as well. Fig. 77 shows that implemented grid-forming converter is capable of working with a grid with SCR=3.



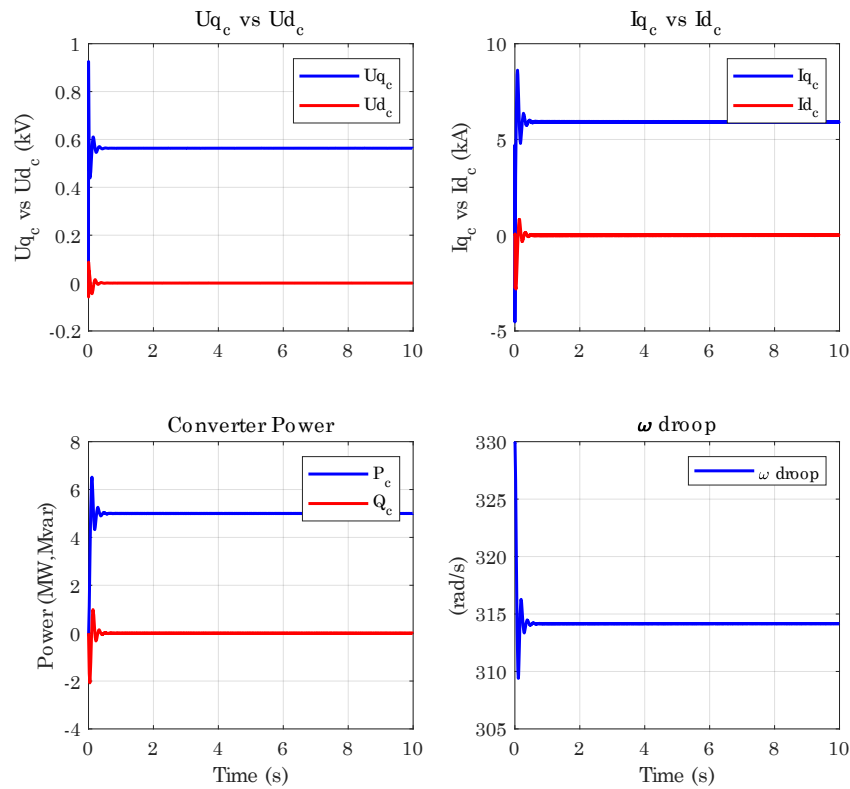


Figure 77: Voltage, current, power, and angular speed of GFOR converter connected to the grid with SCR=3

- SCR=5

By comparing the findings in Fig. 76, Fig. 77, and Fig. 78 it can be deduced that the grid-forming converter is more stable with weak grids or low SCR ratios. It should be emphasized that stronger grids can confront the grid-forming converter considerably more than weak grids, hence the cause for the instability at the start, according to Fig. 78, is related to the grid-forming converter's virtual inertia. The greater the virtual inertia value, the more difficult it is to link grid-forming converters to more powerful grids.



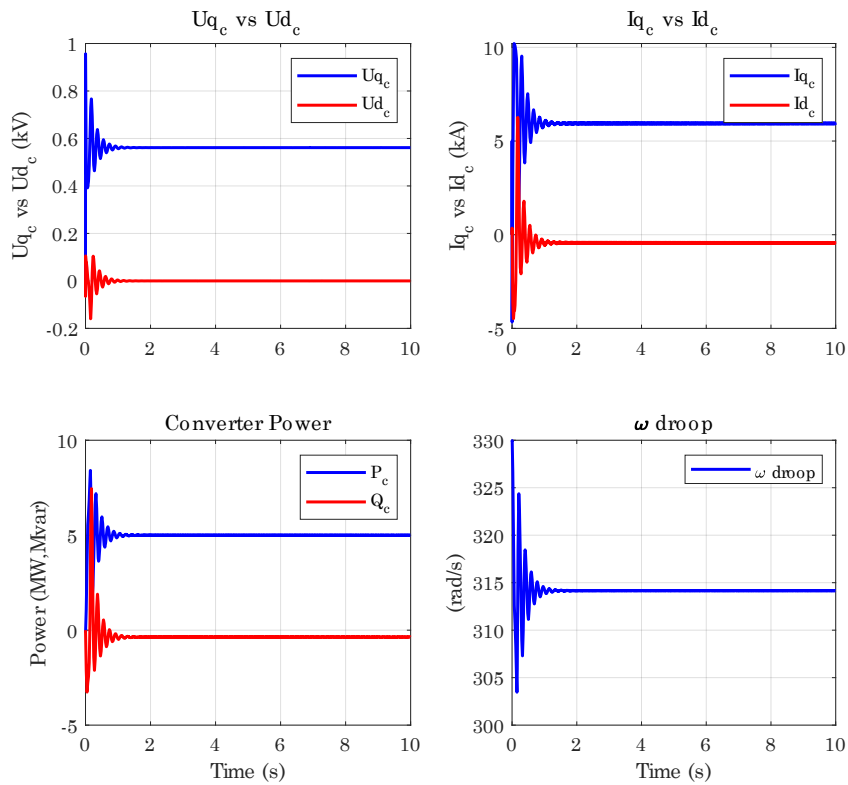


Figure 78: Voltage, current, power, and angular speed of GFOR converter connected to the grid with SCR=5

- SCR=0 or Island mode

To execute grid-forming converter island mode simulation, the grid-forming converter is connected to a grid with SCR=3 and a load of 50% (2.5 MW) of grid-forming converter power is connected between them. Feeding the load is divided evenly between the grid and the converter until the grid is removed after 5 seconds, at which point the converter will be the sole remaining source of power to supply the load.

As results shown in Fig. 79, when the grid disconnects after 5 seconds, the grid-forming converter is capable of maintaining stability and supplying the load as intended. This is accomplished as follows: immediately upon grid disconnection, the converter maintains a steady voltage while increasing current, resulting in increased power and decreased frequency.



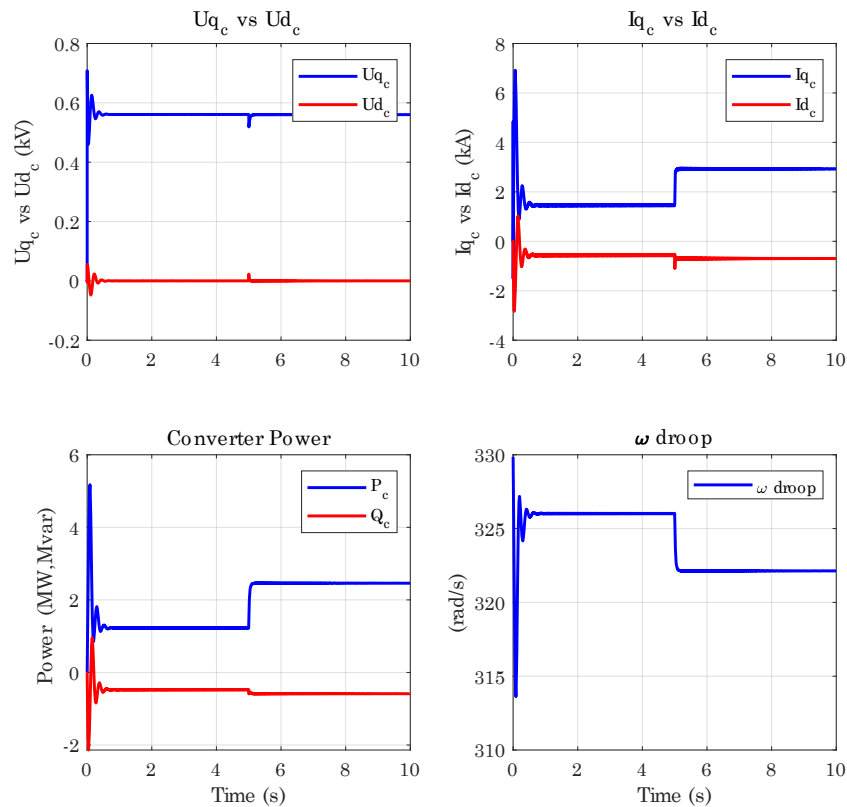


Figure 79: Voltage, current, power and angular speed of GFOR converter in island mode

5.2 IEEE 9-bus system with GFOL converter

This Section describes the IEEE 9-bus benchmark system, with the characteristics as stated in Section (4.16), plus integrating a grid-following converter to it. At first, the wind turbine with the grid-following converter will replace the generator at the PQ bus and the results will be illustrated and analyzed.

5.2.1 Normal operation

All the required parameters in order to run the power flow of an IEEE 9-bus system are illustrated in Tables 8, 10 and 9. After completing the power flow, it is necessary to check the results with those from the raw file. The model is run and the values are displayed in this phase.

Two synchronous generators are connected to the Slack bus and the PV bus alongside the grid-following converter which is linked to the PQ bus and the power flow results are indicated in Fig. 80. When comparing the findings to the raw data, it is clear that the active and reactive power levels agree with the raw data but the voltage remains slightly below the raw data value.



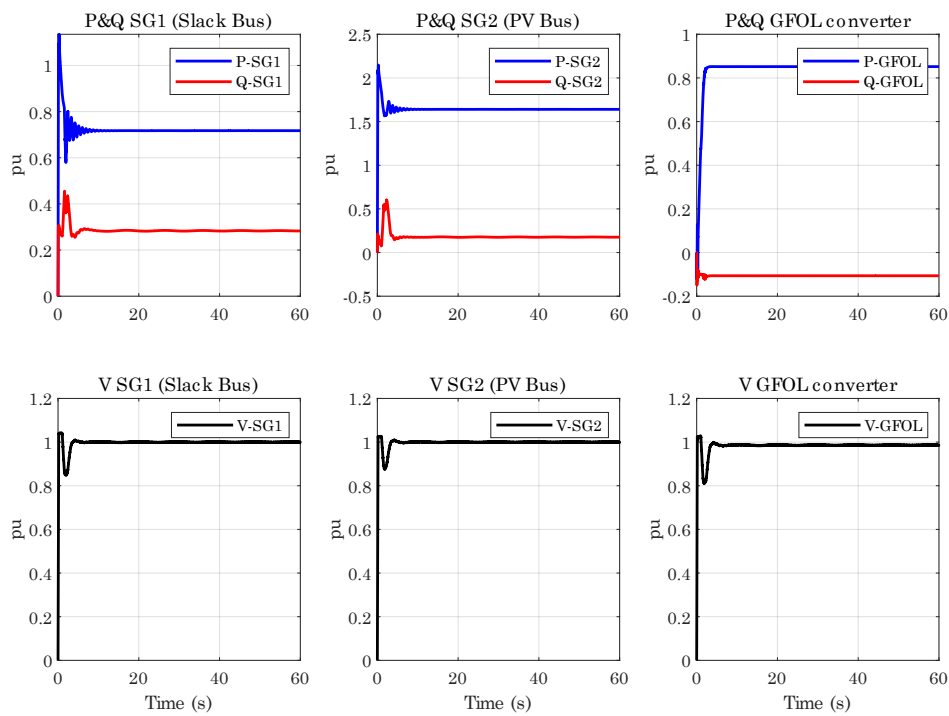


Figure 80: IEEE 9-bus system with GFOL converter in normal operation

5.2.2 Symmetric fault

This scenario shows the response of the IEEE 9-bus system with a grid-following converter during a symmetrical fault at bus 6. The time for this fault has been set to 30 seconds with a duration of 10 ms and a short circuit impedance of 0.01Ω . By concentrating on the voltage in Fig. 81, it can be seen that the voltages of the PQ and slack buses to which the converter is attached decrease more than those of the PV bus. This is because the fault is at bus 6, which is situated between the PQ and slack buses. It can be observed that all the generators and the converter work together to preserve stability, which in the end the system response is acceptable, by taking into account the active and reactive power fluctuation during and after the faults.



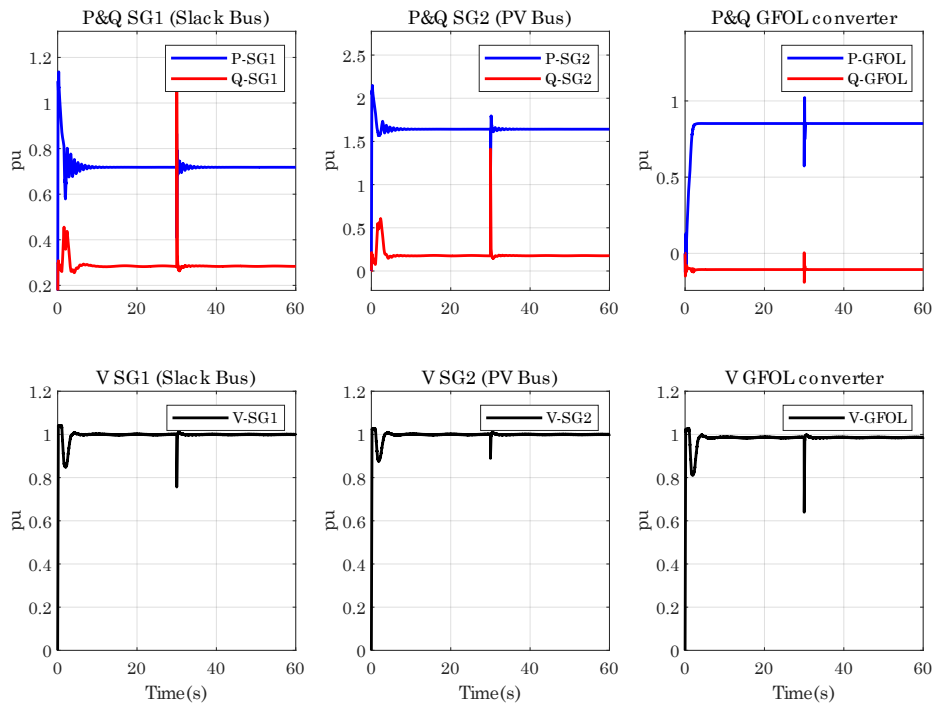


Figure 81: IEEE 9-bus system with GFOL converter with a symmetric fault

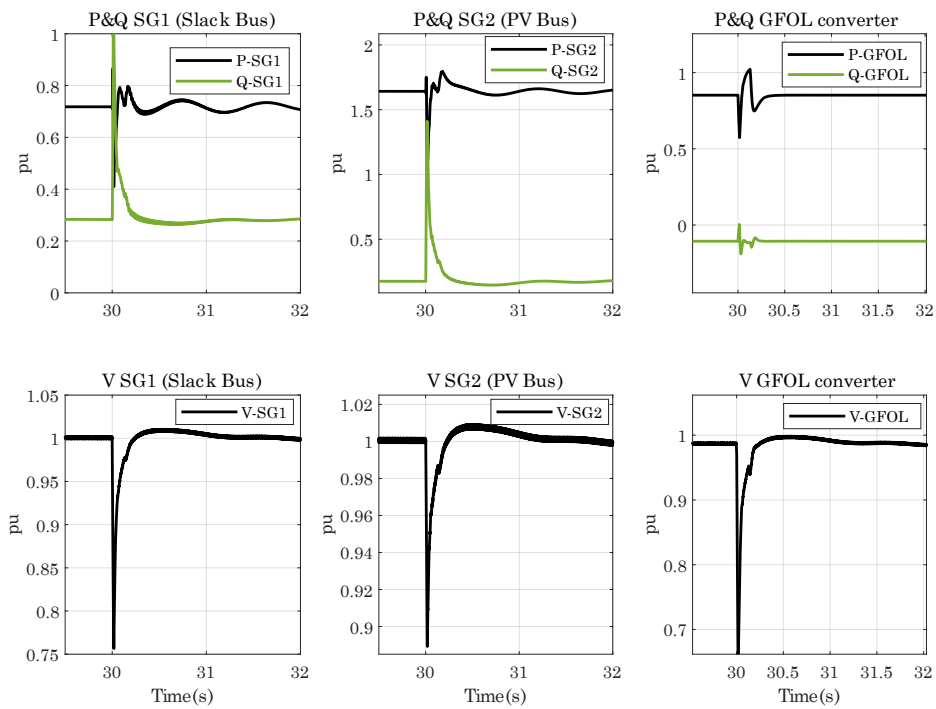


Figure 82: IEEE 9-bus system with GFOL converter with a symmetric fault (detailed view)



5.2.3 Load increase

The objective of this scenario is to examine the system by applying a 20 MW resistive load to bus 6 in 30 seconds and investigating how the generators and GFOL converter react. As shown by the results in Fig. 83, Fig. 84, it can be observed that the system operates normally for the first 30 seconds until a switch adds a 20 MW resistive load, changing the power flow results. The result is that, because the slack and PV buse have more power reserved for them, by increasing the load, each generator's governor activates and adds more power to the system, while the converter, which is already operating at maximum capacity, is unable to produce any more because there is no more power available. To add to that, it can be deduced from the voltage data that voltage declines in all buses as a result of an increase in load values, which is within a reasonable range.

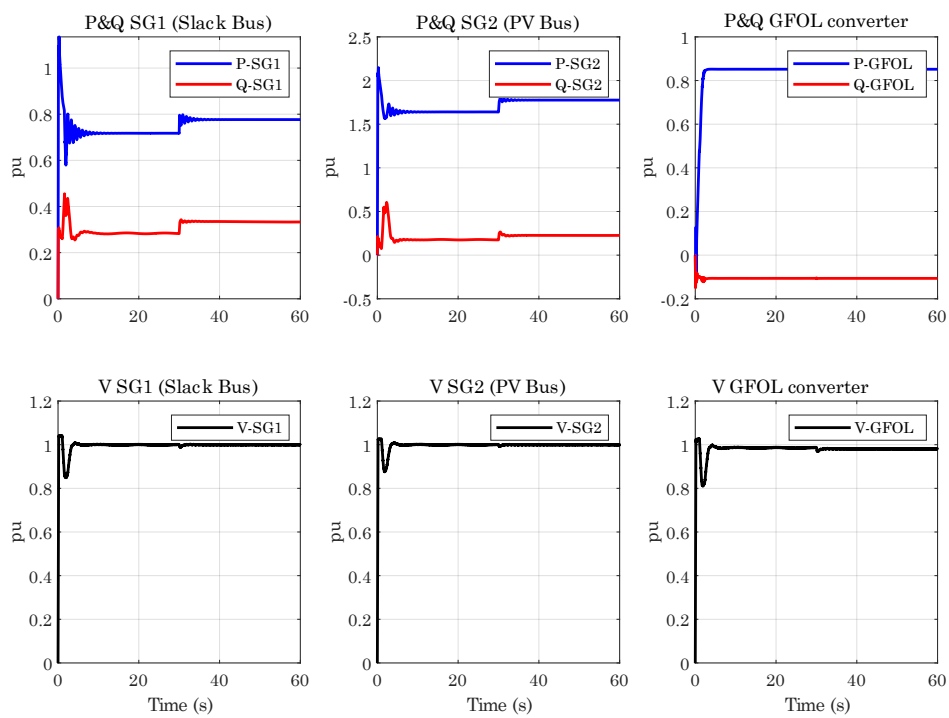


Figure 83: IEEE 9-bus system with GFOL converter with an added load



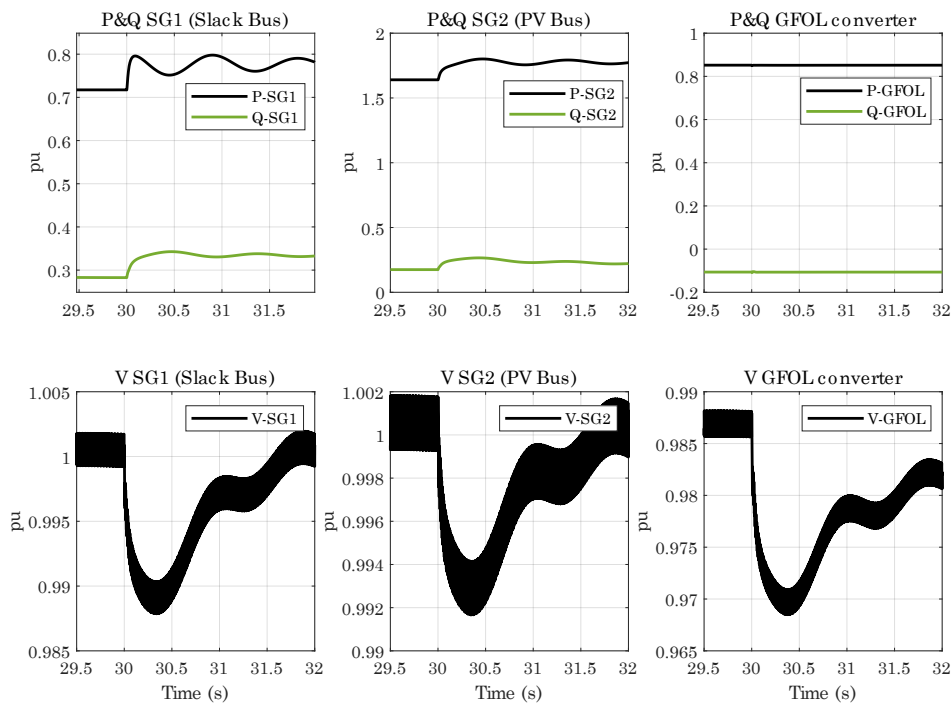


Figure 84: IEEE 9-bus system with GFOL converter with an added load (detailed view)

5.2.4 Generator disconnection

In this scenario, one of the two synchronous generators, in this case, the SG of the Slack bus, will be removed from the system after 30 seconds, and the other sources' behavior will be analyzed. As indicated in Fig. 85, the system operates smoothly for 30 seconds. Then, the SG1 is removed, and the SG2 begins to increase its power to its maximum permissible level. As previously indicated, the converter is unable to increase its power since it is operating at 100% of its allowable limits level. Due to the presence of the loads and the absence of the SG1, it can be seen that the system maintains stability, albeit to a marginal extent. This is because the remaining two sources are insufficient for the system to function normally, as seen in the voltage values at buses 1 and 3, where they have fallen noticeably.



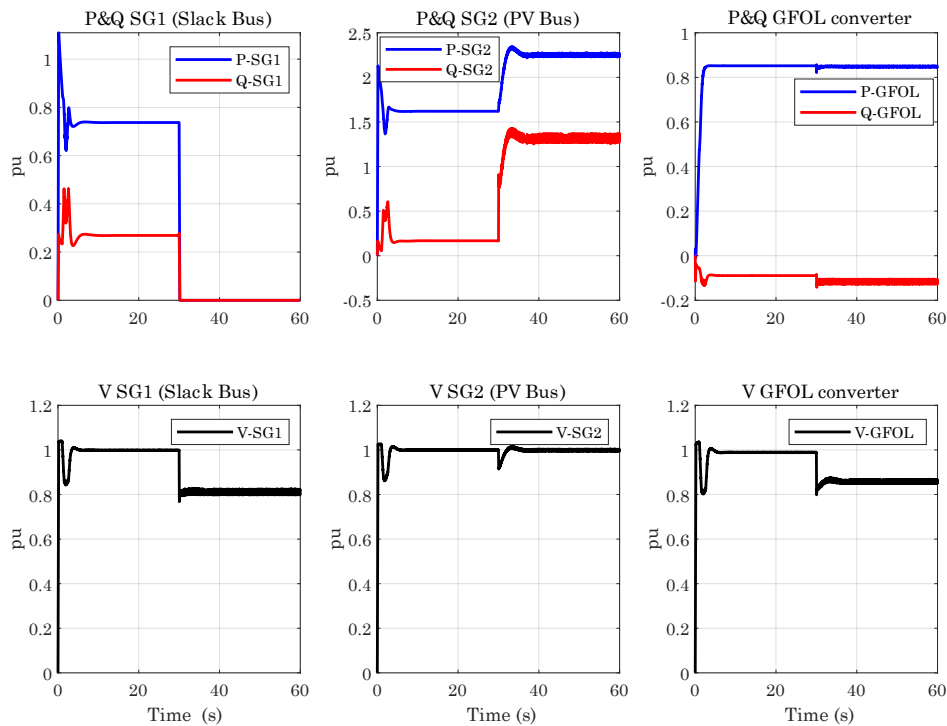


Figure 85: IEEE 9-bus system with GFOR converter and a generator disconnection condition

5.3 IEEE 9-bus system with GFOR and GFOR converters

With one exception, this part repeats the Section before it. At the PV bus, a grid-forming converter will take the place of the synchronous generator, identical scenarios will be applied and results will be shown.

5.3.1 Normal operation

The sole purpose of this Section is to observe the results of the power flow and determine whether the system is stable. In this case, there are two power converters, one connected to the PQ bus with GFOR control and the other to the PV bus with GFOR control, and a synchronous generator is connected to the slack bus with the same characteristics as in the previous Section. As shown in Fig. 86, the results of the system match with power flow results in the raw file.



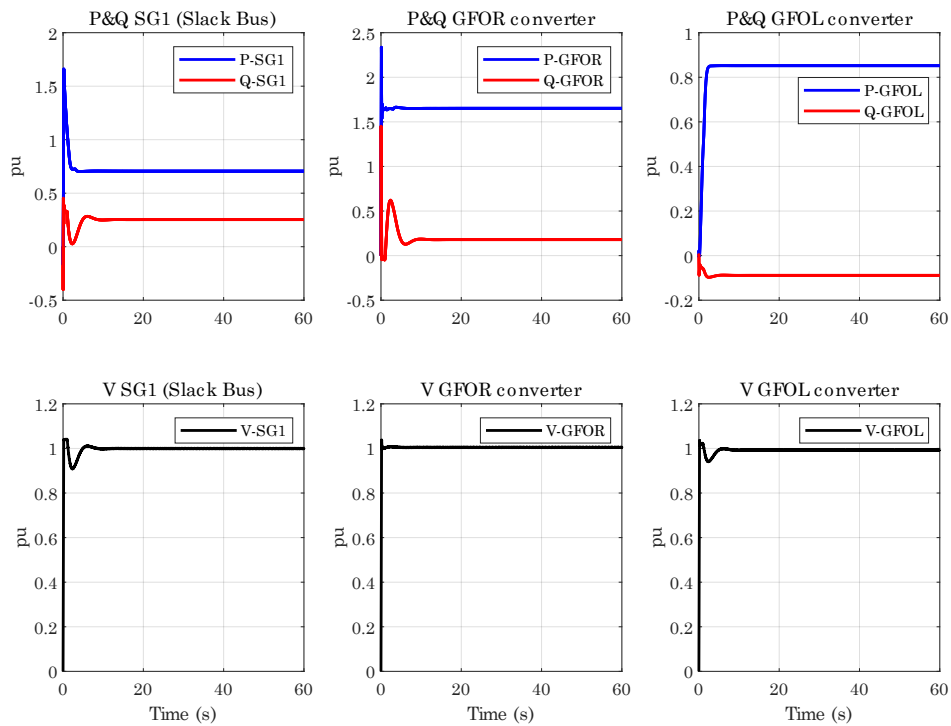


Figure 86: IEEE 9-bus system with GFOL and GFOR converters

5.3.2 Symmetric fault

As demonstrated in Fig. 87, a symmetric fault with 0.01Ω of resistance for a length of 10 ms occurs at 30 seconds at bus 6. This fault results in a significant voltage drop across all buses. To keep the voltage at the same level, the synchronous generator and the GFOR converter increased their reactive power injection. It should be mentioned that the system could function even in a failure situation thanks to the GFOR converter that took the role of the synchronous generator at the PV bus.



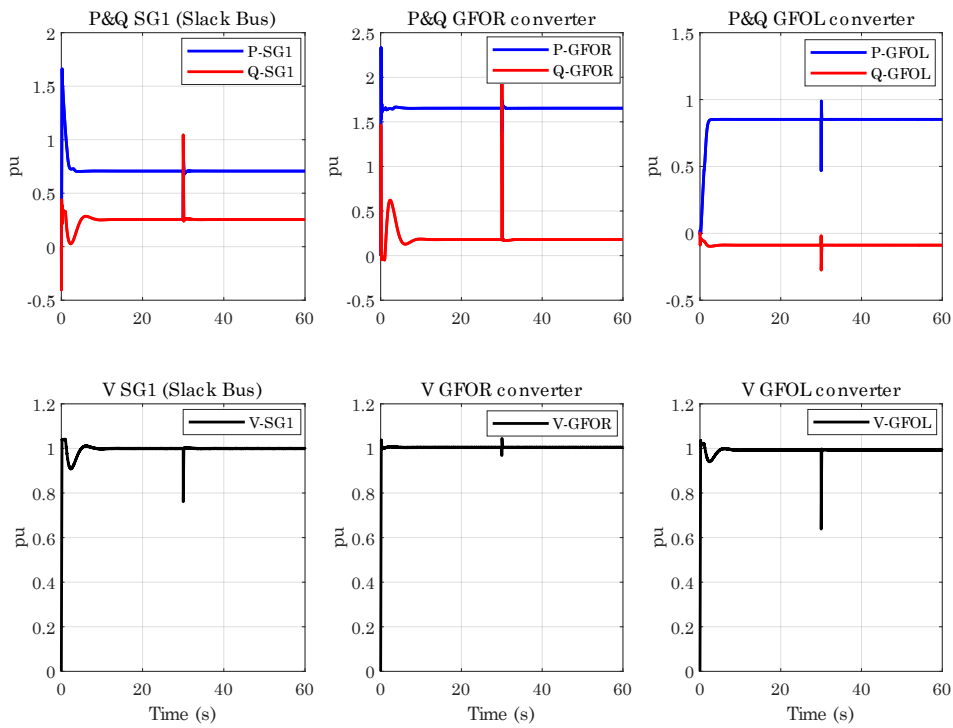


Figure 87: IEEE 9-bus system with GFOL and GFOR converters with a symmetric fault

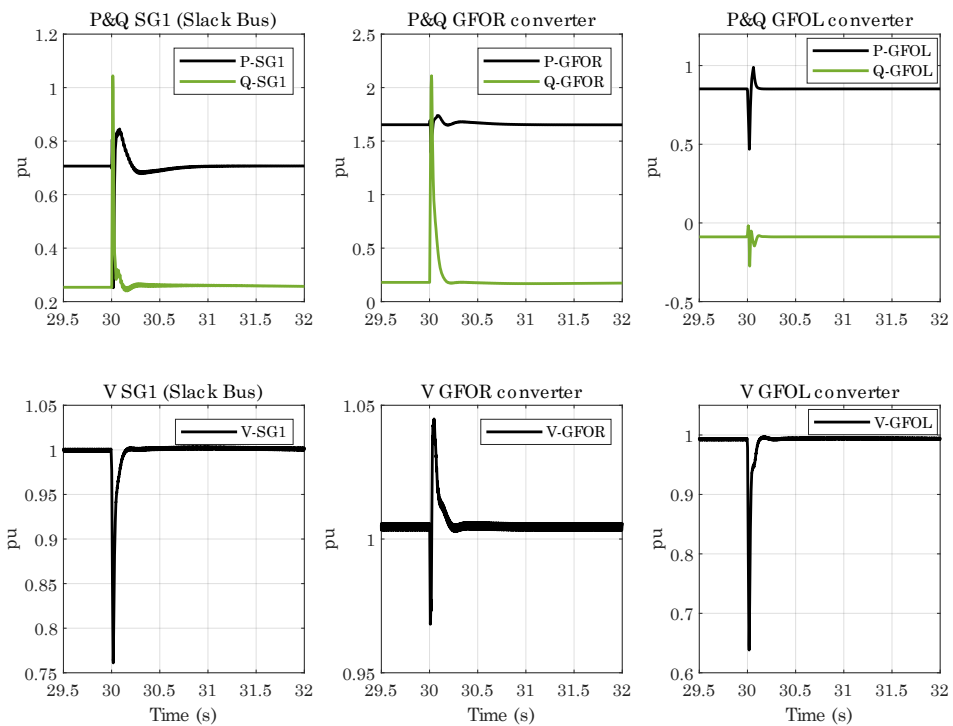


Figure 88: IEEE 9-bus system with GFOL and GFOR converters with a symmetric fault (detailed view)



5.3.3 Load increase

In this scenario a load with 20 MW of power after 30 seconds will be linked to the system at bus 6 and the results are shown in Fig. 89.

After 30 seconds, when the load is applied to the system, the GFOR and SG1 boost their output power to handle the additional load. The GFOR converter virtual inertia is set to 0.01 s in the low pass filter and is much faster than a synchronous generator in this case, and as a result, when the load is added to the system, the GFOR converter reacts rapidly and covers the majority of the load share. However, after about 10 seconds, the synchronous generator, which is much slower due to its bigger inertia and the speed of its governor and other factors, regains its share.

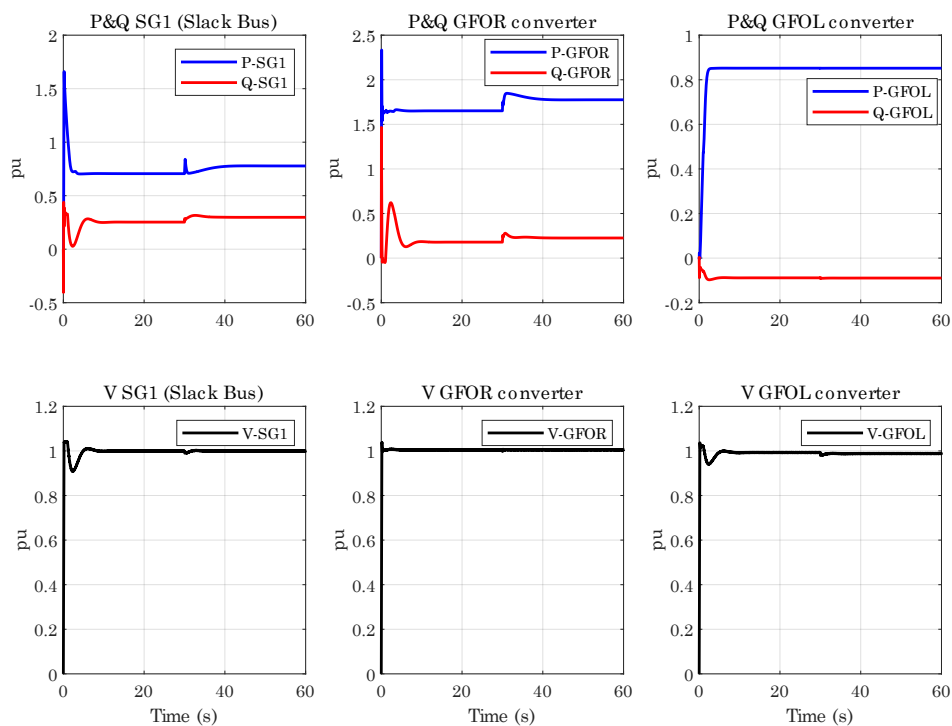


Figure 89: IEEE 9-bus system with GFOL and GFOR converters with an added load

To investigate the influence of virtual inertia on the system for the same scenario, different values will be placed in the frequency droop low pass filter, and the results are shown in Fig. 90. The values to be set are 1 ms, 10 ms, and 500 ms. As observed in the findings, when there is a larger virtual inertia, the rate of change of frequency (ROCOF) is smaller. This is because, as shown in Fig. 90, the converter with higher virtual inertia will inject more power at the time of the occurrence, resulting in smoother frequency mitigation.



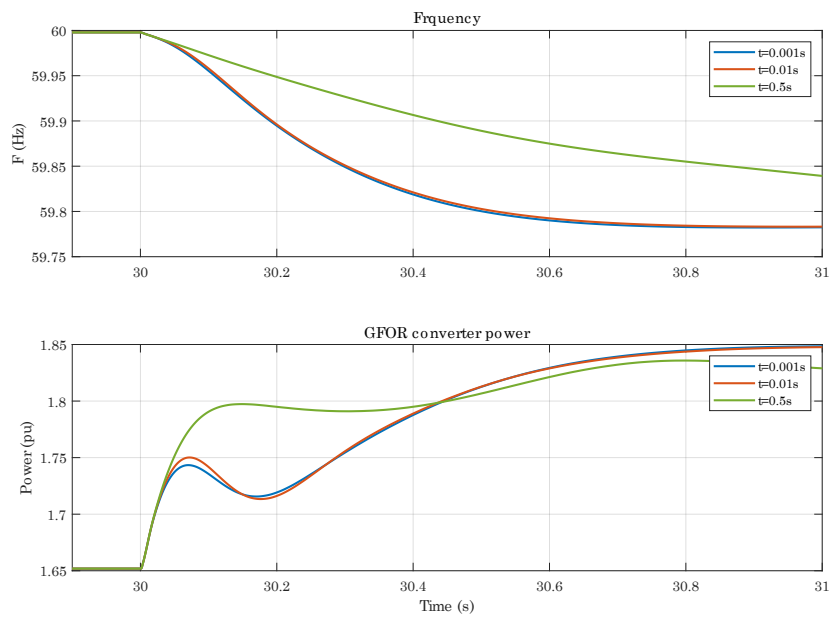


Figure 90: Effects of different virtual inertia values on the system

5.3.4 Generator disconnection

In this scenario the SG1 which now is the only synchronous generator in the system will be removed after 30 seconds and the only existing sources will be the GFOR converter and the GFOL converter and the system behavior will be assessed.

When the synchronous generator is removed from the system, there will be no conventional sources left; instead, there will only be two remaining power converters, as shown in Fig. 91, maintaining the stability of the system. This illustrates the significance of the GFOR control structure in this situation. The GFOL converter can receive the references from the GFOR converter, which is now serving as the system's slack bus. The GFOR converter has the ability to increase its power and level to its maximum levels.



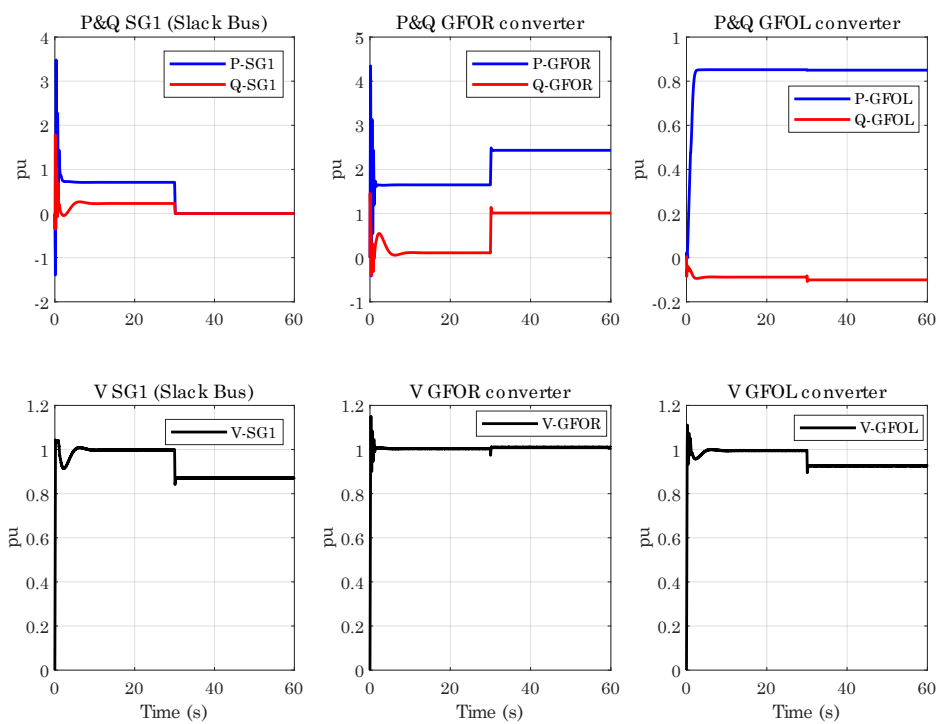


Figure 91: IEEE 9-bus system with GFOL and GFOR converters and a generator disconnection condition



Conclusions

For more than a century, the wind power sector has helped meet the need for energy, and since then, wind power technology has also advanced. This development may be seen in the transition from fixed-speed wind turbines to variable-speed wind turbines with full-scale converters or from on-shore to offshore wind farms. Power networks are not exempt from this change, therefore the power grids are switching from a system with a preponderance of heavy, inert synchronous generators to fast power electronic converters.

In this study, the grid-following control, which is the traditional method of controlling the converters, has been evaluated using robust simulation tools, and it has been demonstrated that the grid-following control, which had previously worked extremely well, may now have issues with the new structure of the power networks, where the majority of the sources are power converters. We may infer that the SCR levels and inertia will be reduced in a new power system with greater penetration of power converters. In this study, it is demonstrated that weak grids or low SCR values make it impossible for grid-following converters to operate.

Grid-forming control mechanism has recently been developed to address the aforementioned issue, and it is examined in this research. In spite of the grid-forming control's complexity, it is demonstrated in this study that two power converters can supply a small system simultaneously without the need for a synchronous generator, whereas in grid-following control, two converters are unable to do so because a voltage and angle reference are required. It has also been demonstrated that a system with grid-forming and grid-following in addition to other sources can withstand faults and disturbances, which is crucial for future power networks.

Apart from that, it is proven in this study that the virtual inertia in grid-forming control can influence the rate of change of frequency (ROCOF), which is directly related to the inertia of the system. Being able to change the inertia allows us to move more quickly toward a network with full power converter penetration.

As wind energy is expected to be one of the main sources of electricity in the future, this research attempted to look at both present and emerging wind energy technologies.



Economics and environmental impact of the project

Economics

To make this project, a personal computer is used and to create the models and perform the analysis software such as PSCAD and Matlab/Simulink are utilised. Table 11 shows the cost of the project and it can be noted that by taking into account the human resource, software and hardware the total cost for this thesis is equal to 15783.93€.

Table 11: Cost of the project

<i>Concept</i>	<i>Type</i>	<i>Unit</i>	<i>Cost(€)</i>
Lenovo Thinkpad	Hardware	1	1200
PSCAD	Software	1 Year	4813.93
Matlab/Simulink	Software	1 Year	250
Research	Human Resource	350 Hours	2800
Building Simulink model	Human Resource	80 Hours	640
Building PSCAD model	Human Resource	250 Hours	2000
Building the code	Human Resource	60 Hours	480
Scenarios and validation	Human Resource	150 Hours	1200
Writing	Human Resource	300 Hours	2400
		Total	15783.93

Environmental Impact

Due to the author's presence throughout the project in Spain, the value of CO₂ emission is taken into account in accordance with the Spanish national grid (Red Eléctrica de España). The environmental impact assessment of this project is computed and displayed in Table 12.

Table 12: Environmental impact of the project

<i>Concept</i>	<i>Total Consumption (kWh)</i>	<i>Unitary kgCO₂/kWh emissions</i>	<i>Total emissions (kgCO₂-eq)</i>
PC	30	0.19	5.7
Lighting	900	0.19	171
Heating	1250	0.19	237.5
Ventilation	25	0.19	4.75
		Total	418.95



Acknowledgements

First of all, I would want to express my gratitude to my family for their support during the entirety of my studies. Without their help, it would have been very challenging for me to advance.

I'd want to convey my appreciation to Eduardo Prieto Araujo and Vinicius Albernaz Lacerda for their supervision and guidance; it was a privilege learning alongside you.

I want to acknowledge and thank Joan Bergas, Saman Dadjoo Tavakoli, Daniel Westerman Spier and Vahid Moshari for their advice and support with this thesis; I will always be grateful for what you did.

I also want to thank Jaume Girona Badia for helping me with the grid-forming part and for sharing his unpublished article, which enabled me to complete that chapter.

Overall, it was a pleasure to have the opportunity to participate in the UPC renewable energy master's program. It was an honor to be able to know Onur Alican and Oscar Cabrera Redondo in this program, and I was very fortunate to have their company during my studies.



Bibliography

- [1] 9-Bus System (WSCC Test Case). Power Systems and Evolutionary Algorithms. URL: <https://al-roomi.org/power-flow/9-bus-system>.
- [2] Thomas Ackermann. *Wind power in power systems*. Wiley, 2012. URL: https://books.google.es/books/about/Wind_Power_in_Power_Systems.html?id=y7430s86pQAC&redir_esc=y.
- [3] Thomas Ackermann et al. "Paving the Way: A Future Without Inertia Is Closer Than You Think". In: *IEEE Power and Energy Magazine* 15 (Nov. 2017), pp. 61–69. DOI: 10.1109/mpe.2017.2729138.
- [4] P. Anderson and Anjan Bose. "Stability Simulation Of Wind Turbine Systems". In: *IEEE Transactions on Power Apparatus and Systems* PAS-102 (Dec. 1983), pp. 3791–3795. DOI: 10.1109/tpas.1983.317873.
- [5] Luis Arturo Soriano, Wen Yu, and Jose de Jesus Rubio. "Modeling and Control of Wind Turbine". In: *Mathematical Problems in Engineering* 2013 (2013), pp. 1–13. DOI: 10.1155/2013/982597. (Visited on 08/11/2019).
- [6] Arasan Aruliah. *average-annual-wind-capacity-factor-mapped-across*. Energypost.eu, July 2019. URL: <https://energypost.eu/wp-content/uploads/2019/07/average-annual-wind-capacity-factor-mapped-across.jpeg>.
- [7] Valérie Besson Associée. *How the Russia/Ukraine crisis impacts energy industry?* KPMG, Sept. 2022. URL: <https://home.kpmg/fr/fr/blogs/home/posts/2022/03/how-the-russia-ukraine-crisis-impacts-energy-industry.html>.
- [8] Rahul Awati. *What is a Phase-locked Loop (PLL)?* SearchNetworking. URL: <https://www.techtarget.com/searchnetworking/definition/phase-locked-loop>.
- [9] M. Balat. "A Review of Modern Wind Turbine Technology". In: *Energy Sources, Part A: Recovery, Utilization, and Environmental Effects* 31 (Oct. 2009), pp. 1561–1572. DOI: 10.1080/15567030802094045.
- [10] Alex Bath. *Global Wind Report 2021*. Global Wind Energy Council, Mar. 2021. URL: <https://gwec.net/global-wind-report-2021/#Download>.
- [11] Marisa Blackwood. "Maximum Efficiency of a Wind Turbine". In: *Undergraduate Journal of Mathematical Modeling: One + Two* 6 (May 2016). DOI: 10.5038/2326-3652.6.2.4865.
- [12] Tony Burton et al. *Wind energy Handbook*. J. Wiley Sons, 2011. DOI: 10.1002/9781119992714. URL: <https://onlinelibrary.wiley.com/doi/book/10.1002/9781119992714>.
- [13] Marc Cheah Mañé. *Assignment 3: Wind Generation Model*.
- [14] Aleh Cherp et al. "National growth dynamics of wind and solar power compared to the growth required for global climate targets". In: *Nature Energy* 6 (July 2021), pp. 742–754. DOI: 10.1038/s41560-021-00863-0. URL: <https://www.nature.com/articles/s41560-021-00863-0>.
- [15] Se-Kyo Chung. "A phase tracking system for three phase utility interface inverters". In: *IEEE Transactions on Power Electronics* 15 (May 2000), pp. 431–438. DOI: 10.1109/63.844502. (Visited on 12/19/2021).
- [16] Joel Colby. *Wind Power: Onshore vs Offshore Wind Farms*. ArcGIS StoryMaps, Nov. 2019. URL: <https://storymaps.arcgis.com/stories/b96f4db23c4449849deb60c0953b2509>.
- [17] Aubryn Cooperman and Marcias Martinez. "Load monitoring for active control of wind turbines". In: *Renewable and Sustainable Energy Reviews* 41 (Jan. 2015), pp. 189–201. DOI: 10.1016/j.rser.2014.08.029.
- [18] O Daniyan and K Ibekwe. "Design and Simulation of a Wind Turbine for Electricity Generation". In: *International Journal of Applied Engineering Research* 13 (2018), pp. 16409–164717. URL: https://www.ripublication.com/ijaer18/ijaerv13n23_33.pdf.



- [19] Wei Du et al. "A Comparative Study of Two Widely Used Grid-Forming Droop Controls on Microgrid Small-Signal Stability". In: *IEEE Journal of Emerging and Selected Topics in Power Electronics* 8 (June 2020), pp. 963–975. doi: [10.1109/jestpe.2019.2942491](https://doi.org/10.1109/jestpe.2019.2942491).
- [20] Agustí Egea-Alvarez, Adrià Junyent-Ferré, and Oriol Gomis-Bellmunt. "Active and Reactive Power Control of Grid Connected Distributed Generation Systems". In: *Modeling and Control of Sustainable Power Systems* (2012), pp. 47–81. doi: [10.1007/978-3-642-22904-6_3](https://doi.org/10.1007/978-3-642-22904-6_3). (Visited on 09/10/2022).
- [21] Satria Eko et al. "Precision Measurement of Drag Force Acting on a Spherical Body Dropping in the Air". In: (Mar. 2017), pp. 7–15. URL: https://www.researchgate.net/publication/339899234_Precision_Measurement_of_Drag_Force_Acting_on_a_Spherical_Body_Dropping_in_the_Air.
- [22] *Evolution of Net Maximum Electrical Capacity for Renewables and Renewable Waste in EU-27 (MW)*. ec.europa.eu, 2019. URL: https://ec.europa.eu/eurostat/statistics-explained/index.php?title=Main_Page.
- [23] F. M. Gardner. "Phaselock techniques". In: *IEEE Transactions on Systems, Man, and Cybernetics SMC-14* (Jan. 1984), pp. 170–171. doi: [10.1109/tsmc.1984.6313286](https://doi.org/10.1109/tsmc.1984.6313286).
- [24] *Global Wind Explained | EARTH 111: Water: Science and Society*. www.e-education.psu.edu. URL: <https://www.e-education.psu.edu/earth111/node/1013>.
- [25] Oriol Gomis and Eduardo Prieto. *Wind Power V6-1 Wind turbines types Fixed-speed and limited speed wind turbines*.
- [26] John J. Grainger and William D. Stevenson. *Power System Analysis*. McGraw-Hill, 1994. URL: https://books.google.es/books/about/Power_System_Analysis.html?id=a10zQgAACAAJ&redir_esc=y.
- [27] Wenyong Guo et al. "Evaluation of the Performance of BTFCLs for Enhancing LVRT Capability of DFIG". In: *IEEE Transactions on Power Electronics* 30 (July 2015), pp. 3623–3637. doi: [10.1109/TPEL.2014.2340852](https://doi.org/10.1109/TPEL.2014.2340852). URL: <https://ieeexplore.ieee.org/document/6860299>.
- [28] Mohammed Haddad. *Infographic: How much of Europe's energy comes from gas?* www.aljazeera.com, Sept. 2022. URL: [https://www.aljazeera.com/news/2022/9/6/infographic-how-much-of-europes-energy-gas#:~:text=In%5C%202021%5C%2C%5C%20two%5C%2Dthirds%5C%20\(,](https://www.aljazeera.com/news/2022/9/6/infographic-how-much-of-europes-energy-gas#:~:text=In%5C%202021%5C%2C%5C%20two%5C%2Dthirds%5C%20(,)
- [29] Martin O. L. Hansen. *Aerodynamics of Wind Turbines*. Earthscan from Routledge, 2015. URL: https://books.google.com.bn/books/about/Aerodynamics_of_Wind_Turbines.html?hl=ms&id=Hbg5swEACAAJ&utm_source=gb-shareAerodynamics.
- [30] Lennart Harnefors et al. "Robust Analytic Design of Power-Synchronization Control". In: *IEEE Transactions on Industrial Electronics* 66 (Aug. 2019), pp. 5810–5819. doi: [10.1109/TIE.2018.2874584](https://doi.org/10.1109/TIE.2018.2874584). URL: <https://ieeexplore.ieee.org/document/8490668>.
- [31] Dirk Van Hertem, Oriol Gomis-Bellmunt, and Jun Liang. *HVDC Grids : for Offshore and Supergrid of the Future*. Ieee Press ; Hoboken, New Jersey, 2016.
- [32] IEA. *Wind Power – Analysis*. IEA, Nov. 2021. URL: <https://www.iea.org/reports/wind-power>.
- [33] Md Rabiul Islam, Youguang Guo, and J.G Zhu. "Power Converters for Wind turbines: Current and Future Development". In: (Aug. 2013). URL: https://www.researchgate.net/publication/262974138_Power_converters_for_wind_turbines_Current_and_future_development.
- [34] *Jachens Steam Turbines Their Construction PDF*. Scribd, 1966. URL: <https://www.scribd.com/document/355456515/1966-Jachens-Steam-Turbines-Their-Construction-pdf>.



- [35] Madhumitha Jaganmohan. *Global wind energy share in electricity mix 2021*. Statista, Apr. 2022. URL: <https://www.statista.com/statistics/1302053/global-wind-energy-share-electricity-mix/>.
- [36] Jafar Jallad, Saad Mekhilef, and Hazlie Mokhlis. "Frequency Regulation Strategies in Grid Integrated Offshore Wind Turbines via VSC-HVDC Technology: A Review". In: *Energies* 10 (Aug. 2017), p. 1244. DOI: 10.3390/en10091244.
- [37] Andrew de Juan and Safa Al Tameemi. "Wind Energy Analysis Wind Energy Modelling". In: (Sept. 2013). DOI: 10.13140/2.1.3075.1047.
- [38] Adrià Junyent Ferré. *Control of power electronic converters for the operation of wind generation*. www.tdx.cat, July 2011. URL: <https://www.tdx.cat/handle/10803/108501#page=5>.
- [39] Sohail Khan et al. "On Small Signal Frequency Stability under Virtual Inertia and the Role of PLLs". In: *Energies* 11 (Sept. 2018), p. 2372. DOI: 10.3390/en11092372. URL: <https://www.mdpi.com/1996-1073/11/9/2372>.
- [40] Yitong Li, Yunjie Gu, and Tim Green. "Revisiting Grid-Forming and Grid-Following Inverters: A Duality Theory". In: *IEEE Transactions on Power Systems* (2022), pp. 1–1. DOI: 10.1109/tpwrs.2022.3151851. (Visited on 05/19/2022).
- [41] Jiannan Liu et al. "A hybrid AC/DC microgrid control system based on a virtual synchronous generator for smooth transient performances". In: *Electric Power Systems Research* 162 (Sept. 2018), pp. 169–182. DOI: 10.1016/j.epsr.2018.05.014.
- [42] *Load Bus, Generator Bus and Slack Bus*. Electrical Concepts, Mar. 2018. URL: <https://electricalbaba.com/load-generator-slack-bus/>.
- [43] Dr. Richard M. Andres. *Betz Limit* | REUK.co.uk. Reuk.co.uk, 2016. URL: <http://www.reuk.co.uk/wordpress/wind/betz-limit/>.
- [44] Yanfeng Ma et al. "Research on Improved VSG Control Algorithm Based on Capacity-Limited Energy Storage System". In: *Energies* 11 (Mar. 2018), p. 677. DOI: 10.3390/en11030677. URL: <https://www.mdpi.com/1996-1073/11/3/677>.
- [45] Tarek Hassan Mohamed et al. "Model predictive based load frequency control-design concerning wind turbines". In: *International Journal of Electrical Power Energy Systems* 43 (Dec. 2012), pp. 859–867. DOI: 10.1016/j.ijepes.2012.06.032. URL: <https://www.sciencedirect.com/science/article/abs/pii/S0142061512002943>.
- [46] BBC News. "Climate change: EU to cut CO2 emissions by 55% by 2030". In: *BBC News* (Apr. 2021). URL: <https://www.bbc.com/news/world-europe-56828383>.
- [47] Kenneth E. Okedu et al. "Wind Farms Fault Ride Through Using DFIG With New Protection Scheme". In: *IEEE Transactions on Sustainable Energy* 3 (Apr. 2012), pp. 242–254. DOI: 10.1109/TSTE.2011.2175756. URL: <https://ieeexplore.ieee.org/document/6170989>.
- [48] Dinesh Pattabiraman, R. H. Lasseter., and T. M. Jahns. *Comparison of Grid Following and Grid Forming Control for a High Inverter Penetration Power System*. IEEE Xplore, Aug. 2018. DOI: 10.1109/PESGM.2018.8586162. URL: <https://ieeexplore.ieee.org/document/8586162>.
- [49] *PSCAD-THE ELECTROMAGNETIC TRANSIENTS SOFTWARE*. June 2011. URL: <http://www.powerqualityworld.com/2011/06/pscad-power-systems-computer>.
- [50] Pengwei Qiao and Ganesh Venayagamoorthy. "Dynamic Modeling of Wind Farms with Fixed-Speed Wind Turbine Generators Grid integration of RE using Smart Technologies and Innovation for Smart Cities View project IoT and Intelligent Technologies for Efficient Energy Management View project". In: (2007). DOI: 10.1109/PES.2007.386283.
- [51] Mohsen Rahimi. "Control and Performance Assessment of Variable Rotor Resistance Based Wind Turbines Regarding the Aerodynamic Power Fluctuations". In: *Scientia Iranica* 0 (Aug. 2017), pp. 0-0. DOI: 10.24200/sci.2017.4363.



- [52] Peter J. Schubel and Richard J. Crossley. "Wind Turbine Blade Design". In: *Energies* 5 (Sept. 2012), pp. 3425–3449. DOI: 10.3390/en5093425.
- [53] Jean-Jacques E. Slotine and Weiping Li. *Applied Nonlinear Control*. Pearson education Taiwan, 2005. URL: https://books.google.es/books/about/Applied_Nonlinear_Control.html?id=fdvPbwAACAAJ&redir_esc=y.
- [54] Vishnu Sidaarth Suresh. "Comparison of Solvers Performance for Load Flow Analysis". In: *Transactions on Environment and Electrical Engineering* 3 (Feb. 2019), p. 26. DOI: 10.22149/teee.v3i1.131.
- [55] M.A Tabrizi. "Integration of Renewable Energy sources: Strong Challenge for a Weak Grid". In: (2015). URL: <https://blogs.dnvgl.com/energ%20y/integration-of-renewable-energy-sources-strong-challenge-fora-%20weak-grid>.
- [56] Yehezkiel Tumewu, Petrone Crescenzo, and Mettupalayam Sivaselvan. "Numerical Simulation of the Influence of Platform Pitch Motion on Power Generation Steadiness in Floating Offshore Wind Turbines". In: *International Journal of Environmental Science Sustainable Development*. 2 (July 2017), p. 92. DOI: 10.21625/essd.v1i2.39.
- [57] TYNDP 2018 - Scenario Report. tyndp.entsoe.eu, 2018. URL: <https://tyndp.entsoe.eu/tyndp2018/scenario-report/>.
- [58] Peter Unruh et al. "Overview on Grid-Forming Inverter Control Methods". In: *Energies* 13 (May 2020), p. 2589. DOI: 10.3390/en13102589.
- [59] NOAA US Department of Commerce. *NWS JetStream - Origin of Wind*. www.weather.gov. URL: <https://www.weather.gov/jetstream/wind>.
- [60] Xiaohe Wang et al. "A Modified Self-Synchronized Synchronverter in Unbalanced Power Grids with Balanced Currents and Restrained Power Ripples". In: *Energies* 12 (Jan. 2019), p. 923. DOI: 10.3390/en12050923. URL: <https://www.mdpi.com/1996-1073/12/5/923/htm>.
- [61] Xiongfei Wang et al. "Grid-Synchronization Stability of Converter-Based Resources—An Overview". In: *IEEE Open Journal of Industry Applications* 1 (2020), pp. 115–134. DOI: 10.1109/OJIA.2020.3020392. URL: <https://ieeexplore.ieee.org/document/9181463> (visited on 09/10/2022).
- [62] David.E Watson. *Wind Turbine Power Coefficient*. Ftexploring.com, 2015. URL: <https://www.ftexploring.com/wind-energy/wind-power-coefficient.htm>.
- [63] *What is Simulink?* 2005. URL: <https://ewh.ieee.org/r1/ct/sps/PDF/MATLAB/chapter8.pdf>.
- [64] *What Is the Purpose of Exciter in Generator*. generatortech, June 2019. URL: <https://startlight.wixsite.com/generatortech/single-post/2019/06/20/what-is-the-purpose-of-exciter-in-generator>.
- [65] *Wind, Wind Information, Facts, News, Photos – National Geographic*. Science, Oct. 2009. URL: <https://www.nationalgeographic.com/science/article/wind>.
- [66] Kah Yung Yap, Charles R. Sarimuthu, and Joanne Mun-Yee Lim. "Virtual Inertia-Based Inverters for Mitigating Frequency Instability in Grid-Connected Renewable Energy System: A Review". In: *Applied Sciences* 9 (Dec. 2019), p. 5300. DOI: 10.3390/app9245300.
- [67] Bo Zhang et al. "Stable Operation and Small-Signal Analysis of Multiple Parallel DG Inverters Based on a Virtual Synchronous Generator Scheme". In: *Energies* 11 (Jan. 2018), p. 203. DOI: 10.3390/en11010203.
- [68] Jianzhong Zhang et al. *Pitch angle control for variable speed wind turbines*. IEEE Xplore, Apr. 2008. DOI: 10.1109/DRPT.2008.4523867. URL: <https://ieeexplore.ieee.org/document/4523867>.



- [69] Haoran Zhao and Qiuwei Wu. "Status of Wind Power Technologies". In: *Modeling and Modern Control of Wind Power* (2018), pp. 1–10. doi: [10.1002/9781119236382.ch1](https://doi.org/10.1002/9781119236382.ch1). URL: <https://orbit.dtu.dk/en/publications/status-of-wind-power-technologies>.
- [70] Chong Wei Zheng et al. "An overview of global ocean wind energy resource evaluations". In: *Renewable and Sustainable Energy Reviews* 53 (Jan. 2016), pp. 1240–1251. doi: [10.1016/j.rser.2015.09.063](https://doi.org/10.1016/j.rser.2015.09.063).
- [71] Qing-Chang Zhong and George Weiss. "Synchronverters: Inverters That Mimic Synchronous Generators". In: *IEEE Transactions on Industrial Electronics* 58 (Apr. 2011), pp. 1259–1267. doi: [10.1109/TIE.2010.2048839](https://doi.org/10.1109/TIE.2010.2048839). URL: <https://ieeexplore.ieee.org/abstract/document/5456209>.
- [72] Qing-Chang Zhong et al. "Self-Synchronized Synchronverters: Inverters Without a Dedicated Synchronization Unit". In: *IEEE Transactions on Power Electronics* 29 (Feb. 2014), pp. 617–630. doi: [10.1109/tpel.2013.2258684](https://doi.org/10.1109/tpel.2013.2258684).
- [73] Dao Zhou and Frede Blaabjerg. "Optimized Demagnetizing Control of DFIG Power Converter for Reduced Thermal Stress During Symmetrical Grid Fault". In: *IEEE Transactions on Power Electronics* 33 (Dec. 2018), pp. 10326–10340. doi: [10.1109/tpel.2018.2803125](https://doi.org/10.1109/tpel.2018.2803125). (Visited on 09/25/2022).



Appendix

MATLAB script

```

%% General parameters
%% Wind turbine data
rho=1.225;      %Air density
Pn=5e6;        %WT nominal power
D=88;          %WT diameter
N=80;          %Transmission ratio of gearbox
wg=2*pi*50/2;  %WT nominal mechanical speed
Jtot=9*10^4;   %inertia
rt=D/2;
A=pi*rt^2

%PMSG paramaters
wn=2*pi*50;    %Rotatioanl speed
P=2;           %Pole pairs
Rs=0.01;       %Series resiastant
Ld=0.159;      %Inductance d-component
Lq=0.159;      %Inductance q-component

%Power coefficient values
c1=0.73;
c2=151;
c3=0.58;
c4=0.002;
c5=2.14;
c6=13.2;
c7=18.4;
c8=-0.02;
c9=-0.003;

% AC grid: Thevenin equivalent
Sn1=5e6;       % Base power
Un1=690;       % Base AC voltage
f1=50;         % Base frequency
SCR1=5;        % Short-circuit ratio
Scc1=SCR1*Sn1; % Short-circuit power
Xcc1=Un1^2/Scc1; % Short-circuit impedance
Lcc1=Xcc1/(2*pi*f1); % Shot-circuit inductance
Rcc1=Xcc1/10;  % Short-circuit resistance

% DC grid: ideal
Vdcref=1200;

%% 2L-VSC
Sn_n1=Sn1;     % Base power
f_n1=f1;       % Frequency
w_n1=2*pi*f_n1; % Angular speed
Un_n1=Un1;     % Line-line voltage
Vpeak_n1=Un_n1/sqrt(3)*sqrt(2); % Peak voltage
Xn_n1=Un_n1^2/Sn_n1; % Base impedance
Ln_n1=Xn_n1/(2*pi*f_n1); % Base inductance
Rg_n1=Rcc1;    % Thevenin resistance

```



```

Lg_n1=Lcc1; % Thevenin inductance
Rc_n1=0.01*Xn_n1; % Converter grid coupling filter resistance
Lc_n1=0.1*Ln_n1; % Converter grid coupling filter inductance

%Grid thevenin equivalent Configuration
vaini_n1=Vpeak_n1; % Three-phase system initial voltages
vbini_n1=-1/2*Vpeak_n1;
vcini_n1=-1/2*Vpeak_n1;

Vdcref_n1=Vdcref; % Base DC voltage
tau_C=0.04; % Time response of DC capacitor
Cdc=2*tau_C*Sn_n1/Vdcref_n1^2; % DC capacitor
Kcp=0.5*rho*A*(D/2)^3*(c1*(c2+c6*c7)^3*exp((-c2-c6*c7)/c2))/(c2^2*c7^4)

% PLL tuning
ts_pll_n1=0.025;
xi_pll_n1=0.707;
omega_pll_n1=4/(ts_pll_n1*xi_pll_n1);
kp_pll_n1=xi_pll_n1*2*omega_pll_n1/Vpeak_n1;
tau_pll_n1=2*xi_pll_n1/omega_pll_n1;
ki_pll_n1=kp_pll_n1/tau_pll_n1;

% Current control
taus=1e-3;
kp_s_n1=Lc_n1/taus;
ki_s_n1=Rc_n1/taus;

% Power loops
tauPQ=1e-2;
kp_P_n1=taus/tauPQ;
kp_Q_n1=kp_P_n1;
ki_P_n1=1/tauPQ;
ki_Q_n1=ki_P_n1;

% DC voltage control
psi_Vdc=2;
wn_Vdc=100*2*pi; %100*2*pi
kp_dc=2*Cdc*psi_Vdc*wn_Vdc;
ki_dc=Cdc*wn_Vdc^2;

%% Parameters PMSG
wr=2*pi*f1;
fluxm=2.5;
p=2;
Rs=0.01;
Lqd=0.05/(2*pi*50);
Lq=Lqd;
Ld=Lqd;

%Control parameters
tau_m=5e-3;
kp_mq=Lq/tau_m;
kp_md=Ld/tau_m;
ki_m=Rs/tau_m;

```



```
lambda= wt*rt ./ vw; % Calculation of the tip speed ratio
k1=(lambda+c8*angle_pitch).^(-1)-c9/(1+angle_pitch^3); % aux variable for the cp calcul
Cpp=max(0,c1*(c2*k1-c3*angle_pitch-c4*angle_pitch^c5-c6).*exp(-c7*k1));
Kcp=0.5*rho*A*(D/2)^3*(c1*(c2+c6*c7)^3*exp((-c2-c6*c7)/c2))/(c2^2*c7^4)
```



Initialization code for WT in Python

```

import mhi.pscad
from mhi.pscad.utilities.file import File
import sys, os
import win32com.client
import shutil
import grg_pssedata
import math
# -----
# Configuration
# -----
print("Automation Library:", mhi.pscad.VERSION)

settings = {'fortran_version': 'GFortran 4.6.2'}
fortran_ext = '.gf46'
project_name = 'Final_model_Gfollow'

# Working directory
working_dir = os.getcwd() + "\\\"

# -----
# Main script
# -----

# Launch PSCAD and Fortran version
pscad = mhi.pscad.launch(version='5.0.1', settings=settings)

#Defining parameters of the Wind turbine
rho=1.225           #Air density in (kg\m^3)
Pn=5                #WT nominal power in (MVA)
rt=44               #WT diameter in (m)
wrat=314.1592      #WT nominal mechanical speed in (rad\sec)
A=math.pi*rt**2   #Rotor area in (m^2)
Gr=80.1             #Gearbox ratio
Ge=1                #Gearbox efficiency in(pu)

#PMSG parameters
Pg=5                #Generator power
Vg=1                #Generator voltage
Fg=50               #Generator frequency
Rs=0.01             #Stator winding resistance
Xs=0.064            #Stator leakage reactance
Xd=0.55             #Unsaturated reactance(Xd)
Xq=0.85             #Unsaturated reactance(Xq)
time=1              #Time to switch from source to machine

#Grid parameters
Sgrid=5              #Grid base power
Vgrid=0.69           #Grid L_L base voltage
Fgrid=50             #Grid frequency
SCR=5                #Short circuit ratio
Sccgrid=Sgrid*SCR   #Short circuit power
Zccgrid=Vgrid**2/Sccgrid #Short circuit impedance
Lccgrid=Zccgrid/(2*math.pi*Fgrid) #Short circuit inductance

```



```

Rccgrid=Zccgrid/100                                #Short circuit resistance

#Converter parameters
SC=Sgrid                                           #Converter Base power
fC=Fgrid                                           #Converter Base frequency
WC=2*math.pi*fC                                   #Converter Base angular speed
ZbC=Vgrid**2/SC                                   #Converter Base impedance
LbC=ZbC/(2*math.pi*fC) #Converter Base inductance
RC=0.01*ZbC                                       #Converter grid coupling filter resistance
LC=0.1*LbC                                       #Converter grid coupling filter inductance
Vpeak_n1 = Vgrid*(math.sqrt(2)/math.sqrt(3))

#Dc bus parameters
Vdc_ref=1.2                                       #DC bus voltage
tauc=0.04                                         #Time response of the DC capacitor
Cdc=(2*tauc*SC/Vdc_ref**2)*2e6 #DC capacitor(2 in series)

#PLL tuning
ts_pll_n1=0.025                                  #PLL time constant
xi_pll_n1=0.707                                  #PLL damping ratio
omega_pll_n1=4/(ts_pll_n1*xi_pll_n1)             #PLL angular speed
kp_pll_n1=(xi_pll_n1*2*omega_pll_n1)/(Vpeak_n1*10**3) #PLL propotional value
tau_pll_n1=2*xi_pll_n1/omega_pll_n1             #PLL tau
ki_pll_n1=kp_pll_n1/tau_pll_n1                 #PLL integral value
f_PLL=50                                         #PLL frequency

#G-side Current controller
taus=0.001
kp_s_n1=LC/taus
ki_s_n1=RC/taus

#Power loops
tauPQ=1e-2
kp_P_n1=taus/tauPQ
kp_Q_n1=kp_P_n1
ki_P_n1=1/tauPQ
ki_Q_n1=ki_P_n1

if pscad:
    try:
        # Load the project
        pscad.load([r'(PSCAD file loation)'])
        project = pscad.project(project_name)
        project.focus()

        # Get the "Main" canvas
        main = project.canvas('Main')

        #Getting wind turbine data
        WT=project.component(956528011)

        #Getting generators data
        G=project.component(862029781)

```




```
#Getting timer data
Timer=project.component(1294302219)

#Getting grid data
Vgg=project.component(1657895110)
fgg=project.component(603474630)
Zgg=project.component(135393464)

#Getting converter filter Data
RLCg=project.component(869123953)

#Getting capitors Data
C1=project.component(1894479177)
C2=project.component(533623950)

#Getting PLL Data
kp_pll=project.component(1052788259)
ki_pll=project.component(759565932)
fppll=project.component(267265109)

#Getting power loops Data
kp_P_g=project.component(1338049127)
ki_P_g=project.component(342682449)
kp_P_m=project.component(744561321)
ki_P_m=project.component(383861948)

# -----
# Sending Data to PSCAD
# -----

# Sending Wind turbine data
WT.parameters(Gmva=Pn,Wrat=wratt, Rad=rt, Area=A, Airden=rho, Eff=Ge, Gratio=Gr)

# Sending Generators datas
G.parameters(MVA=Pg, VRAT=Vg, F=Fg, Rs=Rs, Xls=Xs, Xd=Xd, Xq=Xq)

# Sending Generator Timer data
Timer.parameters(X=time)

# Sending Grid datas
Vgg.parameters(Value=Vgrid)
fgg.parameters(Value=Fgrid)
Zgg.parameters(R=Rccgrid, L=Lccgrid)

# Sending Converter filter data
RLCg.parameters(R=RC, L=LC)

# Sending DC capacitors data
C1.parameters(C=Cdc)
C2.parameters(C=Cdc)

# Sending Data to PLL
kp_pll.parameters(Value=kp_pll_n1)
```



```
ki_pll.parameters(Value=ki_pll_n1)
fp11.parameters(G=f_PLL)

# Sending Datas to power loops
kp_P_g.parameters(Value=kp_P_n1)
ki_P_g.parameters(Value=ki_P_n1)
kp_P_m.parameters(Value=kp_P_n1)
ki_P_m.parameters(Value=ki_P_n1)

project.run()
print("Script is Done!")

else:
    print("Failed to launch PSCAD")

# -----
# End of script
# ~~~~~
```



Initialization code for IEEE 9-bus in Python

```

import mhi.pscad
import mhrc.automation
from mhi.pscad.utilities.file import File
import sys, os
import win32com.client
import shutil
import grg_pssedata
import math
# -----
# Configuration
# -----
print("Automation Library:", mhi.pscad.VERSION)

settings = {'fortran_version': 'GFortran 4.6.2'}
fortran_ext = '.gf46'
project_name = 'IEEE9bus_WT_with_automation'

# Working directory
working_dir = os.getcwd() + "\\\"

# -----
# Main script
# -----

# Launch PSCAD and Fortran version
pscad = mhi.pscad.launch(version='5.0.1', settings=settings)

#Getting Data from raw file
INPUT_FILE = "Raw file location"
data = grg_pssedata.io.parse_psse_case_file(INPUT_FILE)

#Defining Generators parameters from raw file
vt1=(data.buses[0].vm)           #Initial voltage magnitudte of G1
vt2=(data.buses[1].vm)           #Initial voltage magnitudte of G2
ph1=(data.buses[0].va)           #Initial phase angle of G1 in (radians)
ph2=((data.buses[1].va)*0.0174533) #Initial phase angle of G2 in (radians)
pg1=(data.generators[0].pg)      #Initial active power of the G1
pg2=(data.generators[1].pg)      #Initial active power of the G2
qg1=(data.generators[0].qg)      #Initial reactive power of the G1
qg2=(data.generators[1].qg)      #Initial reactive power of the G2

#Defining Load datas
pl1=(data.loads[0].pl)/3         #Load 1 active power
pl2=(data.loads[1].pl)/3         #Load 2 active power
pl3=(data.loads[2].pl)/3         #Load 3 active power
ql1=(data.loads[0].ql)/3         #Load 1 reactive power
ql2=(data.loads[1].ql)/3         #Load 2 reactive power
ql3=(data.loads[2].ql)/3         #Load 3 reactive power

#Defining parameters of the Wind turbine
rho=1.225           #Air density
Pn=5                #WT nominal power

```



```

rt=44                #WT diameter
wrat=314.1592        #WT nominal mechanical speed(rad\sec)
A=math.pi*rt**2     #Rotor area
Gr=80.1              #Gearbox ratio
Ge=1                  #Gearbox efficiency

#PMSG parameters
Pg=5                  #Generator power
Vg=1                  #Generator voltage
Fg=50                 #Generator frequency
Rs=0.01               #Stator winding resistance
Xs=0.064              #Stator leakage reactance
Xd=0.55               #Unsaturated reactance(Xd)
Xq=0.85               #Unsaturated reactance(Xq)
time=1                #Time to switch from source to machine

#Grid parameters
Sgrid=5               #Grid base power
Vgrid=0.69            #Grid L_L base voltage
Fgrid=50              #Grid frequency
SCR=5                  #Short circuit ratio
Sccgrid=Sgrid*SCR     #Short circuit power
Zccgrid=Vgrid**2/Sccgrid #Short circuit impedance
Lccgrid=Zccgrid/(2*math.pi*Fgrid) #Short circuit inductance
Rccgrid=Zccgrid/100   #Short circuit resistance

#Converter parameters
SC=Sgrid              #Converter Base power
fC=Fgrid              #Converter Base frequency
WC=2*math.pi*fC      #Converter Base angular speed
ZbC=Vgrid**2/SC       #Converter Base impedance
LbC=ZbC/(2*math.pi*fC) #Converter Base inductance
RC=0.01*LbC           #Converter grid coupling filter resistance
LC=0.1*LbC            #Converter grid coupling filter inductance
Vpeak_n1 = Vgrid*(math.sqrt(2)/math.sqrt(3))

#Dc bus parameters
Vdc_ref=1.2           #DC bus voltage
tauc=0.04             #Time response of the DC capacitor
Cdc=(2*tauc*SC/Vdc_ref**2) #DC capacitor
Cdc_PSCAD=Cdc*2e6     #2 Capacitor in series in PSCAD

#PLL tuning
ts_pll_n1=0.025      #PLL time constant
xi_pll_n1=0.707      #PLL damping ratio
omega_pll_n1=4/(ts_pll_n1*xi_pll_n1) #PLL angular speed
kp_pll_n1=(xi_pll_n1*2*omega_pll_n1)/(Vpeak_n1*10**3) #PLL propotional value
tau_pll_n1=2*xi_pll_n1/omega_pll_n1 #PLL tau
ki_pll_n1=kp_pll_n1/tau_pll_n1      #PLL integral value
f_PLL=60              #PLL frequency

#G-side Current controller
taus=0.001
kp_s_n1=LC/taus
ki_s_n1=RC/taus

```



```
# DC voltage control
psi_Vdc=2
wn_Vdc=10*2*math.pi
kp_dc=2*Cdc*psi_Vdc*wn_Vdc
ki_dc=Cdc*wn_Vdc**2

#Power loops
tauPQ=1e-2
kp_P_n1=taus/tauPQ
kp_Q_n1=kp_P_n1
ki_P_n1=1/tauPQ
ki_Q_n1=ki_P_n1

if pscad:
    try:
        # Load the project
        pscad.load([r'(PSCAD file location)'])
        project = pscad.project(project_name)
        project.focus()

        # Get the "Main" canvas
        main = project.canvas('Main')

        #Getting Generators Datas
        G1 =project.component(148919121)
        G2 =project.component(1869282479)

        #Getting load Datas
        l1=project.component(1391543602)
        l2=project.component(393679904)
        l3=project.component(1512264491)

        # Getting wind turbine data
        WT = project.component(956528011)

        # Getting PMSG parameters
        G = project.component(862029781)

        # Getting timer data
        Timer = project.component(1294302219)

        # Getting converter filter Data
        RLCg = project.component(869123953)

        # Getting capitors Data
        C1 = project.component(1894479177)
        C2 = project.component(533623950)

        # Getting PLL Data
        kp_pll = project.component(1052788259)
        ki_pll = project.component(759565932)
        fpll = project.component(267265109)
```



```

# Getting power loops Data
kp_P_g = project.component(1338049127)
ki_P_g = project.component(342682449)
kp_P_m = project.component(744561321)
ki_P_m = project.component(383861948)

#Getting DC voltage regulator Data
kp_DC=project.component(600618823)
ki_DC=project.component(1120448045)

# -----
# Sending Data to PSCAD
# -----
print("Run 1, set IEEE9bus datas, run,")

# Sending Generators datas
G1.parameters(VT=vt1,Pheta=ph1,P0=pg1,Q0=qg1)
G2.parameters(VT=vt2,Pheta=ph2,P0=pg2,Q0=qg2)

#Sending Loads parameters
l1.parameters(P0=pl1, Q0=ql1)
l2.parameters(P0=pl2, Q0=ql2)
l3.parameters(P0=pl3, Q0=ql3)

# Sending Wind turbine data
WT.parameters(Gmva=Pn, Wrat=wratt, Rad=rt, Area=A, Airden=rho, Eff=Ge, Gratio=G)

# Sending Generators datas
G.parameters(MVA=Pg, VRAT=Vg, F=Fg, Rs=Rs, Xls=Xs, Xd=Xd, Xq=Xq)

# Sending Generator Timer data
Timer.parameters(X=time)

# Sending Converter filter data
RLCg.parameters(R=RC, L=LC)

# Sending DC capacitors data
C1.parameters(C=Cdc_PSCAD)
C2.parameters(C=Cdc_PSCAD)

# Sending Data to PLL
kp_pll.parameters(Value=kp_pll_n1)
ki_pll.parameters(Value=ki_pll_n1)
fpll.parameters(G=f_PLL)

# Sending Datas to power loops
kp_P_g.parameters(Value=kp_P_n1)
ki_P_g.parameters(Value=ki_P_n1)
kp_P_m.parameters(Value=kp_P_n1)
ki_P_m.parameters(Value=ki_P_n1)

```



```
    #Sending parameters to DC voltage regulator
    kp_DC.parameters(Value=kp_dc)
    ki_DC.parameters(Value=ki_dc)

    project.run()

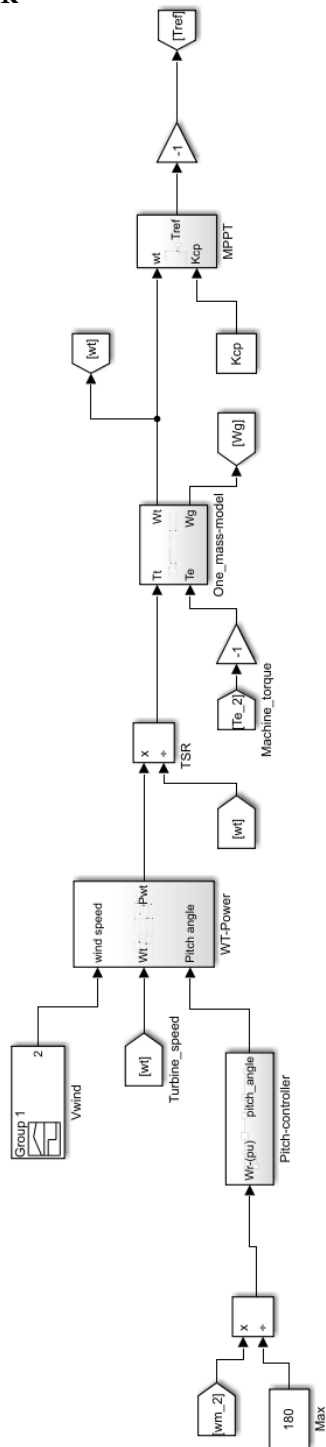
else:
    print("Failed to launch PSCAD")

# -----
# End of script
# ~~~~~
```

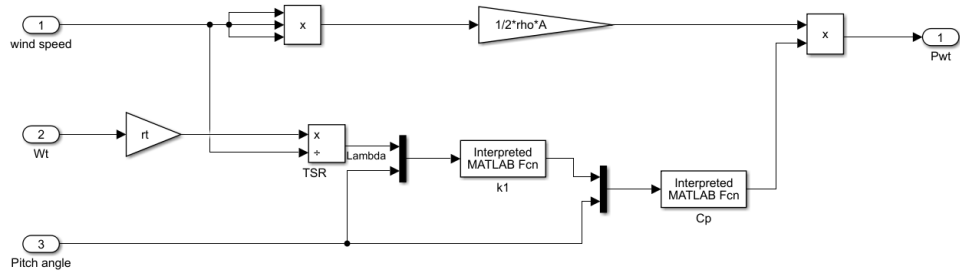


Simulink Figures

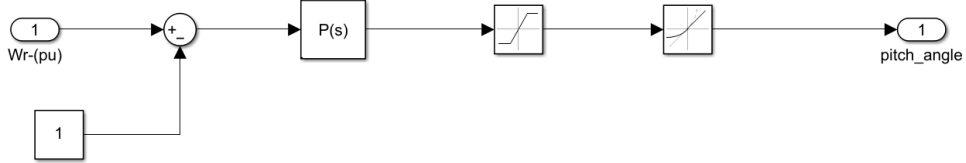
Wind Turbine model in Simulink



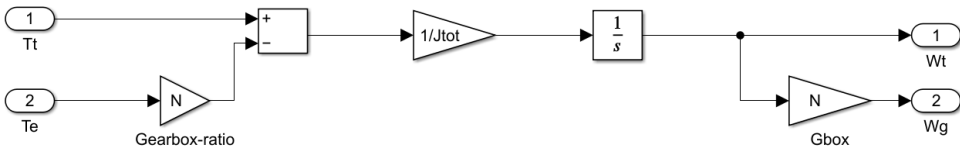
Wind Turbine power model in Simulink



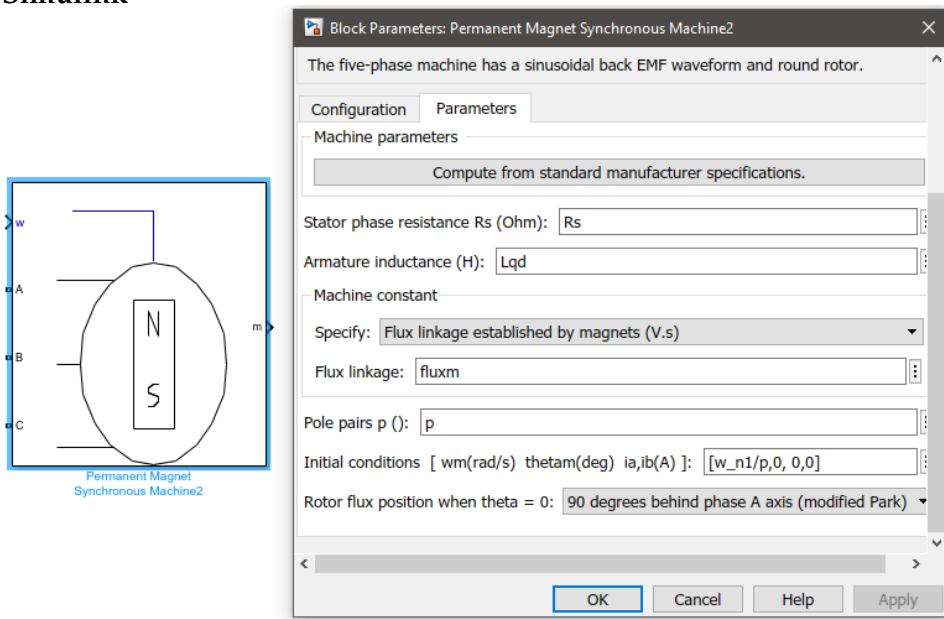
Pitch controller model in Simulink



Shaft model in Simulink



PMSG in Simulink

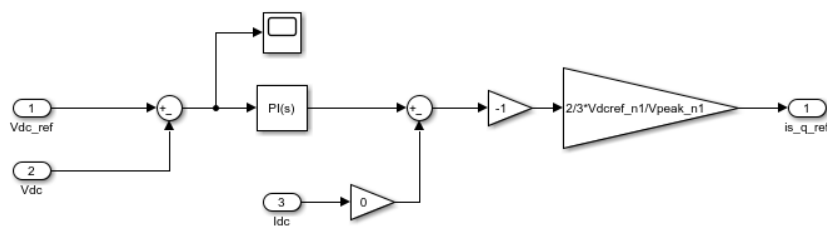


The diagram on the left shows a cross-section of a Permanent Magnet Synchronous Machine (PMSG) with a round rotor. The rotor has North (N) and South (S) poles. The stator has three phases labeled A, B, and C, and a winding labeled 'w'. The machine is labeled 'Permanent Magnet Synchronous Machine2'.

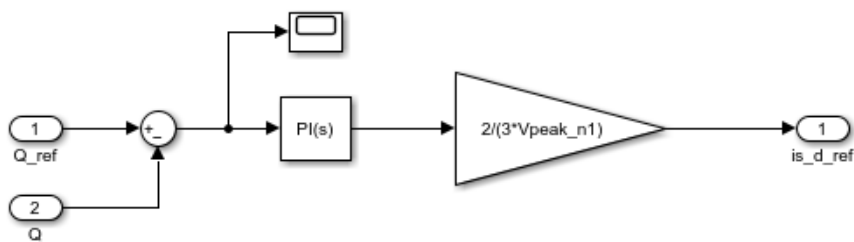
The 'Block Parameters: Permanent Magnet Synchronous Machine2' dialog box on the right contains the following parameters:

- Configuration:** Parameters
- Machine parameters:** Compute from standard manufacturer specifications.
- Stator phase resistance R_s (Ohm):** R_s
- Armature inductance (H):** L_{qd}
- Machine constant:** Specify: Flux linkage established by magnets (V.s)
- Flux linkage:** fluxm
- Pole pairs p ():** p
- Initial conditions [ω_m (rad/s) θ_{tam} (deg) i_a, i_b (A)]:** $[\omega_{n1}/p, 0, 0, 0]$
- Rotor flux position when $\theta = 0$:** 90 degrees behind phase A axis (modified Park)

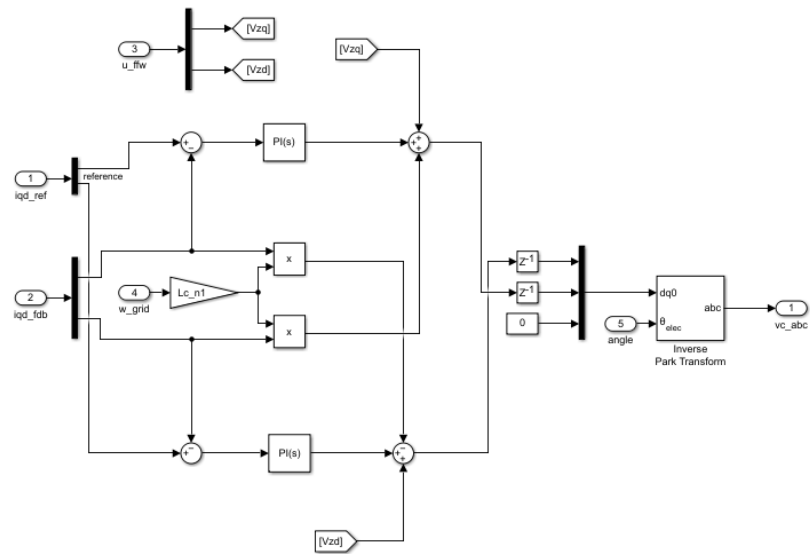
DC voltage regulator in Simulink



Qloop in Simulink



Grid-side current regulator in Simulink



Machine-side current regulator in Simulink

